NANOPARTICLE DYNAMICS IN SIMPLE FLUIDS

Thesis submitted in accordance with the requirements of the University of Liverpool for the degree of Doctor of Philosophy

By

Diego Coglitore

December 2016

ABSTRACT

The Stokes-Einstein relation is considered a benchmark in the transport of small particles in fluids, predicting an increase in diffusion with decreasing particle size. However, there is doubt about its validity at the nano-scale where some theoretical studies have predicted deviations from it. Experimental data from single nanoparticle tracking are presented in this thesis, collected using a recently-developed technique based on the optical phenomenon of caustics to detect the particle in a conventional inverted optical microscope. Experiments were performed on gold and polystyrene nanoparticles dispersed in water and glycerol-water mixtures, with viscosities ranging from 0.00008 to 0.15 Pa·s, to investigate the effect of nanoparticle size, density, concentration, and liquid viscosity on diffusion rates at a fixed temperature of 30°C. It is shown that below a critical concentration and critical size of particle diffusion falls orders of magnitude below the Stokes-Einstein prediction and it is better represented by the fractional Stokes-Einstein relation. At these experimental conditions, the diffusion coefficient was found to be constant with particle size and independent of material, but dependent on fluid viscosity. This thesis is aimed at enriching the knowledge on nanoparticle motion in simple fluid. The validity of the Stokes-Einstein diffusion at the nanoscale is addressed by experiments, within the context of simple, isotropic fluids.

ACKNOWLEDGEMENTS

I would like to express my sincere gratitude to Professor Eann Patterson, for providing me with tremendous support and guidance throughout my time as a PhD student at University of Liverpool. Without his insights and drive, the completion of this thesis would not have been possible.

I am grateful to Professor Maurice Whelan, who drove me through this project giving an imprescindible contribution to this research with his ideas, intuitions and knowledge of the nanoworld.

Furthermore, I am thankful to Dr. Stuart Edwardson for his essential supervision, always available for any kind of help and leading me with advices at each step of my research.

Profound gratitude goes to Dr. Peter Macko, who supported me from my first visit at the JRC of the European Union, and donated his point of view as a physicist among four engineers.

I would also like to acknowledge Professor Rob Poole and Dr. John Bridge from University of Liverpool for letting me use their laboratories, Taina Palosaari and Dr. Douglas Gilliland for their helpful advices.

Finally I would like to thank my parents and dedicate this thesis to them, and wish them every happiness in life.

TABLE OF CONTENTS

"These motions were such as to satisfy me, after frequently repeated observation, that they arose neither from currents in the fluid, nor from its gradual evaporation, but belonged to the particle itself"

Robert Brown

"Brownian motion, unique among physical processes, makes visible the constant state of internal restlessness of bodies, in the absence of any external cause."

Georges Gouy

ABBREVIATIONS AND NOTATIONS

Abbreviations

DLS: dynamic light scattering

FFS: fluorescence fluctuation spectroscopy

FRAP: fluorescence after photobleaching

MSD: mean square displacement

NTA: Nanoparticle tracking analysis

PDF: probability density function

SPT: single-particle tracking

STED: stimulated emission depletion

TEM: transmission electron microscope

TIRF: total internal reflection fluorescence

Notations

C : numerical constant in the fractional Stokes-Einstein equation

d: particle diameter

D: diffusion coefficient

f(kr): Henry's function

H_A : Hamaker constant

I: intensity of light

J: particle flux

k_b: Boltzmann constant

m: mass of the particle

P: probability that the x-coordinate of a single particle at the time *t* will lie in the interval (x, x+dx)

q: wave vector

r: particle radius

T: temperature

U_{DLVO}: DLVO potential

U_{DH}: Debye-Huckel potential

U_{SR}: short range potential

U_E: electrophoretic mobility

ε_r: dielectric constant

η: viscosity of the fluid

ξ: frictional coefficient

λ: wavelength of light

μ: mean of Gaussian distribution

ζ: random change of the particle position

ρ: particle density

σ^2: variance of Gaussian distribution

τ_p: relaxation time

Γ: decay time

CHAPTER 1

Introduction

This experimental research is concerned with the dynamics of nanoparticles in simple, isotropic fluids. The core of the thesis addresses this topic through an experimental study on two different types of metallic and non-metallic nanoparticles, where the variation of different parameters is used to test the validity of the Stokes-Einstein diffusion at the nanoscale. The lack of a systematic investigation on the nanoparticles diffusion in simple fluids was the initial motivation leading to this research. Simple fluid is intended as a continuous hydrodynamic system, in which the characteristics are the same in all directions, and no highly specific interactions (long-range interactions can be neglected, fluid molecules interact only by van der Waals forces) are present; the shape and size of the fluid molecule are the main parameter to characterize the system. Most of the studies found in the literature do not present a parametric investigation of the nanoparticle motion, in order to understand its characteristics when, for instance, particle concentration or viscosity are changed. The idea that the classical Stokes-Einstein diffusion could break down at the nanoscale has been proposed by few authors, but no experimental evidence was given to support it. The aim of this research was to investigate the role that interaction forces could play at this scale, where their effect is stronger because of the particle size and leads to deviations from expected behaviour, or can be simply neglected as for bigger particles, where the Stokes-Einstein diffusion has been demonstrated to predict their motion. The

study was conducted at low concentrations both for a better identification of the nanoparticle and to study its behaviour when isolated from interactions with other nanoparticles. At these concentrations only the nanoparticle-fluid molecule interactions can be considered, since Brownian motion is generated by the collisions between them.

A characterization of the nanoparticle behaviour in simple and complex media is necessary, for instance, for a toxicological investigation; as the comprehension of all the properties of the nanomaterials is something impractical, a set of the characteristics has to be established to describe their behaviour. Diffusion could be a direct, physical, quantity to measure, in order to classify the level of toxicity of a nanomaterial. As this research concerns simple fluids, the work can find applications, or can be extended, to biological fluids. Carbon nanotubes, silica and metal oxides generate several problems when absorbed by the living organism and cell damages occur. The widespread use of nanoparticles, as in cosmetics of food production (silica nanoparticles are used as stabilizer in soups!), makes necessary a full comprehension of the associated phenomena.

In the next chapter a history of the diffusion is presented, starting from the exploratory work of Thomas Graham, which later inspired Adolf Fick's diffusion equations, and through the work of scientists who achieved the milestones in the history of diffusion and Brownian motion. The first systematic investigation of the random motion of a particle was made by Robert Brown, but it was Albert Einstein who first gave it a mathematical form. Einstein derived Fick's second law taking into consideration the random nature of the motion, introducing a Gaussian

distribution to take account of the random displacement of the particle. While for Fick the diffusion coefficient was “a constant dependent upon the nature of substances”, Einstein explored its nature in depth and through statistical considerations he defined the mean square displacement of the particle and the well-known Stokes-Einstein diffusion. After describing the history and theory of Brownian motion, the chapter follows with a description of the deviations from the classical Brownian motion. Anomalous diffusion is presented, for instance, in biological systems, for which the assumption of continuous hydrodynamic fluid does not hold, and so deviations are expected. In such cases, the diffusion coefficient and mean square displacement have different characteristics to those of particles moving in isotropic fluids. Another exemplar deviation from the classical Stokes-Einstein diffusion is introduced to explain dynamics at the molecular scale: the fractional Stokes-Einstein equation is often used to represent the motion of molecules and tracers. In this equation the diffusion coefficient has a fractional dependence on the viscosity, while in the classical relation is linearly proportional. As will be shown later, the fractional Stokes-Einstein relation has been found to nicely represent the diffusion of nanoparticles under well-defined circumstances.

Chapter 3 is intended to introduce the following experimental method chapter. An overview of the main particle tracking techniques shows the benefits and disadvantages of the most used single-particle and single-molecule methodologies. These techniques allow the study of dynamics in many fields, such as physics, biophysics and cell biology. Fluorescence and confocal microscopy are probably the most widespread methodologies for single-particle tracking, but the emergence

of non-fluorescent nanoparticles, due to their non-toxicity and their importance for *in vivo* studies, is making important the development of more suitable nanoparticle tracking techniques. Dynamic light scattering is described and discussed because of its versatility and wide use in different applications. A system based on dynamic light scattering was used in this experimental work as a confirmation of the data collected with the main apparatus used in this thesis. The experiments in this investigation were indeed performed in an inverted optical microscope where a recently developed nanoparticle tracking technique was applied, based on the optical phenomenon of caustics. This technique allows non-fluorescent particles to be easily identified and followed in their motion. The caustics and their applications are described before their formation in an inverted optical microscope is explained. The last two sections introduce the experimental technique and the setup that were employed to track gold and polystyrene nanoparticles dispersed in simple fluids.

Chapter 4 is the materials and methods section. The first part is dedicated to the commercial nanoparticles used in the experiments and their characterization, followed by a description of the fluids in which the nanoparticles are dispersed. Then the methodology used to prepare the nanoparticles dispersions, the experimental setup and the experimental methodology are reported. Particular care is taken to describe the 2D tracking software used to process the collected videos and to obtain the nanoparticle coordinates over the time of the experiment. The final section of chapter 4 is dedicated to the Nanosight system, which utilizes the properties of both light scattering and Brownian motion to obtain the particle size

distribution in liquid suspensions: a general description, the setup and the data analysis are discussed.

The results of the experimental investigation are presented in Chapter 5. The first two sections show how nanoparticles moving in simple fluids comply with some of the essentials characteristics of the Brownian motion: the linear dependence of the diffusion coefficient on time, typical of the isotropic liquids, and the Gaussian distribution of the particle displacements, i.e. the random nature of the motion. Even if the nanoparticles motion met these two conditions, Stokes-Einstein prediction is shown to overestimate the diffusion coefficients. Nanoparticles with diameters below 150nm, at low concentrations, were found to deviate from the classical Stokes-Einstein relation, which is a surprising result. Comparing the collected data with experimental data found in the literature, and performing further experiments for a better understanding of the phenomenon, the borders between the classical model and its deviation emerge: a critical concentration and a critical size below which diffusion is no more defined by the Stokes-Einstein relation. The experimental data were confirmed by the failure of a Nanosight system to correct size the particles. Finally, the experimental data were fitted to the fractional Stokes-Einstein equation, giving a mathematical form to the nanoparticle motion at low concentrations.

The experimental results are then discussed in Chapter 6. A spatial interpretation of the deviation of the nanoparticle diffusion at low concentrations is proposed as a first step in understanding of the phenomenon. Since a nanoparticle is mostly surrounded by fluid molecules under these conditions, the behaviour of simple

fluids is taken into account and the fractional Stokes-Einstein approach is interpreted. It is speculated that the van der Waals forces could play an important role at the nanoscale and a theoretical justification using models for interparticle interactions is presented, highlighting the relevance of these attraction forces below a critical size. The results find a possible interpretation in terms of hydrodynamics, where classical approaches fail under these experimental circumstances. An interpretation of the fractional Stokes-Einstein behaviour at low concentrations is presented and compared with possible explanations given by other authors.

The main findings and conclusions of the thesis are summarized in Chapter 7.

CHAPTER 2

Theoretical Background

2.1 - Diffusion and Brownian motion: historical background

Almost 200 years ago, the Scottish botanist Robert Brown was the first who systematically investigated the motion of suspended microscopic particles, observing, in his microscope, the random motion of pollen particles of few micrometres [1]. In his honour, the name "Brownian Motion" has been used to refer to the random walk of particles suspended in a fluid. One of its most popular and best representations was given by George Gamow [2] through his drunkard's walk (Figure 1). The origin of this random motion was successfully studied by Albert Einstein [3], who was able to link the microscopic with the macroscopic world: he expressed the microscopic data, i.e. the never-ending movement of a particle, in terms of a macroscopic quantity: the coefficient of diffusion.

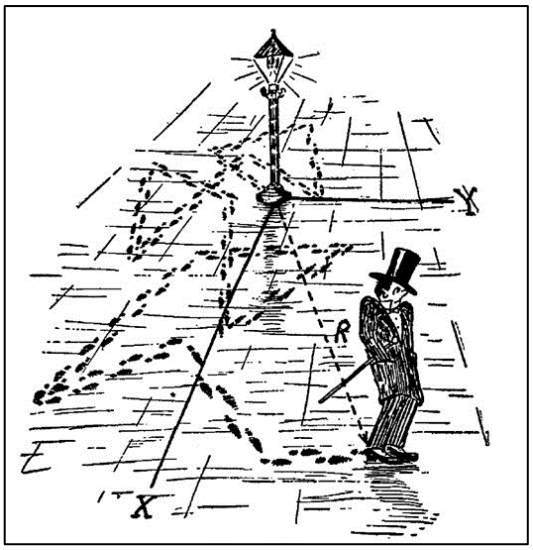

Figure 1 - Drunkard's walk [2]

To trace back the first systematic study on diffusion, we have to refer to another Scottish scientist, the chemist Thomas Graham, inventor of the dialysis. He performed the first quantitative experiment on diffusion, even if the notion of "coefficient of diffusion" was introduced later by Adolf Fick [4]. Graham observed that gases of different nature, when in contact, do not arrange themselves according to their density, but they spontaneously diffuse through each other [5]. To understand the importance of his work, we have to consider that his results were used by Maxwell for the determination of the diffusion of CO_2 in air [4].

It was a German doctor, Adolf Fick, mainly interested in physiology, who dedicated a couple of years of his life to physics and left us the well-known Fick's equations of diffusion [6, 7]. Physiologists began to have an interest in membranes and the related osmotic and diffusive processes. In this sense, Fick admitted that hydrodiffusion through membranes was at the origin of his studies [6]. Fick, in 1855, had the idea, thinking about Graham's results on salt diffusion, of the analogy with the conduction of heat [4]. Employing this analogy, he assumed the flux of matter proportional to the concentration gradient through a constant dependent on the nature of the substances [6].

A microscopic approach was at that time something difficult to accept. If we consider that famous scientists, as Lavoisier or Gay-Lussac, thought that diffusion in solids was not credible [4], we can understand the difficulties of an "atomistic" approach. It was the British metallurgist Roberts-Austen who performed, some years after Fick's paper, systematic experiments on the diffusion in metals [8].

In 1889, the French physicist Georges Gouy performed experiments on different particles suspended in different fluids to investigate Brownian motion. Through his results, he demonstrated that the motion is independent of external forces and it is more intense when the fluid is less viscous. His conclusion gives a clear idea of the deep understanding he reached: "Brownian motion, unique among physical processes, makes visible the constant state of internal restlessness of bodies, in the absence of any external cause." [9]

But Gouy's approach had no theoretical basis, so he moved on from the study of Brownian motion. The first mathematical form was given some years later, in 1905, by Albert Einstein. He published five papers between 1905 and 1908 [10]. At that time Einstein, while employed as an engineer at the Patent Office in Bern, was interested in the movement of small particles suspended in a liquid, because he considered it as a demonstration of the molecular kinetic theory of heat [3]. At that time the "Atomic Theory" was still at the centre of discussion and controversy [4]. Einstein assumed that the movement of a particle, in a considered time interval, sufficiently small, is independent of the successive intervals and from the motion of other particles, thus identifying the main assumptions of the Brownian motion [3]. Thanks to Einstein, diffusion became a macroscopic quantity defined in terms of a microscopic one: the mean square displacement of the particle.

Marian von Smoluchowski, one year after Einstein's first publication, came essentially to the same conclusion with a kinetic approach, considering as the principle causes the interactions and collisions between particles rather than the molecular kinetic theory of heat [11]. The only difference between the two

equations is a numerical factor. For this reason, the relation between diffusion and mean square displacement is also known as Einstein-Smoluchowski equation.

It is necessary to cite another milestone in the study of diffusion and Brownian motion: the French physicist Paul Langevin, who, with a simpler approach than Einstein and Smoluchowski, starting from Newton's second law, explained the motion of a particle as generated by a viscous resistance and a fluctuating force independent of the velocity, generated by the impacts of the fluid molecules on the particles [12].

In the same year Langevin published his studies, another French physicist tested experimentally Einstein's theory: Jean Perrin, armed with a microscope and particles (few tenths of micron in diameter) suspended in a fluid, proved Einstein's explanation of Brownian motion [13] (Figure 2). These experiments, together with others on the sedimentation of particles for the calculation of the Avogadro constant, allowed Perrin to demonstrate the atomic nature of matter, for which he was honoured with the Nobel Prize for Physics in 1926.

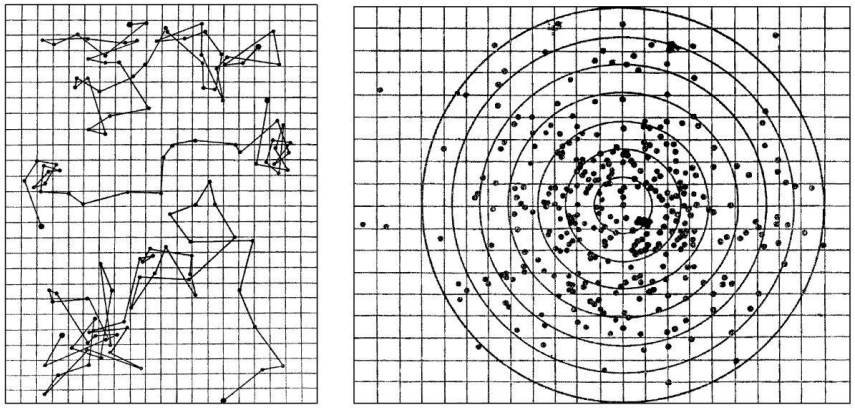

Figure 2 - Recorded random walk trajectories by Jean Baptiste Perrin [13]

If Brownian motion was at the centre of debate from the very beginning, in the early nineties even the name "Brownian" was subject of discussion, when Daniel Deutsch, an American businessman, claimed Brown could not have been able to observe particles with his microscope [14]. Gerhard Cadée promptly answered [15], and the dispute was finally solved by Brian Ford, who repeated the experiments with Clarkia pollen and Brown's setup [16], restoring Brown's findings.

If Brownian motion began to be studied with particles suspended in a fluid, people soon started to be interested in the random walk applied in any kind of field [17]. The mathematician Louis Bachelier did probably the first study on the random walk five years before Einstein exploring the fluctuations of the stock-market prices, describing the process as a law of diffusion of probability [18]. Nowadays Brownian motion is widely applied in the financial world, it's a main topic in mathematics, biology, genetics or evolution models [4, 19].

2.2 - Einstein's theory of diffusion

Before it was universally accepted that a fluid consists of moving molecules, thanks to Einstein [3] and the experimental confirmation of Perrin [13], Fick's diffusion equation were widely accepted [20]. Fick's macroscopic theory of diffusion focuses on two quantities: the solute density $\rho(\mathbf{r}, t)$ and the solute flux $J(\mathbf{r}, t)$, defined as the average number of particles per unit volume at the position $\mathbf{r}$ and at the time t. He assumed, employing the analogy with the diffusion of heat and the conduction of electricity [7], an empirical relation between the two quantities:

$$J_u(\mathbf{r}, \mathrm{t}) = -D \frac{\partial \rho(\mathbf{r}, \mathrm{t})}{\delta u} \quad (1)$$

Where $u = x,y,z$ and D is the diffusion coefficient, that in Fick's original paper is called k, "a constant dependent upon the nature of substances" [7]. The former equation represents Fick's first law.

If one considers an infinitesimal volume element $dxdydz$ at the position $\mathbf{r}$ in the infinitesimal time interval $t+dt$, we must have

$$\begin{aligned} \rho(\boldsymbol{r}, t + dt)dxdydz \; - \; \rho(\boldsymbol{r}, t)dxdydz \quad (2) \\ = \; (J_x(\boldsymbol{r}, t)dydzdt \; - \; J_x(\boldsymbol{r} + \boldsymbol{x}dx, t)dydzdt) \\ + \left(J_y(\boldsymbol{r}, t)dxdzdt \; - \; J_y(\boldsymbol{r} + \boldsymbol{y}dy, t)dxdzdt\right) \\ + \; (J_z(\boldsymbol{r}, t)dxdydt \; - \; J_z(\boldsymbol{r} + \boldsymbol{z}dz, t)dxdydt) \end{aligned}$$

The equation is represented in Figure 3: the increase during dt in the number of solute particles (black spheres), i.e. the solid particles dispersed in a liquid (solvent), inside the infinitesimal volume element $dxdydz$ at the point (x, y, z) (the small dot) is equal to the average number of particles entering the volume element through the left side in dt, $J_x(r,t)dydzdt$, minus the average net number of particles leaving the volume element through its right face in dt, $J_x(r+xdx,t)dydzdt$. The same contributions are summed from the back and front of the volume element, and its bottom and top faces.

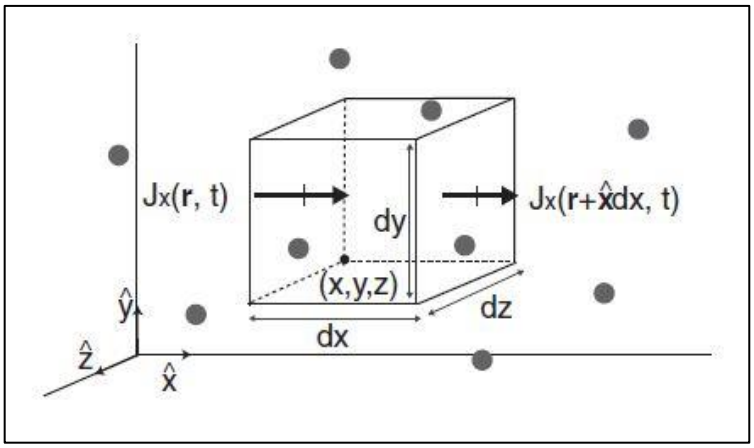

Figure 3 – Representation of the continuity equation [20]

Dividing the equation by *dxdydzdt*, we obtain the continuity equation [20]

$$\frac{\partial \rho(\boldsymbol{r},t)}{\partial t} = -\left(\frac{\partial J_x(\boldsymbol{r},t)}{\partial x} + \frac{\partial J_y(\boldsymbol{r},t)}{\partial y} + \frac{\partial J_z(\boldsymbol{r},t)}{\partial z}\right) \tag{3}$$

If we substitute equation (1) in the right side of equation (3), we obtain

$$\frac{\partial \rho(\boldsymbol{r},t)}{\partial t} = D\left(\frac{\partial^2 \rho(\boldsymbol{r},t)}{\partial x^2} + \frac{\partial^2 \rho(\boldsymbol{r},t)}{\partial y^2} + \frac{\partial^2 \rho(\boldsymbol{r},t)}{\partial z^2}\right) \tag{4}$$

Where the solution depends on the initial conditions and the boundary conditions, determined by the characteristics of the specific problem [20]. The former equation is generally known as Fick's second law. What Einstein essentially did was to derive Fick's second law taking into consideration a random motion. Fick instead started from the continuity equation (3) to derive his second law.

Einstein chose a time interval infinitesimally small considering a macroscopic scale, but long enough that many collisions happen between the solute molecule and the fluid molecules. Considering a one-dimensional system, he introduced a

probability density function (PDF) $\Phi(\zeta;\delta t)$, defined so that $\Phi(\zeta;\delta t)\delta\zeta$ is the probability that the solute molecule in the x-direction during time δt will change by an amount ζ+δζ. The variable ζ represents the random change in position due to the collisions, i.e. the stochastic displacement of the solute, and it is defined as $\zeta = x/\sqrt{4Dt}$. Einstein observed that the average number of solute molecules between *x* and *x*+*dx* can be written in terms of a PDF

$$\rho(x, t+\delta t)dx = \int_{-\infty}^{\infty} \Phi(\zeta;\delta t)\rho(x-\zeta)dxd\zeta \tag{5}$$

Cancelling *dx* on both sides and expanding $\rho(x-\zeta)$ in a Taylor series gives:

$$\begin{aligned}\rho(x, t+\delta t) &= \int_{-\infty}^{\infty} \Phi(\zeta;\delta t)\,[\rho(x,t) + \sum_{k=1}^{\infty} \frac{(-\zeta)^k}{k!}\frac{\partial^k \rho(x,t)}{\partial x^k}] \\ &= \rho(x,t)\int_{-\infty}^{\infty} \Phi(\zeta;\delta t)d\zeta \\ &+ \sum_{k=1}^{\infty} \frac{\partial^k \rho(x,t)}{\partial x^k}\left[\frac{1}{k!}\int_{-\infty}^{\infty}(-\zeta)^k \Phi(\zeta;\delta t)\,d\zeta\right]\end{aligned} \tag{6}$$

Since Φ is a PDF in ζ, the first term in the integral is a unity. The solute molecule has the same probability to move in the positive or negative x-directions, so $\Phi(\zeta;\delta t)$ is an even function of ζ and consequently all the odd integers *k* in the summation vanish. Moving the first term ρ(x, t) to the right side and dividing by *dt*, he obtained

$$\frac{\partial \rho(x,t)}{\partial t} = \sum_{k=1}^{\infty}\left[\frac{1}{\delta t}\frac{1}{(2k)!}\int_{-\infty}^{\infty}\zeta^{2k}\Phi(\zeta;\delta t)\,d\zeta\right]\frac{\partial^{2k}\rho(x,t)}{\partial x^{2k}} \tag{7}$$

Assuming that the series converges rapidly so that all the terms beyond $k = 1$ can be ignored, we have

$$\frac{\partial \rho(x,t)}{\partial t} = D \frac{\partial^{2k} \rho(x,t)}{\partial x^{2k}} \tag{8}$$

Where D is

$$D = \frac{1}{2\partial t} \int_{-\infty}^{\infty} \zeta^2 \Phi(\zeta; \delta t)\, d\zeta \tag{9}$$

Equation (8) is exactly the one-dimensional case for Fick's second law, derived reasoning from the random motion of a particle and its collisions with the fluid molecules. Its solution, for k=1, is given by

$$\rho(x,t) = \frac{1}{\sqrt{4\pi D t}} e^{\left(-\frac{x^2}{4Dt}\right)} \tag{10}$$

2.3 - Einstein's new perspective: the mean square displacement

A more detailed explanation of the innovation introduced by Einstein, considering a random variable, is given by Gillespie [20].

Let's consider N solute particles. At the time t = 0, we have the initial condition $\rho(x,0) = N\delta(x)$, when all the *N* particles are contained at the origin x=0 and represented as the Dirac delta function of the particles, which has value 0 everywhere except at x=0. The average fraction of the N solute particles, in the spatial interval (x, x+dx) in the time interval dt, is then given by $N^{-1}\rho(x,dt)dx$. The

solute particles move randomly and independently of each other, so that their average fraction has to be also the probability that one of them will have, in the time interval dt, its position between (x, x+dx). In this way the PDF Φ is related to the solute density ρ by

$$\Phi(x, \delta t) = N^{-1}\rho(x, \delta t), \text{when } \rho(x, 0) = N\delta(x) \tag{11}$$

The PDF Φ is also the probability P that the x-coordinate of a single particle at the time t will lie in the interval (x, x+dx). We can write

$$P(x + \zeta, t + \delta t) = \Phi(\zeta, \delta t) \tag{12}$$

But also P and ρ are related, and following the same reasoning that brought to equation (11), we have

$$P(x, t) = N^{-1}\rho(x, t) \tag{13}$$

Given equation (13), considering equation (8), we can write

$$\frac{\partial P(x,t)}{\partial t} = D\frac{\partial^2 P(x,t)}{\partial x^2} \tag{14}$$

Equation (14) is exactly the diffusion equation (8) in a probabilistic perspective. If the solution for equation (8) is the average number of particles in the interval [x, x+dx], the solution for equation (14) gives us the probability that a particular solute particle will be in the interval [x, x+dx]. Similarly to equation (10), i.e. the solution for equation (8), the solution to equation (14) is

$$P(x,t) = \frac{1}{\sqrt{4\pi D(t-t_0)}} e^{\left(-\frac{(x-x_0)}{4D(t-t_0)}\right)} \quad (15)$$

If we compare equation (15) with a Gaussian distribution *N* with mean μ and variance σ^2

$$N(x) = \frac{1}{\sqrt{2\pi\sigma^2}} e^{(-\frac{(x-\mu)^2}{2\sigma^2})} \quad (16)$$

the mean of the probability distribution *P* is x_0 and its variance is $2D(t-t_0)$.

The probability that a particle will be at the position *x* at the time *t* can be written in terms of the Gaussian distribution *N*

$$x(t) = N(x_0, 2D(t-t_0)) \quad (17)$$

Similar reasoning can be done for the y- and z- components. Thanks to the properties of the Gaussian distribution for which

$$\alpha + N(\mu, \sigma^2) = N(\alpha + \mu, \sigma^2) \quad (18)$$

from equation (17), we have

$$x(t) - x_0 = N_x(0, 2D(t-t_0)) \quad (19)$$

By definition, in a probability density function, the variance is given by the difference between the second moment and the square of the first moment

$$var(x) \equiv \langle x^2 \rangle - \langle x \rangle^2 \equiv \langle (x - \langle x \rangle)^2 \rangle \quad (20)$$

where the symbol ⟨ ⟩ represents, in general, the statistical moment. In general, the statistical moment is a quantitative measure of the shape of a set of points; for instance, if the points represent the mass, the zero moment is the total mass, the first moment is the centre of mass and the second moment is the rotational inertia. In a probability distribution, the zero moment is the total probability, the first moment is the mean and the second moment is the variance. In equation (20) the first moment ⟨x⟩ represents the mean of the distribution, which is μ=0 from equation (19). Equation (19) implies that the mean square displacement $x(t) - x_0$ is equal to its variance σ^2, i.e. $2D(t - t_0)$. Considering equation (20) it is possible to write

$$\langle (x(t) - x_0)^2 \rangle = 2D(t - t_0) \tag{21}$$

Equation (21) can be easily generalized in three dimensions, because

$$\begin{aligned} &(r(t) - r(0))^2 \\ &\quad = (x(t) - x(0))^2 + (y(t) - y(0))^2 + (z(t) - z(0))^2 \end{aligned} \tag{22}$$

and in two-dimensions

$$\langle (r(t) - r(0))^2 \rangle = 4Dt \tag{23}$$

or in three-dimensions

$$\langle (r(t) - r(0))^2 \rangle = 6Dt \tag{24}$$

While for Fick the diffusion coefficient is "a constant dependent upon the nature of substances", Einstein explored the coefficient *D* more in depth. Assuming that the particles have the same kinetic energy as the gas molecules at the same temperature [21], the diffusion coefficient is

$$D = \frac{k_b T}{\xi} \tag{25}$$

Where

$$\xi = 6\pi\eta r \tag{26}$$

In equation (25) k_b is the Boltzmann constant, T is the temperature and ξ is the frictional coefficient. The latter, defined in equation (26), is the Stokes' law and represents the force experienced by a perfect sphere of radius r moving in a liquid of viscosity η. Equation (25) is also known as the Stokes-Einstein relation and it represents the diffusion coefficient, i.e. the velocity, independent of the direction, of a particle undergoing Brownian motion in a fluid of viscosity η.

These mean square displacements formulas (equation (21), (23) and (24)) were used from the beginning, for instance by Perrin [13], to confirm Einstein's theory of Brownian motion. When a concentration gradient is absent, diffusion is usually described by Einstein's equation of Brownian motion rather than Fick's laws, i.e. equation (21), (23), (24) and considering the diffusion coefficient as in equation (25).

If the solvent can be described as a continuous hydrodynamic fluid and the characteristics of its structure can be ignored, the diffusion of the particle is expected to be constant. In this case it is common to talk about simple, or normal diffusion, so that the diffusion coefficient D in equations (21), (23) and (24), is constant during the period of observation of the particle motion.

On the basis of equation (22), which describes the position of the particle at the initial time of observation and at the time *t*, it is possible to extend it for the whole period of observation of the particle motion

$$MSD_n = \frac{1}{N-n}\sum_{i=0}^{N-n}((x_{i+n}-x_i)^2+(y_{i+n}-y_i)^2+(z_{i+n}-z_i)^2) \qquad (27)$$

based on the coordinates, (x_i, y_i, z_i) of the particle's location at the i^{th} step and similarly for the (i+n)th step of N steps. Equation (27) allows the determination of the mean square displacement from an experimentally measured trajectory. Particle positions are recorded as a time sequence, with the data acquisition time interval corresponding to the length of the step. In this way it is possible to plot the mean square displacement as a function of time. In the case of simple diffusion the dependence of the mean square displacement on the time is linear, where the diffusion coefficient represents the constant slope of a straight line.

In terms of probability, a particle undergoing simple diffusion can be represented as a Gaussian process. The displacement in each direction is Gaussian-distributed if the squared deviation from the origin is finite (central limit theorem) and if the displacements themselves are Markovian, i.e. the probability of a particular displacement is independent of previous displacements [22]. Displacements that do not follow the previous conditions, such as displacements that are correlated or that are not Gaussian-distributed, do not lead to simple diffusion, but to anomalous diffusion [23].

The mean square displacement is the most common way to analyse the trajectory of a particle. From it, and its dependence on time, it is possible to obtain information about the motion characteristics and properties of a particle suspended in a fluid.

2.4 - Deviations from Stokes-Einstein diffusion: from simple diffusion to anomalous diffusion

If the simple diffusion is based on the assumption of a continuous hydrodynamic fluid, a biological system does not obey this definition. Cytoplasm, for instance, contains different solutes of different sizes [24], so that its structure cannot be regarded as a continuous hydrodynamic fluid. Other effects, such as interactions, boundary effects, and a solute that approaches the cell membrane, have to be considered [23]. Diffusion that does not follow Stokes-Einstein prediction is often defined as anomalous diffusion [25], described by the following equation

$$MSD = 6Dt^{\alpha} \tag{28}$$

Where the numerical coefficient α in equation (28) is the generalization for the three-dimensional case, as in equation (24). In the case $\alpha<1$, the diffusion is generally called subdiffusion; if $\alpha>1$, diffusion is generally called superdiffusion [25].

Anomalous diffusion is typical of crowded systems, where the crowder in the solvent can be either mobile or fixed. In terms of diffusion, it represents an obstacle

for the solute motion, so that, for long times and distances, the motion of the solute is slowed down, leading to subdiffusion [26].

Anomalous diffusion was first reported by Richardson in 1926, during his studies on turbulent diffusion [27] and then mathematically formulated by Scher and Montroll [28] while they were trying to describe the dispersive transport in amorphous semiconductors, a system where the traditional models could not be applied [29]. If a biological environment is a good host for anomalous diffusion, it has been observed also in other kinds of systems, such as polymeric network [30,31], rotating flows [32], porous glasses [33,34,35], single molecule spectroscopy [36,37], bacterial motion [38-42], and many others, including the flight of the albatross [43].

Various models have been proposed to model anomalous diffusion. Generalization of the diffusion equation [44] and of Langevin equation [45], continuous random walk model [46], fractional Brownian motion [47] are some of the most used approaches. The last two have been widely studied in the past years. The continuous random walk model has been criticized [29,48] mainly because it does not incorporate force fields, and boundary condition problems. Fractional Brownian motion and fractional kinetics equations, such as the fractional diffusion equations [49-51] or the fractional Fokker-Planck equations [52-54], overcome these limits. Various interpretations have been proposed, using different fractional operators to replace the time or the spatial derivative, or both at the same time.

It is important to notice also that for a particle undergoing simple diffusion, the dependence of the mean square displacement on the time is not completely linear.

It is necessary to distinguish two diffusive regimes: the ballistic and the diffusive regime. The first one is representative of the particle motion over short time scales, when the time t is less than the momentum relaxation time τ_p ($t << \tau_p$). The diffusive regime is instead defined for $t >> \tau_p$. The momentum relaxation is defined as

$$\tau_p = \frac{m}{\xi} \tag{29}$$

Where m is the mass of the particle and ξ is the Stokes drag of equation (26). It essentially represent the crossover between the two regimes

The MSD of a Brownian particle at short time scales, i.e. $t << \tau_p$, is predicted by [55]

$$MSD = \left(\frac{k_b T}{m}\right) t^2 \tag{30}$$

so that the dependence of the MSD on time, at short time scales, is not linear even for a particle undergoing simple diffusion. Experimentally, it is difficult and challenging to study the ballistic regime since, for instance, the relaxation time of a 1μm particle is ~0.1μs and it decreases when the mass of the particle becomes smaller with its size [56]. In this regime the particle motion is time-correlated unlike the diffusive regime [57].

Even if it is widely accepted that crowding effects lead to anomalous diffusion, experimental results showed some disagreement. For instance, diffusion of aquaporin-1 in cell plasma membranes [58] has been experimentally found to be simple, so that anomalous diffusion cannot be considered a universal phenomenon in biological systems.

Simplification, such as superdiffusion and subdiffusion, could be not enough to explain complex phenomena as the particle-biological environment interactions. Considering, for instance, a nanoparticle approaching a cell membrane, one could expect a linear trend of the mean square displacement at a certain distance from the barrier, followed by a change in the particle dynamics when it approaches the membrane. The "capture" of the particle by the membrane could increase the nanoparticle diffusion in presence of attractive forces, or slowing down its motion with other kind of interactions. Future experimental works will, hopefully, clarify theoretical models that still seem far to be able to predict the particle dynamic in a biological environment.

2.5 - Deviations from Stokes-Einstein diffusion: the fractional Stokes-Einstein equation

Another fractional equation was proposed first by Hiss and Cussler [59] to explain the diffusion of n-hexane and naphthalene in hydrocarbon liquids. Hiss and Cussler proposed a fractional Stokes-Einstein equation for the diffusion of small solutes diffusing in high viscosity liquids (in a range from 0.0005 Pa s to 5 Pa s, at 25°C), based on their experimental data, where the diffusion is proportional to a fractional power of the viscosity. If for a large solute the dependence between diffusion and viscosity is

$$D \propto \eta^{-1} \tag{31}$$

They found the diffusion of small solutes to be proportional to a fractional power of the viscosity

$$D \propto \eta^{-p} \tag{32}$$

In their experimental work, they found the diffusion of hexane and naphthalene to be respectively

$$D\eta^{0.66} = constant \tag{33}$$

$$D\eta^{0.69} = constant \tag{34}$$

They tried to plot their results in other ways, for instance diffusion versus the solvent's molecular weight, but none of them gave such simple relations, with a linear trend in a log-log plot. They were quite surprised by their results and tried to give some explanation by comparing the diffusion data with conductance data, since the equivalent conductance is a measure of mass transport in terms of ionic mobility. They admitted, at the very end of the paper, that "this theory can be much more complicated, but we leave that to those who have much more theoretical skill than we".

Values of p=0.5 were found by Hayduk [60, 61] for the diffusion of methane and ethane in solvents ranging in viscosity from 0.0003 Pa s to 0.003.

Few years later, in 1979, Evans et al [62] found experimentally that the diffusion of a number of tetraalkyltins, in a wide range of size and viscosity to be represented by the fractional Stokes-Einstein equation rather than Stokes-Einstein equation, with p in a range from 0.45 to 0.94.

In 1994, Wakai and Nakahara [63] applied the fractional Stokes-Einstein equation to the self-diffusion in simple molecular fluids such as benzene and acetonitrile at high pressure.

In 2008, Funazukuri et al [64] applied the correlation to the diffusion of tracers, with different sizes and structures, in a wide range of solvents. In their study *p* appears to be constant over the range of viscosities, temperatures and pressures, but differs from one solute to another.

Of particular interest is the application of the fractional Stokes-Einstein equation in the study of glassy liquids and supercooled water, as deviations from Stokes-Einstein behaviour are supposed to be indicative of dynamical heterogeneities [65-67], i.e. the anomalous behaviour of glass liquids in the phase transition from the liquid to the glassy state. These dynamical heterogeneities are supposed to be caused by molecules and ions with different distributions of translational and rotational relaxation times, forming clusters with slower motion [67].

The fractional Stokes-Einstein relation has been widely used for ionic and molecular fluids, as reviewed by Harris [68] in 2009, for the study of the self-diffusion and the molecular dynamics of a number of ionic, molecular and Lennard-Jones fluids. Molecular dynamics simulations also found that the fractional Stokes-Einstein relation apply at the molecular scale over a wide range of thermodynamic states [69]. While the dynamical heterogeneities can explain critical conditions such as the supercooled and glassy liquids, they are not necessarily the cause of deviations observed at ambient conditions. Harris [68], for instance, found by simulations water molecules to follow the fractional Stokes-Einstein relationship

for a temperature range from -35°C to 90°C., which was later extended [70] to 350°C using data produced by Yoshida et al. [71]. An experimental confirmation of water behaviour was given, in 2009, by Xu et al [72], where diffusion of liquid water molecules was found to follow a fractional Stokes-Einstein relation at about 27°C. They ascribed the breakdown from a Stokes-Einstein to a fractional behaviour to the water local structure: below 27°C water begins to develop a structure similar to the low-density amorphous solid H_2O.

The fractional Stokes-Einstein equation has been found to characterize the diffusion of bovine serum albumin [73] for concentrations up to 15g/dL. The authors attributed the observed behaviour to interparticle interactions taking into account the possibility of mixed stick-slip boundary conditions at the colloid-water interface.

Zwanig and Harrison [74] criticized the use of the fractional Stokes-Einstein equation for molecular fluids on the grounds that molecules cannot be considered hard spheres. Even if they admitted the consistency of the fractional Stokes-Einstein equation with the experimental data, they preferred to explain the deviation from the classical Stokes-Einstein relation as due to a change in the hydrodynamic radius, because of the lack of physical explanation for the use of the fractional Stokes-Einstein equation. Even if they opposed the widespread use of an empirical formula, they admitted that maybe classical hydrodynamics could not work in the first layer of fluid molecules around the particle, so that the diffusion could not be proportional to the first power of viscosity but to fractional one. Some authors proposed the use of a local "microviscosity" to take into account the fractional power of the viscosity,

but Zwanig and Harrison preferred to regard the deviation from the classical model as being due to solute-solvent interaction [74].

As Harris stated [68], the fractional Stokes-Einstein equation is commonly accepted for tracer diffusion and molecular fluids. Hence it is worth investigating the limits between the classical Stokes-Einstein relation and its fractional version and how temperature, viscosity, particle size and other parameters influence a possible transition from the classical to the fractional behaviour.

CHAPTER 3

Particle tracking techniques

3.1 - An overview on the nanoparticles tracking techniques

Single-particle and single-molecule techniques have become essential tools in the last 30 years in many fields, such as physics, biophysics and cell biology [75]. One of the main reasons of the importance of these techniques is that they allow the experimental determination of essential information on particle and molecule dynamics, giving the opportunity to deeply understand classical models or deviations from expected behaviours [76]. Among these new techniques, single-particle tracking (SPT) represents a remarkable tool for the study of dynamics, for instance, in biological processes [77]. There are several techniques to detect and track nanoparticles. It is difficult to select the best method, it is rather more convenient to choose the most suitable technique according, for instance, to the restrictions of the sample or the information required.

In general, video microscopy allows the acquisition of consecutive images by a camera and the observation of the dynamic movement of a particle in time series. The optical density of the material and light scattering were utilized, for instance in biology, to visualize large organelle, such as mitochondria, of the order of some micrometers [78]. Smaller particles or molecules, which are below the diffraction limit of the light, are usually invisible in conventional. Single particles are usually

tracked by attaching them to a larger object, for instance, polystyrene beads with a high index of refraction [79].

Several fluorescence techniques have been proposed to study the motion of molecules and particles, but two of them are more widely used [76]: fluorescence after photobleaching (FRAP), proposed in the 1970s by Axelrod at al [80], and fluorescence fluctuation spectroscopy (FFS), proposed almost at the same time by Magde et al. [81]. If FRAP averages, in time and space, the behaviour of a large number of particles [80], FFS averages the behaviour of a small number of particles in the observed volume [81]. In these techniques the dynamical properties are determined for an ensemble of particles to give an average of the observed behaviour.

Single particle tracking (SPT) methods can provide information not available from techniques which are based on the behaviour of a large ensemble [79]. SPT provides information on the random trajectory of the particle through the coordinates recorded at successive times by the microscope camera. SPT was first applied in biophysics during the 1980s [82-84], but the number of applications has grown significantly and simultaneously with the advances in microscopy which have led to important improvements in the accuracy and speed of SPT methods [76].

The most used methods to individually track fluorescent particles are based on recording images of the sample as a function of time in a widefield, or confocal microscope and then locating the particle of interest in each frame [85]. Standard fluorescence microscopy, used for SPT, showed from the beginning problems related to the excitation which occurs throughout the entire depth of the sample. As

a direct consequence, the fluorescence coming from regions far from the focus increases the background intensity, so that the effective signal-to-noise ratio of single particles at the focal plane decreases, decreasing the sharpness of the particle. The out-of-focus regions are also unnecessarily photobleached and photodamaged. In the single particle tracking, these factors reduce the accuracy of the measurements and the duration of the tracking experiments [76].

With the introduction of the confocal microscopy for SPT, there were serious improvements due to its ability to reject out-of-focus light. The most common set-ups are based on the epi-illumination of the sample with a laser, while the objective collects the emitted fluorescence [86]: the emission passes through the dichroic mirror and then an emission filter is focused, at a certain confocal aperture, exactly at the focus plane of the objective. The emission is detected by photodiode detectors or a photmultiplier tube. In this way, the fluorescence light from the out-of-focus regions is cut-off, avoiding the effects typical of the standard epifluorescence microscopy. In this set-up the fluorescence is collected from a single point in the sample. The reconstruction of the image needs the laser or the sample to be moved to scan the region of interest. In a conventional set-up, the image acquisition is less than 10 frames per second, so that it can be used only in processes where slow dynamics are observed [87].

To observe faster dynamics, modifications of the set-up have been proposed. The spinning-disk confocal microscope is characterized by a rapidly rotating disk where an array of pinholes is used to generate an array of beams that are focused on the sample. Instead of scanning one single point at time, with this configuration is

possible to scan thousands of points at the same time. The acquisition frequency can be increased up to 300 frame per second [88].

For single particle tracking experiments, an alternative to the standard epi-fluorescence microscopy, is total internal reflection fluorescence (TIRF). In the TIRF microscope, the excitation lasers totally reflected and generates an evanescent field that decays exponentially with the distance normal to the surface, reducing significantly the effects of the out-of-focus regions [89, 90].

In the past decades, several techniques, such as super-resolution and far-field microscopy techniques have been developed to overcome the diffraction limit [91-94]. Among these techniques, stimulated emission depletion (STED) generates fluorescent focal spots that are below the diffraction limit, so that particles with a diameter below the diffraction limit can be imaged. Imaging with these techniques usually takes longer than with conventional widefield techniques, so that they can be mainly applied to the study of fixed specimens [95, 96].

In the last few years, non-fluorescent nanoparticles have emerged as an important tool for different kinds of studies, due to their high photostability and low cytotoxicity [97]. The majority of fluorescent particle studies are limited to *in vitro* experiments due to the fluorescent background and problems such as the photobleaching of the fluorophores in the cellular environment [77, 98]. Non-fluorescent particles have a high photostability and they can be localized with high precision compared to fluorescent particles, where problems of localization are common due to the shape of the speckle [77]. Since no fluorophore is required, non-

fluorescent particles are generally nontoxic [97]. For these reasons they are an essential tool for *in vivo* studies [99-102].

Rayleigh scattering is one of the most used approach to detect non-fluorescent particles [97]. In a complex environment, like a cell, the detection of nanoparticles is not easy because the environment is a highly scattering medium due to the presence of different entities with different values of the refractive index [103]. Noble metal nanoparticles are excellent for applications in these cases, due to their large scattering cross sections [104]. Microscopic scattering images can be obtained in the wide-field with a conventional dark-field microscope, in which oblique illumination is applied through a high numerical aperture. Light from Rayleigh scattering is collected with an objective with a smaller numerical aperture. The resulting image shows the scattering particles as bright spots on a dark background [103].

Bright-field microscopy is a simple optical microscopy: light is transmitted through the sample and the contrast is obtained by the absorption of light by the dense areas [105]. The main limit of bright-field microscopy is the low contrast of the image caused by weak absorbing bodies and the low resolution of the out-of-focus areas. Gold nanoparticles have been used, for instance as labels, due to their large absorption and scattering cross sections. With the development of video-enhancement techniques in the 1980's, small nanoparticles (20-40nm) became visible [100].

Non-fluorescent nanoparticles can be detected by taking advantage of the photoinduced change in the refractive index of the environment around the particle

[106]. Metal nanoparticles are good candidates for detection with photothermal effect-based methods. These methods are sensitive to scattering background, making them suitable for studies in live cells [107]. The use of a laser and the need of a scan of the sample, sacrificing temporal resolution, are limits in terms of studies of particle dynamics.

Since the scattering of a nanoparticle decays with the 6th order of the particle dimension [108], the scattering signal disappears quickly as the particle size decreases. The signal can be amplified by interfering the scattering signal with the illumination background:

$$I = |E_i + E_s| = |E_i|\{1 + s^2 - 2\sin\varphi\} \quad (35)$$

where I is the interference signal, E_i and E_s are respectively the amplitudes of the incident light and scattering light; s and φ are the modulus and phase of the complex scattering electronic vector. The three terms on the right side of the equation represent: the background intensity, the scattering signal that is a function of R^6, and the cross term that scales with R^3. As the particle size decreases, the cross term dominates the interference signal, while the scattering term is negligible. The scattering is amplified by superimposing with the incidence beam and the detection of small nanoparticles is improved [109]. Based on this principle, an interferometric optical detection system was developed to detect 5nm gold nanoparticles at the water–glass interface [110]. A laser beam was employed to generate a large scattering signal. This method, combined with fluorescence microscopy, was employed to locate, track and measure the orientation of labelled quantum dot and virus-like nanoparticles on artificial membranes [111].

Light scattering is one of the most commonly used techniques for tracking and sizing particles. Nanoparticles can be characterized by a variety of techniques to obtain different physical quantities, but for a rapid evaluation of the particle size, experiments have mostly been carried out by dynamic light scattering [112].

Three domains of light scattering can be recognized, based on a dimensionless size parameter α, and defined as follows [113]:

$$\alpha = \frac{\pi d}{\lambda} \tag{36}$$

where πd is the circumference of the particle and λ is the wavelength of incident light. We have:

α<<1: Rayleigh scattering, i.e. when the particle is small compared to wavelength of light.

α ~ 1: Mie scattering, i.e. when the particle is about the same size as wavelength of light.

α>>1: Geometric scattering, i.e. when the particle is much larger than wavelength of light.

In a dynamic light scattering system, particles are illuminated with a coherent light source. Dynamic light scattering measures the Brownian motion of the nanoparticles and relates this movement to an equivalent hydrodynamic diameter. It directly measures the time-dependent fluctuations in scattered intensity resulting from the motion of the nanoparticles in the sample [114]. The motion data are simply processed to obtain the size (or size distribution) of the particle [113].

Dynamic light scattering (DLS) methods have been applied to a wide variety of systems, which have led to further developments such as laser Doppler, photon correlation spectroscopy, quasielastic light scattering and laser speckle methods. All these techniques are based on the same kind of phenomena, but look at them from different perspectives [112].

The pattern generated by the scattered light has the general form of irregular bright spots called speckles. These patterns remain unchanged as long as the particles do not change their position. Particle motion naturally leads to the fluctuation of the pattern and to its temporal evolution, since one interference pattern is continuously replaced by another. Looking at a single speckle spot, this evolution is observed as temporal fluctuations of the speckle intensity [113]. The intensity fluctuations are inherently linked to the scattering dynamics and therefore to the particle displacement [112].

The temporal fluctuation is usually analysed through the intensity or photon correlation function. In the time domain the correlation functions decays starting from a zero delay time, and faster dynamics lead to faster decorrelation of the scattered intensity trace. For a single particle scattering, the dynamic information of the particles is derived from an autocorrelation of the intensity trace as follows [113]:

$$g^2(q,t) = \frac{I(t)I(t+\tau)}{I(t)^2} \tag{37}$$

where $g^2(q,t)$ is the second order autocorrelation function of a particular wave vector q and delay time τ, while I is the intensity.

After a short time, the correlation is high because the particles do not have enough time to move far from the initial state they were in. The two signals are thus essentially unchanged when compared after only a very short time interval. As the lag time becomes longer, the correlation decays exponentially, leading to no correlation between the scattered intensity of the initial and final states [114].

If the sample is monodispersed, the decay is a single exponential. In this case the second order autocorrelation function is related to the first order through the Siegert relation as follows [114]:

$$g^2(q,t) = 1 + \beta[g(q,t)] \tag{38}$$

where the parameter β is a correction factor that depends on the geometry of the laser beam.

The first order autocorrelation function, in the simplest case, is a single exponential decay:

$$g(q,t) = e^{-\Gamma\tau} \tag{39}$$

Where Γ is the decay rate [112].

This exponential decay is related to the motion of the particles, specifically to the diffusion coefficient [114]:

$$\Gamma = q^2 D \tag{40}$$

Where D is the translational diffusion coefficient. In dynamic light scattering techniques the diffusion coefficient is often used to calculate the hydrodynamic

radius of a sphere through the Stokes-Einstein equation. The size determined by a dynamic light scattering system is the size of a sphere moving in the same manner of the scattered pattern. So, for instance, the resulting size includes any other molecules, solvent molecules, surfactant layer, that moves with the particle. If the system is monodispersed, there should only be one population, whereas a polydispersed system would show multiple particle populations [115], always assuming the motion of the particle as governed by Stokes-Einstein equation. Dynamic light scattering does not consider possible deviation from the classical Stokes-Einstein equation. Behaviour far from it, such as anomalous diffusion in biological environments, diffusion in polymers or at the glass transition, cannot be analysed in a DLS system.

3.2 - Optical caustics in natural phenomena

Caustics were described and studied for the first time by Hamilton in 1828. His *Theory of Systems of Rays* deals with geometrical optics. The paper consists of three parts, but only the first part was published while Hamilton was still alive. This first part describes the properties of systems of rays subject to reflection and it also discusses caustic curves and surfaces that occur when light rays are reflected from flat or curved mirrors [116].

To understand what a caustic is, let's consider a mirror: the effect of its curvature is to cause the light rays to concentrate in some regions in space and to be absent from others so that, when a flat screen is placed in their path, bright curves and

corresponding dark areas or shadows are observed. A caustic is defined as the envelope of light rays reflected or refracted by a curved surface or object, or the projection of that envelope of rays on another surface [117]; it is a curve or surface to which each of the light rays is tangent, defining a boundary of an envelope of rays as a curve of concentrated light [118]. A common situation where caustics are visible is when light hits a drinking glass (Figure 4). The glass casts a shadow, but also produces a curved region of bright light [119].

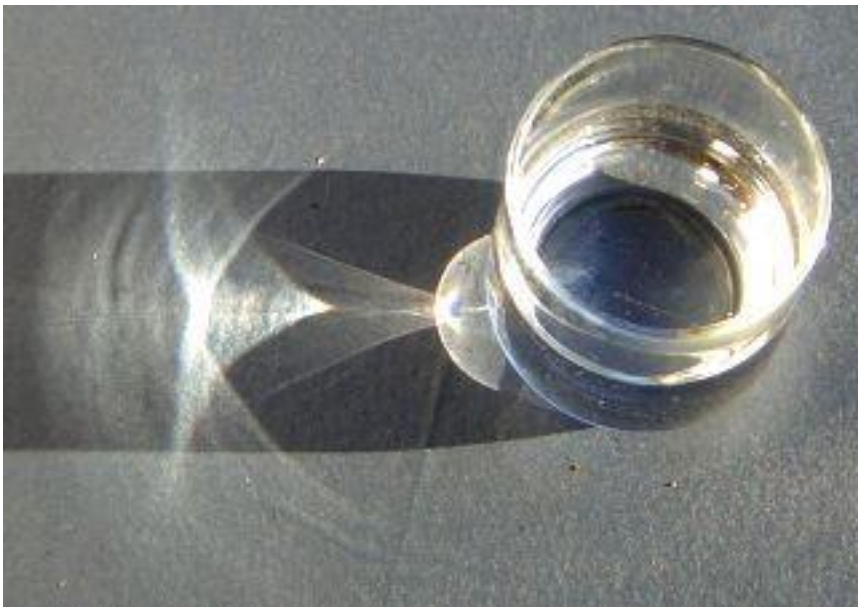

Figure 4 - Caustics produced by a glass of water

Lock and Andrew [117] have explained the formation of caustics occurring in nature, such as in a rainbow: the scattering of light by raindrops causes different wavelengths of light to be refracted into arcs of differing radius, producing, at the end, the bow. Caustics can be found in everyday life, for example in the bottom of a coffee cup or inside a wedding band.

3.3 - Caustics in engineering

Caustics have been used in engineering both in reflection and transmission mode [120, 121] to evaluate the stress distributions, for instance associated with the tips of propagating cracks, to the contact between components and other kind of singular stresses. The method was introduced by Manogg [120] for investigating crack tip stress intensities and it was later extended to investigate other kind of stress singularities. Stresses alter the optical properties of a solid both through the effects of compression/expansion and through changes in the refractive index. When a flat surface is illuminated by a parallel incident light beam, the parts not subject to stress are traversed by light rays, which are not deflected in this case. The stressed areas induce deflections of the light beams that are passing on the surface. In this second scenario the light distribution of the investigated surface is no longer uniform [121].

Experimentally, the required apparatus to generate caustic images includes: an incident beam with the desired characteristics, obtained with a collimating system, and instrumentation for detecting the caustic [121]. The incident beam is required to be spatially and temporally coherent. Spatial coherence can be achieved by generating light from a point light source. Temporal coherence is obtained using a monochromatic source. If both conditions are not fulfilled, the pattern appears unclear or unfocused so that the boundary between the region of shadow and bright illumination is not more represented by a distinct line. However, the quality and sharpness of the caustic increases with the degree of collimation of the light beam [122]. Imaging is usually carried out by a single-standard lens, forming the image directly on the microchip of a CCD camera. These engineering methods measure

characteristics of the caustic curves, which are many times larger than the local deformation of the material due to the stress in the region of interest. The size and shape of the caustic are used, together with the parameters of the optical setup, to study the shape of the localized deformation [121].

Caustics are also observed in astronomy where in gravitomagnetism of supermassive black holes, where radiation is deflected from its path leading to the formation of caustics that are used to investigate the black hole [123, 124].

Kanaka et al [125] studied the formation of caustics in a scanning electron microscope. In this case the theoretical prediction of the caustic shape agreed with their experimental observations when they defocused the microscope slightly. They also found that gold coated spheres produced caustics that were similar in shape to those generated by microholes of few microns in diameter. In their work the caustics represented obstructions in viewing the real shape of integrated circuit specimens and consequently recommendations were made for compensation of third and second order astigmatism to remove them.

3.4 - The formation of caustics in an inverted optical microscope

Patterson and Whelan [126] used the caustic method in the detection of nanoparticles, and used a large caustic to identify small particles. In this case the caustic is used to locate and track the nanoparticles. A similar approach was proposed by Wang [127], who observed the diffraction patterns generated by adjacent ‘optically bound’ particles without using a microscope objective lens.

Wang's work allowed the study of the dynamic motion of an assembly of 70 microspheres of nominal diameter 2 μm [128], using a larger field of view than it is possible to obtain in a conventional high-powered microscope.

Patterson and Whelan [126] started from the consideration that a transparent sphere behaves in a similar manner to a circular aperture, and in the same way it generates a central intense spot, or Airy's disc, surrounded by a series of concentric and much fainter diffraction rings when illuminated with light from a point source [129]. At, or beyond the diffraction limit, i.e. when the diameter of the particle is less than the wavelength of the light, only the Airy's disc is observed. Using this phenomenon, Fedosov et al [130] were able to track 40 nm gold nanospheres using the 1.5 μm bright spot generated by illuminating the nanoparticles with a red laser beam and viewing them with a 40x objective.

Caustics and diffraction patterns often occur at the same time (Figure 5), but the latter show an intensity which varies with distance from the intense spot, as a sine wave of decreasing amplitude, resulting in alterning dark and bright rings of decreasing intensity [126].

Patterson and Whelan [126], using a conventional optical microscope were able to detect and track nanospheres an order of magnitude smaller than those studied by Wang and co-workers [127, 128]. They increased both the spatial coherence by closing the aperture to a minimum and the temporal coherence by including a monochromatic filter, and they were able to generate caustics from the interaction of the light beam and the nanoparticles [126].

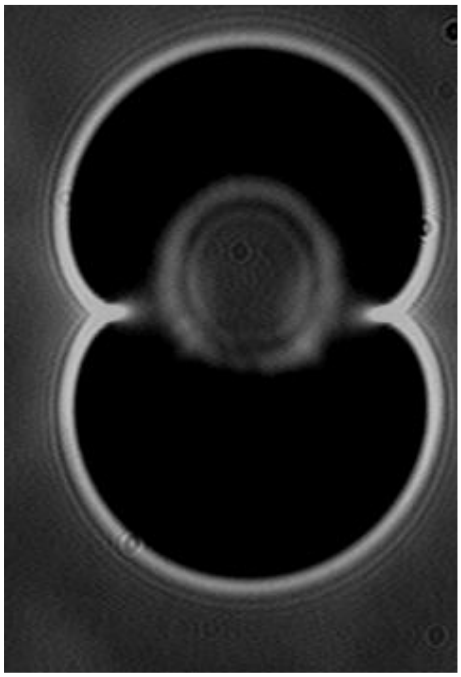

Figure 5 - Caustic formed by light passing through a hole of 4 mm [121]

3.5 - Particle tracking using caustics

Patterson and Whelan [126] demonstrated the formation of caustics in a microscope firstly imaging polystyrene spheres of nominal diameter 30 μm (Figure 6). A conventional microscope, with some simple adjustment, was used in transmission imaging mode. They equipped it with a 100 W halogen lamp, a condenser lens-assembly and a range of objective lenses for imaging at different magnifications. The lamp housing incorporated a weak diffuser, a green interference filter (centred on 550 nm, 45 nm bandwidth) and an adjustable field aperture that could be closed down to a minimum of 1 mm diameter, to increase the spatial coherence of light. A high resolution monochrome CCD camera was employed to record images and videos of the nanoparticles. The field aperture in the lamp housing was left fully

open and the height of the condenser was adjusted to have Kohler illumination [131]. The lamp power was increased to compensate for the lower light level due to the small field aperture.

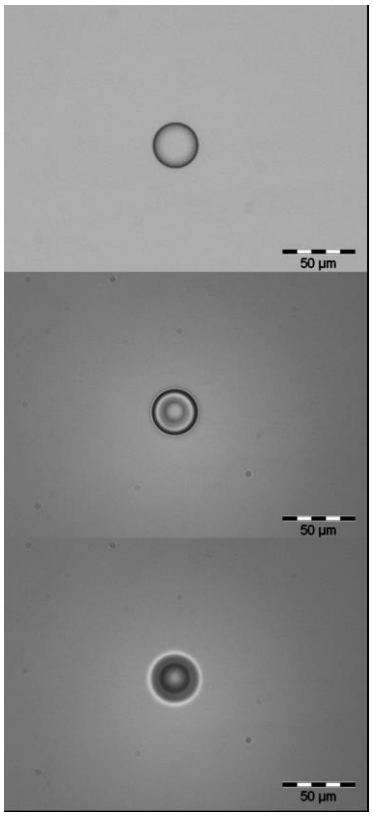

Figure 6 - Polystyrene sphere of 30 µm diameter dispersed in pure glycerol imaged with a conventional optical microscope [126]

With these settings a caustic pattern consisting of bright and dark concentric rings was generated. Moving the objective by few microns, the image was slightly defocused, to obtain a larger caustic with a bigger diameter and contrast.

The experiment was then repeated with much smaller particles, specifically silica nanoparticles of nominal diameter from 300nm to 50nm suspended in glycerol. In these cases the particles had a diameter of the order of, or less than half, the

wavelength of the light ($\lambda/2$ = 275 nm) employed and so theoretically they could not be resolved in a conventional microscope with a conventional set-up. Moving the objective in equal increments along the light path it was possible to collect a z-stack of images and demonstrate the difference in size (Figure 7).

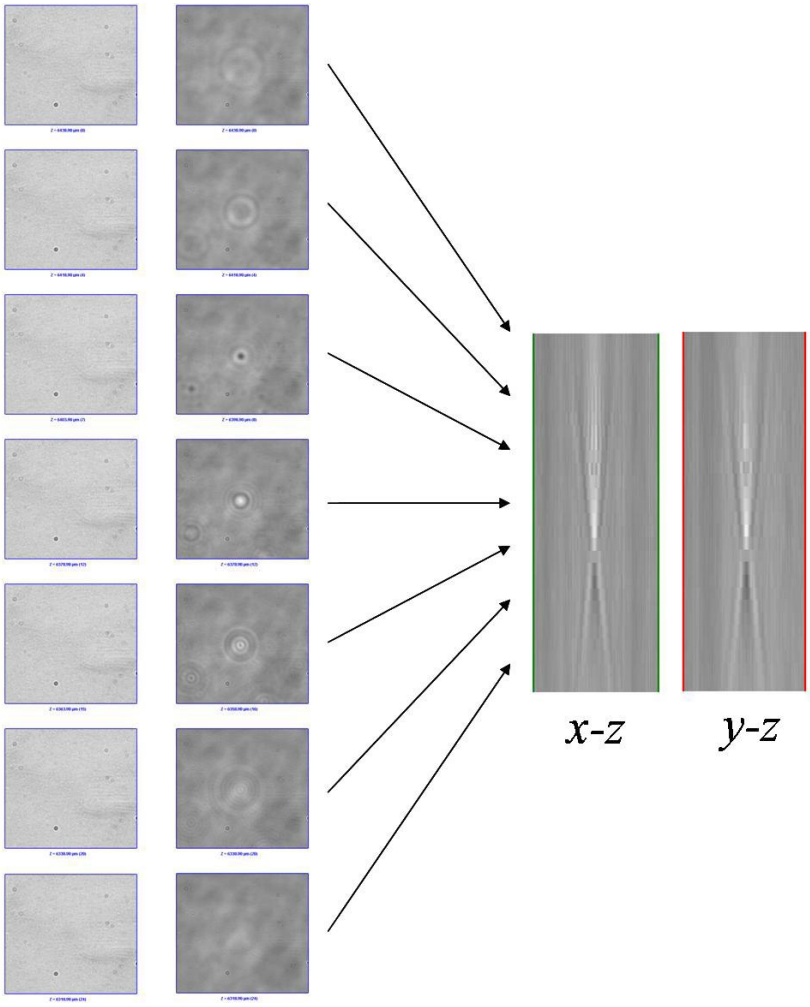

Figure 7 - A z-stack of images at 40 μm intervals with the field aperture opened to its maximum (left), and closed to its minimum (centre) [126]

The caustics produce a magnification of a hundred to a thousand times the particle size (Figure 8) making it possible to track their location and movement, considering the centre of the caustic as the centre of the nanoparticle.

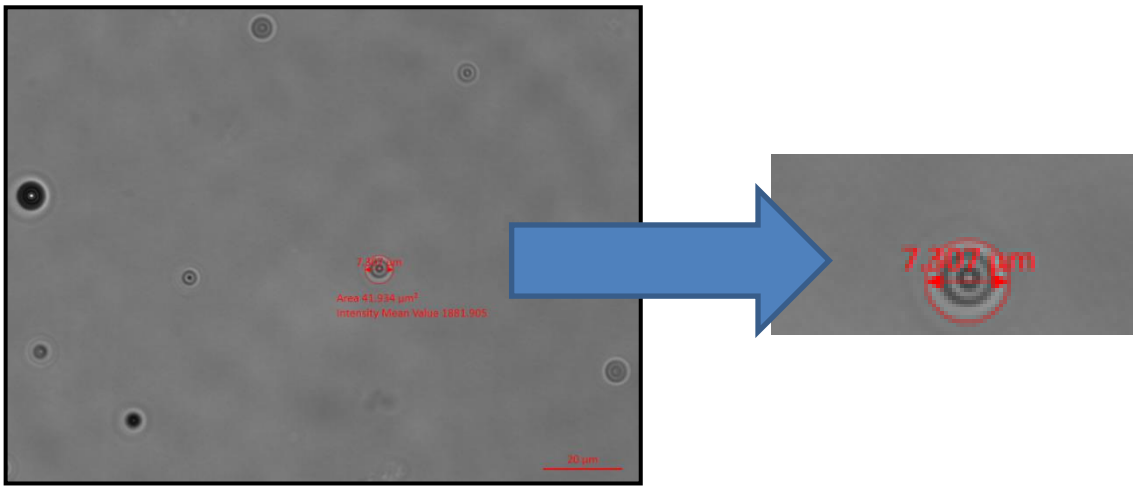

Figure 8 - An 11nm gold nanoparticle (Mintek) generates a caustic of more than 7 micrometers

CHAPTER 4

Materials and Methods

4.1 - Materials

4.1.1 – Gold and polystyrene nanoparticles

Unconjugated gold spherical nanoparticles (BBI solutions OEM Limited) were purchased in monodisperse solution that were supplied in water, having trace amounts of citrate, tannic acid and potassium carbonate as chemical residuals of the manufacture process. The gold nanoparticles were chosen in a range of sizes from 10nm to 150nm diameter (precisely 10nm, 20nm, 30nm, 50nm, 80nm and 150nm).

The standard deviation of the nanoparticle diameter varied with the size, since their production becomes more difficult when the size decreases. So, for the 10nm gold nanoparticles the standard deviation was 10% of the nominal diameter (±1nm) and it decreased to the 8% of the nominal diameter for the 150nm gold nanoparticles (±12nm).

The mass of gold per millilitre was approximatively the same over the whole range of sizes (from 5.76×10^{-5}g for the 10nm dispersion to 5.66×10^{-5}g for the 150nm dispersion). The different size of the particle, but almost the same mass of gold, leads obviously to a different number of particles per millilitre in the monodisperse solutions: for the 10nm gold there were 5×10^{13} particles/ml and for the 150nm gold the number of particles per millilitre decreased to 1.66×10^{9}.

Images of 20, 80 and 150nm diameter gold nanoparticles captured with a transmission electron microscope (Tecnai G2, Fei) confirmed the size and spherical shape of the commercial gold, as shown in Figure 9a-b-c. To prepare the sample for the TEM observation, solutions of gold nanoparticles, at the supplied concentrations, were incubated and then air-dried onto copper grids for 5 minutes; the grids were air dried after the excess gold was removed with a filter paper.

Uniform spherical polystyrene nanoparticles (Magsphere Inc.) were purchased, as for the gold nanoparticles, in monodisperse solutions and supplied already dispersed in water, in a range from 20nm to 500nm diameter (precisely 20, 30, 50, 60, 80, 150, 300 and 500nm).

The standard deviation of the diameter of the polystyrene nanoparticles varied, as for the gold, with size so that for the smallest of the range, 20nm, the standard deviation is 27% of the nominal diameter (±5.4nm), while for the biggest particles in the purchased range, 500nm, the standard deviation is the 9% (±45nm).

TEM images of 20nm, 150nm and 300nm polystyrene nanoparticles were recorded, as for the gold nanoparticles, to confirm their size and shape, as shown in Figure 9.d–e–f. The polystyrene nanoparticles were prepared for the TEM analysis in a similar manner as for the gold nanoparticles, and then stained with aqueous 3% Uranyl Acetate for 30 seconds before drying.

Both gold and polystyrene nanoparticles were observed in the transmission electron microscope at 120kV.

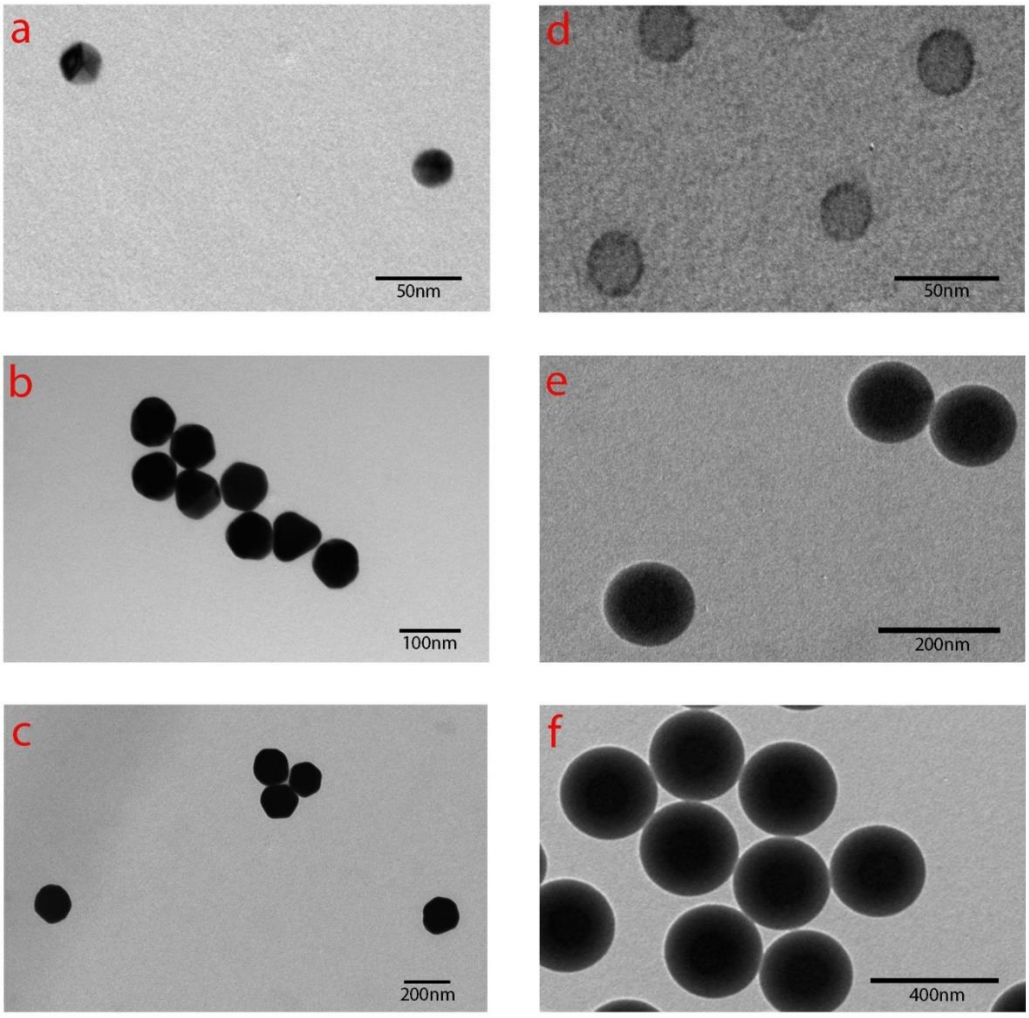

Figure 9 - 20, 80 and 150nm gold particles (A, B and C respectively) and 20, 150 and 300nm polystyrene particles (D, E and F respectively) observed in a transmission electron microscope (Tecnai G2, Fei) at 120kV.

Since all these nanoparticles were stabilized with surfactant, which might influence their behaviour, some surfactant-free polystyrene nanoparticles was tested, to look for possible effects of the stabilizing agent on the particle dynamics. Surfactant can be responsible of change in the shape and size of the nanoparticles, depending on the type of surfactant used during their synthesis and the choice of the temperature too [132]. TEM images confirmed the spherical shape and the size of the

nanoparticle used to perform experiments. Free-surfactant uniform polystyrene nanoparticles (Magsphere Inc.) were purchased with nominal diameters of 60nm and 80nm. Surfactant is usually used as a stabilizer to avoid the aggregation due to the van der Waals forces, but it cannot be employed in biomedical applications [133].

4.1.2 – Base fluids

In order to explore the effect of viscosity on the nanoparticle dynamics, distilled water and different concentrations of glycerol mixed with distilled water were used as the base fluid.

The choice of distilled water was due to the fact that the commercial solutions were already supplied in water. Moreover, the dilution of the population of nanoparticles in the samples, to improve the conditions for the observation, was easier when performed in water or in fluids which were completely miscible with water. Indeed dilution was necessary since the observation of caustics is improved when the field of view is not overwhelmed by nanoparticles, since the generated caustics do not interfere with each other and the background noise is reduced.

Distilled water was provided by a purifier system (Purelab Option-Q, Elga Veolia) at 12MΩ/cm to have a very pure water.

Glycerol was commercially purchased (Fisher Scientific) and was added to distilled water to obtain three mixtures. The three solutions were characterized by different

volume fractions of glycerol in distilled water, i.e. 20%, 50% and 90%, which yielded values from 0.0008Pa·s for distilled water to 0.15Pa·s for a 9:1 mixture of glycerol and water, i.e. a range of three orders of magnitude. The choice of glycerol was due to its complete solubility in water via the formation of hydrogen bonding.

4.2 – Single nanoparticle tracking using caustics

4.2.1 – Experimental setup

Gold nanoparticles were supplied in vials at very high concentrations that varied from 10^9 particles/ml for the 150nm diameter particles to 10^{12} particles/ml for the 10nm diameter particles. The concentrations were reduced substantially by adding the concentrate, which consisted of nanoparticles dispersed in water, to water-glycerol mixtures or water, as appropriate to obtain concentrations of 5×10^{-3}, 5×10^{-5} and 5×10^{-6}mg/ml, which corresponded to 10^{11}, 10^9 and 10^8 particles/ml respectively for the 10nm diameter particles. To obtain the desired concentrations, 100µl were firstly extracted with a pipette (50-1000µl, Fisherbrand) from the commercial vial and added to a 900µl of distilled water. A mixer (Vortex-Genie 2 G560E, Scientific Industries Inc.) was used, for about 2 minutes, to create a uniform distribution of the nanoparticles. Afterwards, an ultrasonic bath (U50, Ultrawave) was employed, for 15 minutes, to avoid aggregation. The choice of an ultrasonic bath instead of an ultrasonic tip was due to a common problem related to the latter, i.e. the release of material by the ultrasonic probe with the consequent, possible, contamination of the sample. The procedure for the preparation of the nanoparticles

samples was tested and suggested by researchers of the Toxicology Unit of the Joint Research Centre (JRC) of the European Union. Following their protocol it was possible to reach a uniform distribution of the nanoparticle dispersions.

Further dilutions were performed to obtain less concentrate solutions: the procedure was repeated three times, extracting 100µl from the obtained diluted vial and adding to another one containing 900µl of distilled water. In this way, every dilution lead to a decrease in the nanoparticle population of one order of magnitude.

A similar procedure was applied when nanoparticles were dispersed in a glycerol-water mixture. Nanoparticles were, again, extracted with a pipette from the commercial vial and then added to the right amount of distilled water and glycerol to maintain the desired percentage of water and glycerol in the mixture. The vortex generator was again used to obtain a uniform distribution and moreover to mix homogenously the distilled water and the glycerol. The ultrasonic bath, when the glycerol-water mixtures were under investigation, was employed again for 15 minutes to avoid nanoparticle aggregation.

Each resultant solution was placed on a glass microscope slide (Marienfeld GmbH) that had a central circular cavity of depth 0.8mm and radius 7.5mm. The cavity was filled with 70µl of nanoparticles solution and then covered by a 0.16mm coverslip (Thermo Fisher Scientific Gerhard Menzel B.V. & Co.). After these simple operations, the slide was placed on the microscope stage.

Experiments to visualize, through the formation of caustics, and measure the diffusion of gold and polystyrene nanoparticles, were performed following the

approach proposed by Patterson and Whelan [126]. The measurements were made in a standard inverted optical microscope (Axio Observer.Z1m, Carl Zeiss) which was mounted on an anti-vibration feet (VIBe, Newport) to isolate the sample from the environment: this steel platform helped to prevent noise due to mechanical vibrations which could affect the Brownian motion measurements (Figure 11).

To start the experiments, the sample was firstly placed on the microscope stage. A constant temperature was achieved using a heated microscope stage (Heatable universal mounting frame KH S1, Pecon GmbH) connected to a temperature controller (Tempcontroller 2000-2, Pecon GmbH). The temperature controller allowed the stage to be regulated in a range of 20-60°C. The sample was maintained at a constant temperature, T=30°C, isolating it from variations in the environment. Before beginning each experiment, the stage was allowed to reach a uniform temperature of 30°C. The choice of T=30°C was to avoid influence from variation of the room temperature over the year and to have a value close to the temperature of biological organisms, but was also to avoid the generation of convection current. Indeed performing experiments at higher temperatures, it was not possible to observe the random motion of the nanoparticles for every size, material or base fluid investigated. In this case, the nanospheres were completely driven by the current. When the temperature controller was set at 40°C, convection current occurred, making impossible the observation of the Brownian motion and consequently the measurement of the nanoparticles diffusion. Further confirmation of the presence of convection current came from experiments performed at 50°C and 60°C, where

again it was impossible to observe Brownian motion, but only the convection current and the nanoparticles flowing with it.

For further confirmation of the temperature value along the stage, two thermocouples (Self-Adhesive Silicone Patch Thermocouples type k, Omega Engineering Inc.) were used for a continuous check.

Each of them, as shown in Figure 11, was connected to a multimeter (Handheld Thermocouple Thermometers, Omega Engineering Inc.), where the measured temperature was displayed.

Figure 11 – The standard inverted optical microscope in which all the experiments were performed.

After 10 minutes the sample was placed on the microscope stage, the experiment started. This ensured the same temperature between the apparatus and the solution when the diffusion measurements on the nanoparticles started.

The experiments to visualize, through the formation of caustics, and measure the diffusion of gold and polystyrene nanoparticles, were performed following the approach proposed by Patterson and Whelan [126]. The microscope setup of the previous work was reproduced (Figure 12)

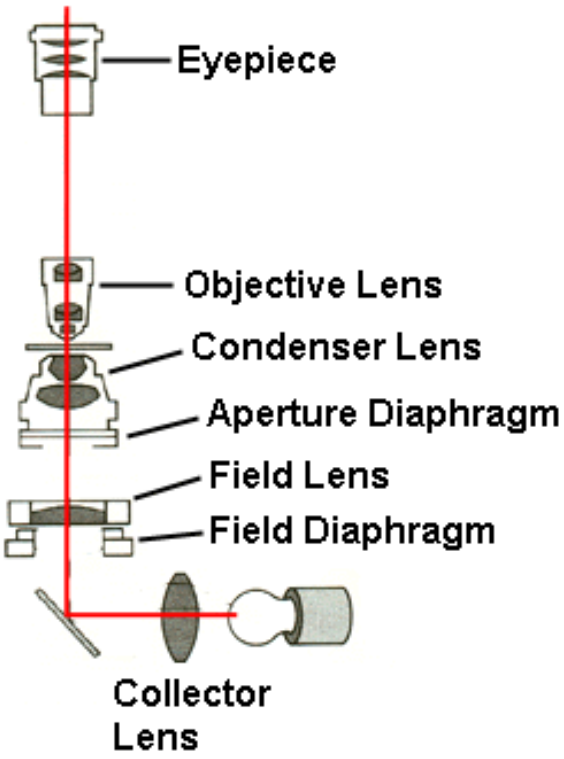

Figure 12 – Scheme of a classical inverted optical microscope.

The microscope was equipped with a range of objectives for different magnifications, from 10x to a 100x oil immerged (EC Plan-Neofluar, Zeiss). The light source (100W halogen lamp) and condenser lens were set-up for Kohler illumination. Then a narrowband filter (Olympus model 43IF550W45, centered on 550 nm, 45 nm bandwidth) was inserted in the light path, in order to improve the

coherence of the light. The condenser aperture was closed to leave only a pin-hole through which light was transmitted, to increase its spatial and temporal coherence. A monochrome high-speed camera (Fastcam mini UX100, Photron) was also employed to reach higher frame rate. The camera was connected to the microscope through a side port.

4.2.2 – Nanoparticles imaging in two-dimensions

Images were captured by the AxioCam ICm 1 camera coupled to the camera port on the microscope. The AxioCam ICm 1 (maximum resolution 1388x1038) allowed a frame rate of ~30frames/second (fps), while the high speed camera was able of up to 6400fps at high definition (1280x720 pixels). At this high frame rate it was not possible to image the caustics. The limit, using a high speed camera, to image the caustics, was observed to be 500fps. At this frame rate, nanoparticles could be observed and the diffusion measurements compared with the results obtained at ~30fps with the AxioCam ICm 1. Michalet has discussed that, in theory, a higher frame rate could improve the accuracy of diffusion measurements [134], but in practice it was found no significant difference between diffusion coefficients based on data captured at 28 fps and 500fps, e.g. D=4.13×10^{-13}±1.6 ×10^{-13}m^2 s^{-1} and D=4.26×10^{-13}±0.11 ×10^{-13}m^2 s^{-1} respectively, for 20nm diameter polystyrene particles in water. At the lower frame rate, the caustics were better defined which supported a more robust analysis, while at the higher frame rate the illumination level was low enough to cause some loss of details.

When tracking was performed with a 40x objective, with the 10x fixed output magnification at the camera port, each pixel corresponded to approximately 0.116µm^2 on the object plane, using the AxioCam ICm 1.

The Zen software suite from Zeiss was used to control the microscope and acquire videos (Figure 13).

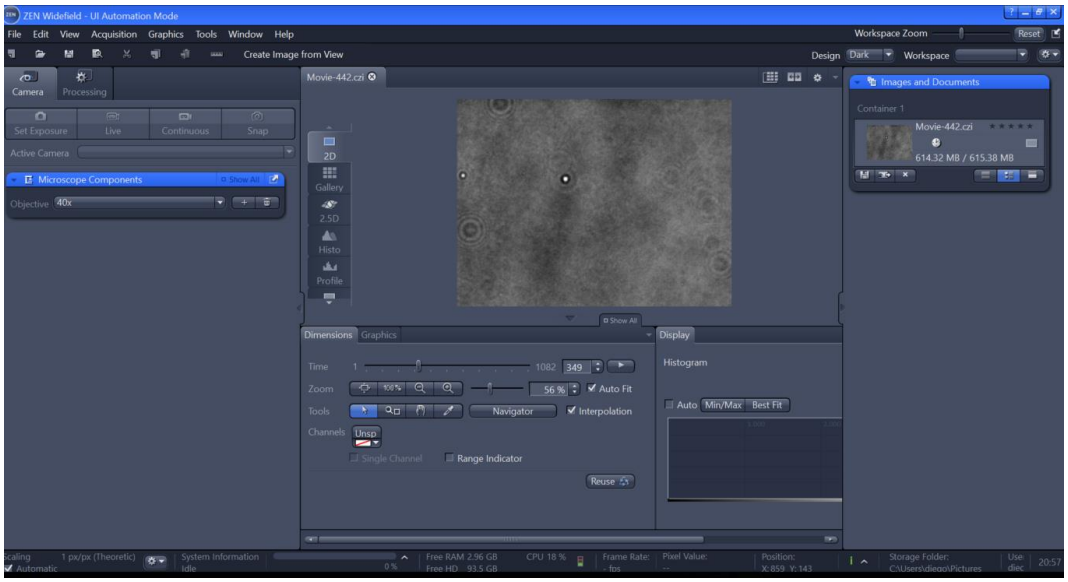

Figure 13 – The Zen software by Zeiss.

The Zeiss suite allowed control of the microscope settings from a software interface, which avoided contact with the microscope during the experiments. Once the video started about 1000 frames, at ~30fps, were recorded to observe the motion of the nanoparticles for at least about 30seconds.

An individual nanoparticle was represented by a single Airy's disk surrounded by rings which became fainter far from the centre (Figure 14).

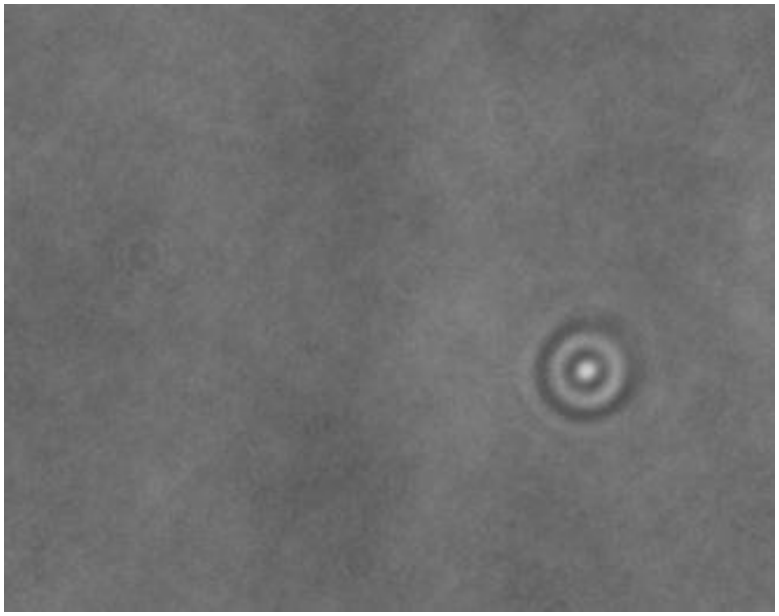

Figure 14 – 10nm gold particle dispersed in water represented by a central intense spot surrounded by fainter rings

When the particles aggregated, the caustic changed shape from a simple circular shape to a set of overlapping circular shapes (Figure 15) so that it was straightforward to ensure single particles were being tracked. Only caustics which were clearly identifiable as a single pattern were analysed.

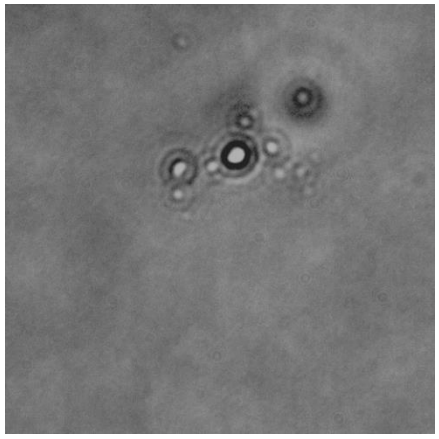

Figure 15 – Nanoparticle aggregation is characterized by a different shape of the caustic than a single nanoparticle.

4.2.3 – Video analysis by 2D tracking software

Once the video was acquired and saved, it was analysed using 2D tracking software (StAT St Andrews Tracker) developed by Milne [135]. The videos were processed using this specially-written software based on feature-matching routines (LabVIEW NI IMAQ Vision, National Instruments). This program allowed the frame-by-frame in-plane co-ordinates of an individual particle to be obtained from the image of the caustic.

LabVIEW is a graphical software development system that can be supplemented by image acquisition and processing add-ons. It includes a wide variety of image analysis virtual instruments (or VIs), including a number of pattern recognition algorithms. The LabVIEW feature-matching algorithms constituted the core of this tracking software.

The software can read video files or image sequences (Figure 16).

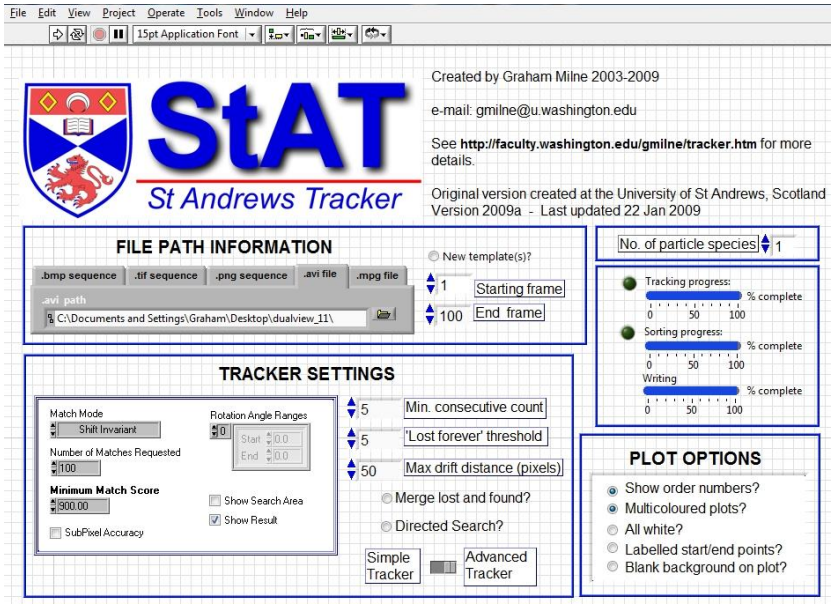

Figure 16 – The user friendly interface of the StaT software for particle tracking.

Once the video source file was selected and the program was started, a box around the particle of interest was drawn (Figure 17).

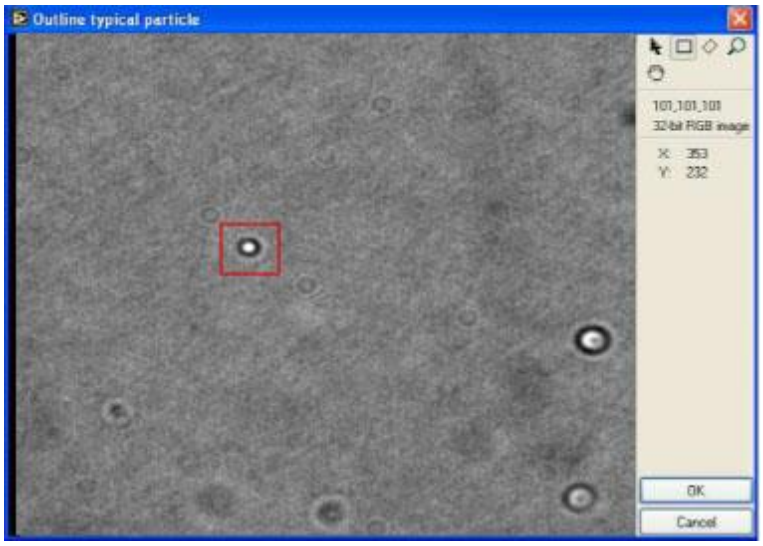

Figure 17 – A box was drawn around the selected particle before the tracking.

Conventional pattern-matching approaches can be computationally heavy. The feature-matching routines was designed to reduce the computation time. This was achieved by introducing a "learning phase" where the image was examined to identify features that could be used to reduce the number of calculations [135]. During the learning phase pixels in the template images were sampled in a random way. The sampled pixels were then tested for stability, which means examining the uniformity of their closest pixels in the image. This method reduced the computation time when compared to standard methods, which would have had to perform analysis for every single pixel in an image.

The program could run in two modes: simple tracker or advanced mode. The first one used the same user-defined templates throughout the entire image sequence.

This was ideal when spherical particles are under investigation, which retain the same appearance, assuming that lighting conditions and the depth of the particles with respect to the focal plane of the microscope objective do not change appreciably over the course of the experiment. The second mode took account of non-spherical shapes, which can occur, for instance, in a biological media. Moreover when running StAT in simple tracker mode, this could present problems, as the program lost the particles when they moved out of focus. If the out-of-plane drift was sufficiently slow, the advanced tracker could deal with the change and the particles could be continuously tracked. For this reason the second mode was preferred to the first one, even if the particle shape was spherical. Anyway, running the tracker in advanced mode presented a problem: the software was much slower, because the program had to "learn" new templates every time they were updated. The videos were not processed in real time, so that the processing time did not influence the outcome. In this advanced mode, the change of size of the caustic was taken into consideration by the program.

Once tracking was completed, the frame by frame particle coordinates were written on a hard disk as a sequence of tab-delimited text files. The single particle coordinates were then used to study the particle motion and its characteristics.

4.3 –Nanoparticle Tracking Analysis (NTA)

4.3.1 – The Nanosight System

Nanoparticle Tracking Analysis (NTA) is a relatively recent technique for nanoparticle sizing. The technique analyses simultaneously the nanoparticles in the field of view, giving the opportunity to investigate polydisperse systems ranging from 10-20nm up to 1-2µm [136].

NTA utilizes the properties of both light scattering and Brownian motion in order to obtain particle size distributions in liquid suspension. A laser beam is passed, through a prism edged glass flat, over a metallized surface within the sample chamber, where the nanoparticle solution is contained (Figure 18).

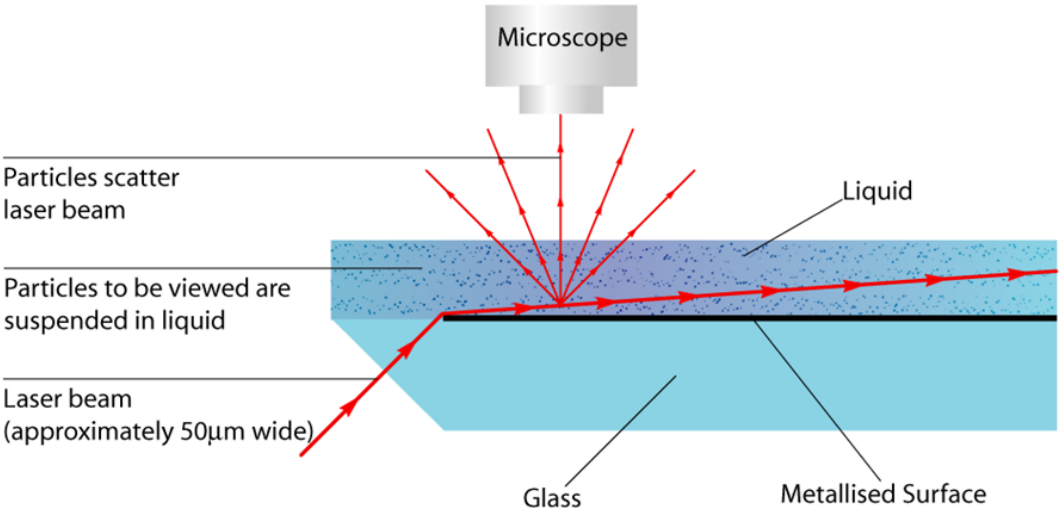

Figure 18 – Scheme of the nanosight system [134].

Particles in the liquid sample which pass through the beam path are observed in the microscope as small white speckles moving under Brownian motion.

The angle of incidence, and refractive index of the glass flat, are designed so that when the laser comes out in the solution, the beam interacts with the particles in suspension.

4.3.2 – Setup

A Nanosight system (Nanosight LM10, Malvern Instruments Ltd) was used to test gold particles with nominal diameters of 20nm, 80nm and 150nm (Figure 19). The system included a small aluminium housing (92x66x47mm) containing a solid-state, single mode laser diode (<20mW, 655nm) configured to generate a focused beam through the 500µl sample chamber. The base of the chamber included a metallised optical flat above which the beam is caused to propagate in close proximity to the metal film. The sample is simply introduced into the chamber using a syringe via the Luer fittings (Figure 20).

The temperature in the chamber was constantly checked by a probe connected to a multimeter.

The particles scattered light so that they could be easily visualized even with a relatively low magnification (x20) microscope objective fitted to a conventional optical microscope. A CCD camera was mounted at the top of the apparatus, operating at 30 frames per second (fps). The camera captured a video file of particles moving under Brownian motion.

Figure 19 – The Nanosight system LM10.

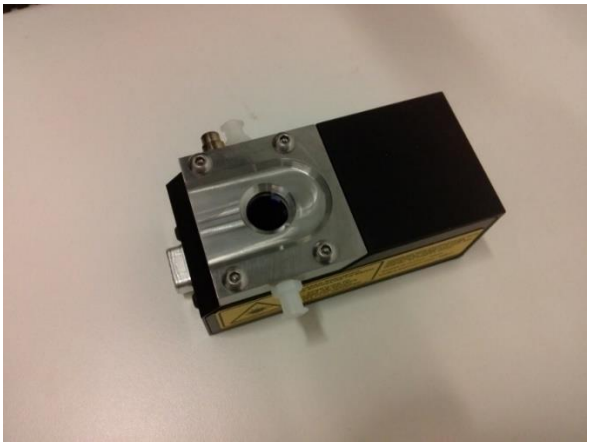

Figure 20 - Aluminium housing where the solution is inserted through the Luer fitting.

4.3.3 – Video analysis

The Nanosight system camera generated videos of a population of nanoparticles moving under Brownian motion in a liquid when illuminated by a laser (Figure 21). The NTA software recorded a video file (typically 30-60 seconds) of the particles and then simultaneously identifies and tracks the centre of each particle on a frame-by-frame basis. The software then determined the mean square displacement of each particle in the x and y directions. The mean square displacements allowed the diffusion coefficient to be experimentally determined and from which, if the temperature T and solvent viscosity η are known, the hydrodynamic diameter of the particles can be calculated using the Stokes-Einstein equation. The software gave information about the particles size and an estimate of the sample concentration by counting the particles in the field of view and considering the volume inside the aluminium housing.

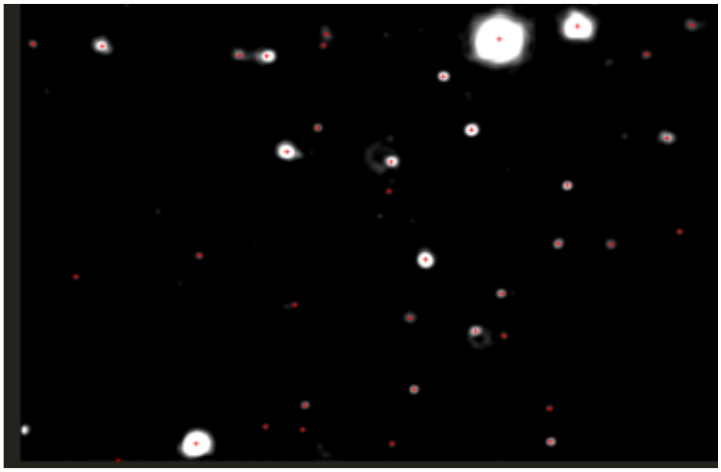

Figure 21 – NTA captures a video of particles under Brownian motion.

CHAPTER 5

Results

5.1 – Simple diffusion of nanoparticles dispersed in simple fluids

Experiments were performed on nanoparticles dispersed in two simple fluids: distilled water and glycerol-water mixtures, adding different concentrations of glycerol to distilled water, to reach different values of viscosities. The target of each experiment was to acquire information on the nanoparticles motion through the acquisition of the frame-by-frame coordinates.

A particle under Brownian motion generates a path of arbitrary movements. From the plot in Figure 22 it is possible to clearly observe the random trajectory of the particle motion.

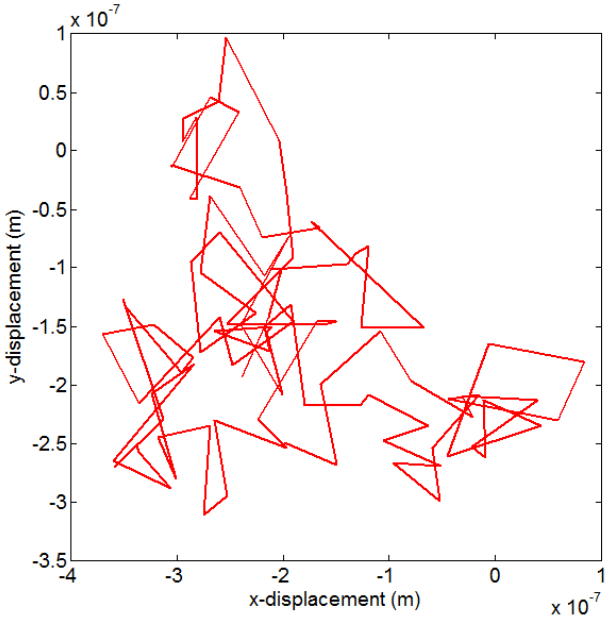

Figure 22 - Typical trajectory of a single particle under Brownian motion (10nm gold particle dispersed in water).

The most common way to analyse particles trajectories is to characterize them through the mean square displacement (MSD). Experimentally, the MSD of a particle is obtained by considering points separated by a fixed lag time Δt, acquiring the position x_i and y_i for each point. The time lag between two consecutive points is imposed by the frame rate of the camera. For every time interval Δt, the displacement on the x and y direction is calculated as follows:

$$x_i = x_i(t), \qquad x_{i+1} = x_{i+1}(t), \qquad \Delta x_i(\Delta t) = x_{i+1} - x_i$$

$$y_i = y_i(t), \qquad y_{i+1} = y_{i+1}(t), \qquad \Delta y_i(\Delta t) = y_{i+1} - y_i \qquad (41)$$

The square displacement for the i[th] time step is the sum of the displacements on each axis:

$$(\Delta r_i(\Delta t))^2 = (\Delta x_i(\Delta t))^2 + (\Delta y_i(\Delta t))^2 \qquad (42)$$

The mean square displacement is obtained as an average of all time steps:

$$MSD_n = \frac{1}{N-n}\sum_{i=0}^{N-n}((x_{i+n} - x_i)^2 + (y_{i+n} - y_i)^2) \qquad (43)$$

Equation (43) is the formula in two dimensions derived from the general equation (27). The mean square displacement can be plotted as a function of its corresponding time step intervals, giving characteristic curves: if the analysed diffusion is of isotropic nature then one would expect the MSD to be a linear function of time. The mean square displacement of gold and polystyrene nanoparticles under investigation was plotted to study their motion when the particles move in an isotropic fluid, such as water and glycerol-water mixtures.

Figure 23 shows the mean square displacement of a 50nm gold particle moving in water, i.e. in a liquid with viscosity of 0.0008Pa·s at 30°C, when the concentration of particles is 5×10^{-6}mg/ml. In Figure 24, the mean square displacement of the same nanoparticle, at the same concentration, is plotted when the particle moves in a mixture with 20% of glycerol and 80% of water, i.e. a viscosity of 0,0015Pa·s. In both figures, it is clear the linear trend of the growing mean square displacement with time.

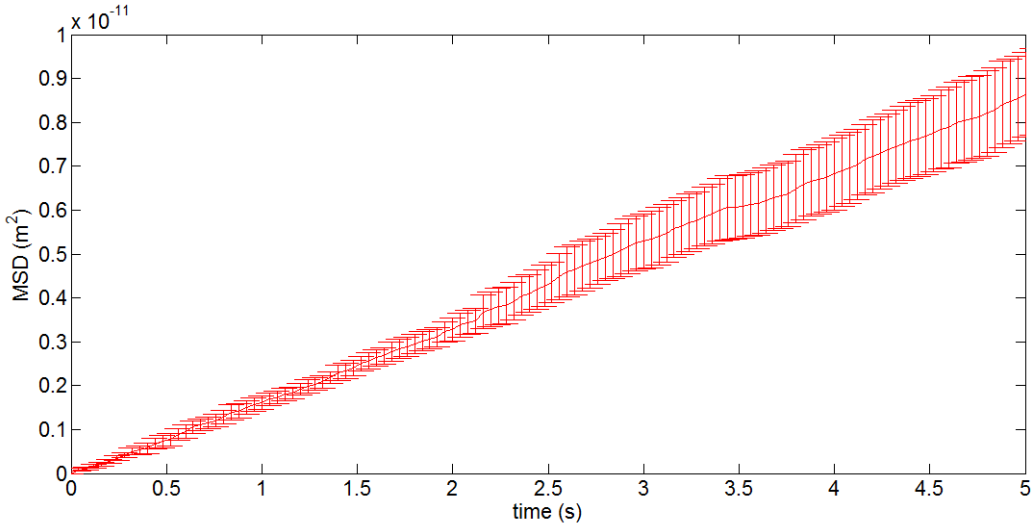

Figure 23 - MSD of a 50nm gold particle in water at $5x10^{-6}$mg/ml. Six measurements performed by single nanoparticle tracking on different nanoparticles from the same sample.

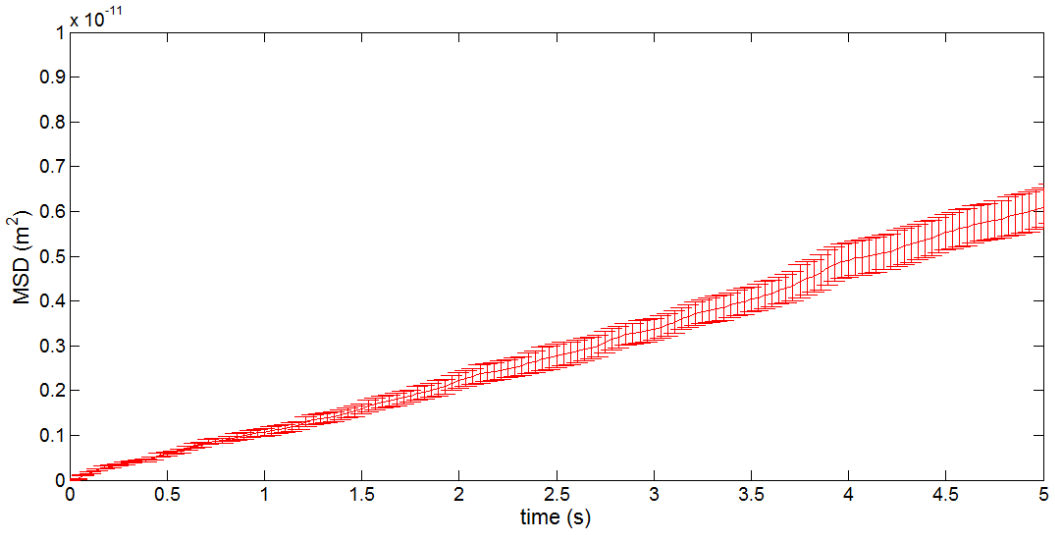

Figure 24 - MSD of a 50nm gold particle in a mixture (20% of glycerol) at $5x10^{-6}$mg/ml. Six measurements performed by single nanoparticle tracking on different nanoparticles from the same sample.

The addition of glycerol to water led to an increase in viscosity and a consequent decrease in the diffusion of the particle, as the Stokes-Einstein relation predicts. Considering the Einstein equation (23), the mean square displacement is linearly related to the time with diffusion representing the slope of the linear trend. Looking to Figure 23 and 24, it is possible to notice the decrease in diffusion due to the higher viscosity, as predicted by the Stoke-Einstein relation (25).

To appreciate the linear trend in Figure 25 and Figure 26, a change of scale on the y-axis, representing the mean square displacement, was necessary compared to Figure 23-24. The increase in viscosity, due to a higher percentage of glycerol, caused a further decrease in diffusion, as can be noticed by the order of magnitude of the mean square displacement on the y-axis. Figure 25 shows the mean square displacement of a 50nm particle in a glycerol-water mixture with 50% glycerol, i.e.

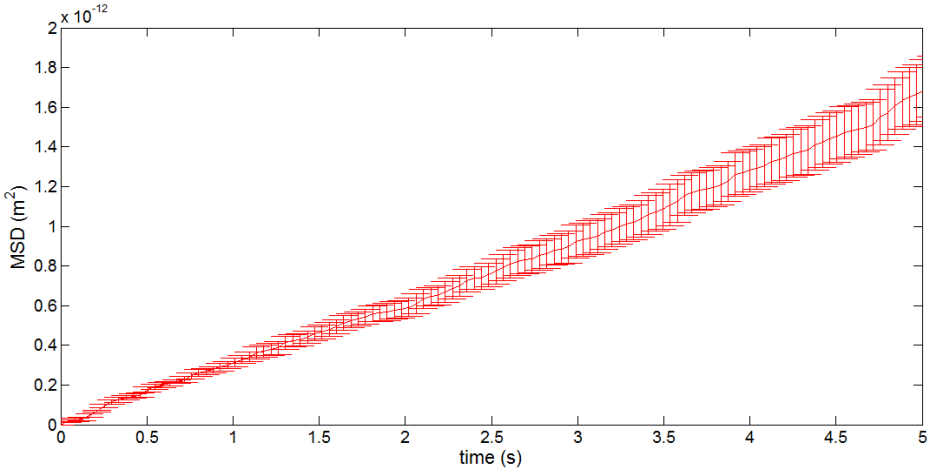

Figure 25 - MSD of a 50nm gold particle in a mixture (50% of glycerol) at 5x10^{-6}mg/ml. Six measurements performed by single nanoparticle tracking on different nanoparticles from the same sample.

a viscosity of 0.006Pa·s, while Figure 26 represents the displacement of the same particle when the glycerol is 90% of the mixture, with a viscosity of 0.15Pa·s.

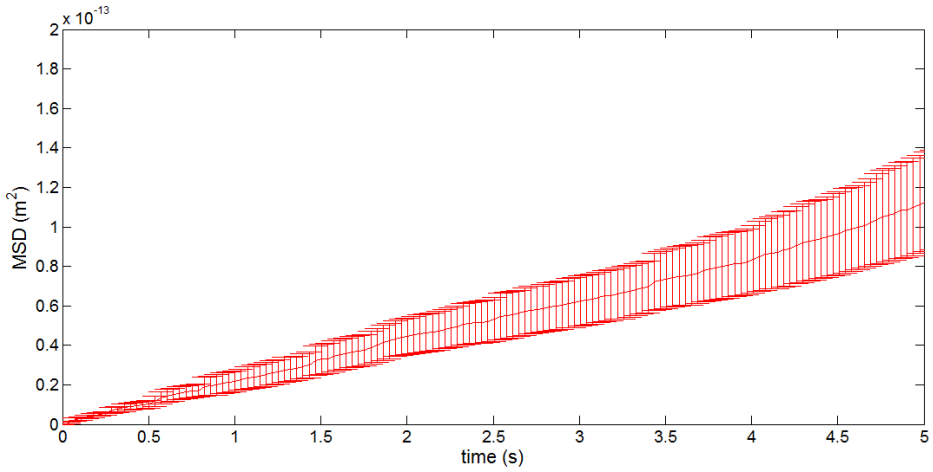

Figure 26 - MSD of a 50nm gold particle in a mixture (90% of glycerol) at 5x10^{-6}mg/ml. Six measurements performed by single nanoparticle tracking on different nanoparticles from the same sample.

5.2 – Gaussian distribution of the nanoparticles displacements

As already described in Chapter 2, Einstein proposed a probability density function (PDF) that takes account of the random change in position, caused by collisions between the particle and the fluid molecules. This probability has the form of equation (15):

$$P_x(x, t \mid x_0, t_0) = \frac{1}{\sqrt{4\pi D(t - t_0)}} e^{\left(-\frac{(x-x_0)}{4D(t-t_0)}\right)}$$

This distribution is essentially a Gaussian distribution, which classically is:

$$f(x) = \frac{1}{\sigma\sqrt{2\pi}} e^{-\frac{(x-\mu)^2}{2\sigma^2}} \quad (44)$$

Comparing the previous equations, the mean, μ of Einstein's PDF is x_0 and the variance, σ is $2D(t - t_0)$. The distribution represents the probability that a particle will be at the position *x* at the time *t*. The variance corresponds to the width of the distribution and it is directly related to the diffusion. The mean of the distribution, x_0 corresponds to the position of the centre of the "bell", and for a particle exhibiting Brownian motion is expected to be zero: there should be almost the same number of displacements at the left and at the right of the initial position.

Gaussian distributions are often used to represent random variables whose distributions are not known. It is possible to plot the distribution of the displacement, which Einstein considered the random variable in his probability distribution function, as described in Chapter 2, in one dimension so to have a confirmation of the random nature of the particle motion.

Figure 27 shows the displacement distribution, for the x-direction, of a 50nm gold particle dispersed in water, whose mean square displacement was plotted in Figure 23 and exhibited linear behaviour.

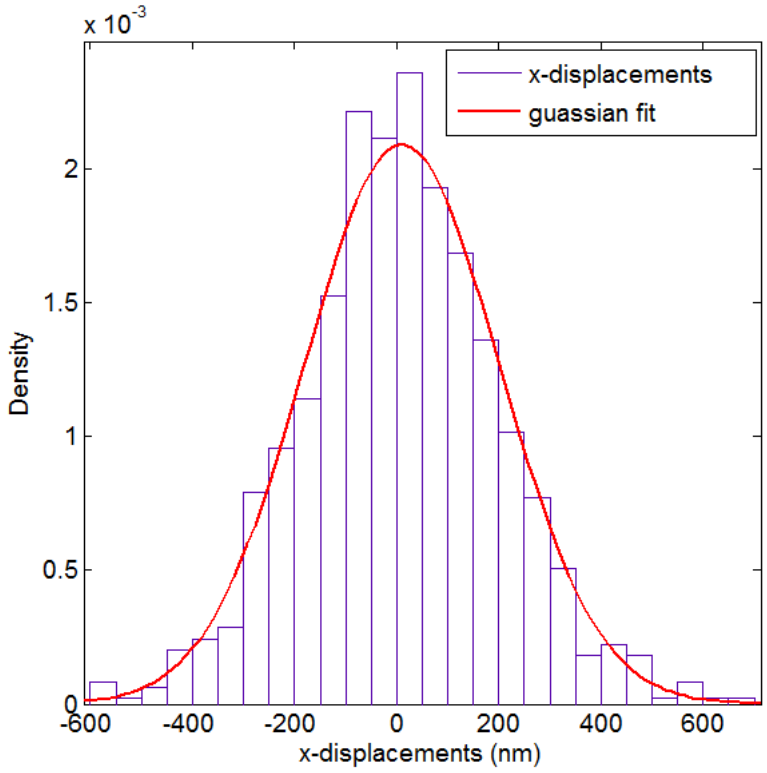

Figure 27 - Gaussian distribution of the x-displacements of a 50nm gold particle dispersed in water at $5x10^{-6}$mg/ml. Six measurements performed by single nanoparticle tracking on different nanoparticles from the same sample.

The histogram is divided in bins, a series of intervals of equal size, and each bin represent a range of values of the displacement. The displacements of the particle (nanometres) are represented on the x-axis of the plot, while, on the y-axis, the density consists in the number of observations in the bin, which is the interval divided by the bin width, which is the typical representation of the PDF, in order to group large sets of displacement data into single bins. The Gaussian distribution in

Figure 27 of the displacements data confirms the random nature of the motion. The same can be observed when the particle is dispersed in a glycerol-water mixture, as shown in Figure 28. In Figure 28, the 50nm gold particle was dispersed in a glycerol-water mixture (9:1). The range of values of the displacements decreases, as can be noticed on the x-axis, because of the increase in viscosity. The displacement distribution is, anyway, again Gaussian.

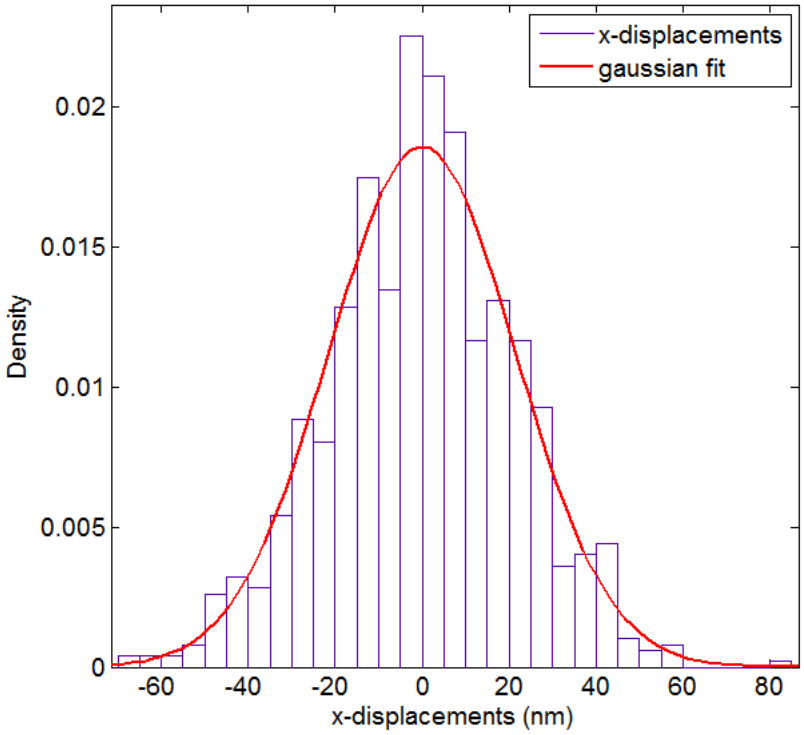

Figure 28 - Gaussian distribution of the x-displacements of a 50nm gold particle dispersed in a mixture with 90% of glycerol and 10% of water at $5x10^{-6}$mg/ml. Six measurements performed by single nanoparticle tracking on different nanoparticles from the same sample.

The displacements data were found, in every case under investigation, to be well represented by a Gaussian fit. The change in dimension, material, concentration or

viscosity did not affect the random nature of the particle motion, as can be noticed in Figure 29, for instance, for a range of polystyrene nanoparticles, from 20nm to 150nm, dispersed in water.

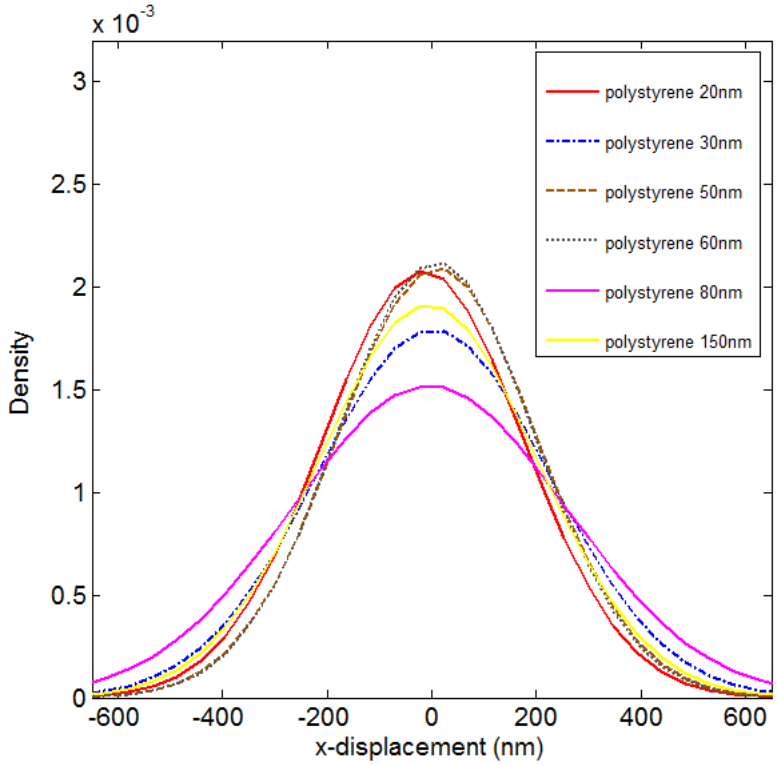

Figure 29 - Gaussian distributions for a range of polystyrene nanoparticles dispersed in water at $5x10^{-6}$mg/ml. Six measurements performed by single nanoparticle tracking on different nanoparticles, for each size, from the same sample.

5.3 – Stokes-Einstein diffusion breakdown approaching the molecular scale

The nanoparticles diffusion was investigated for metallic (gold) and non-metallic materials (polystyrene), as the particle diameter approaches the molecular scale. Gold nanoparticles, in a range from 150nm to 10nm, and polystyrene nanoparticles, from 500nm to 20nm, were dispersed in solutions characterized by different

viscosity values, to investigate the nanoparticle motion in isotropic fluids. The linear trend of the mean square displacement was confirmed for the tested nanoparticles, and the random nature of their motion was verified by the Gaussian distribution of the particle displacements, it appears that Einstein's equation

$$MSD = 4Dt \tag{45}$$

was not able to predict the behaviour of the nanoparticles under investigation. Indeed, looking, for instance, to Figure 23, where a 50nm gold nanoparticle was dispersed in distilled water, and comparing the experimental data to Einstein's mean square displacement prediction, as in Figure 30, it was found that the latter was not able to represent the experimental data.

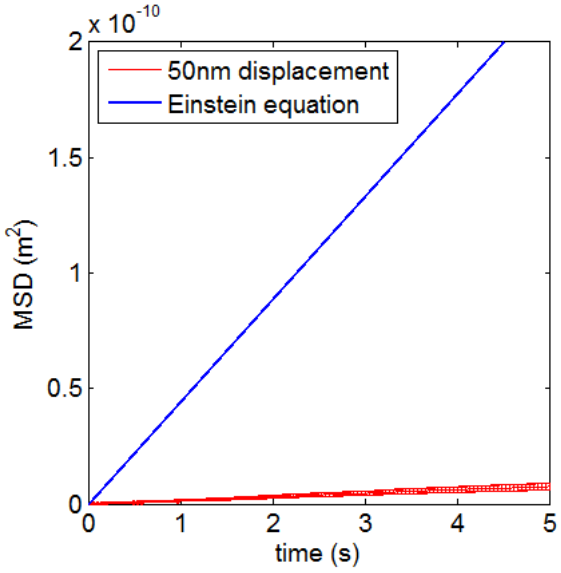

Figure 30 - 50nm gold experimental msd compared to Einstein's prediction in water at $5x10^{-6}$mg/ml. Six measurements performed by single nanoparticle tracking on different nanoparticles from the same sample.

The slope of the experimental trend was found to be about 20 times lower than the value predicted by the Einstein's equation. Similarly, if the 50nm gold particle is

dispersed in a glycerol-water mixture 9:1, i.e. an increase in viscosity of three orders of magnitude, the slope of the experimental trend was found to be about 12 times lower than the prediction as shown in Figure 31.

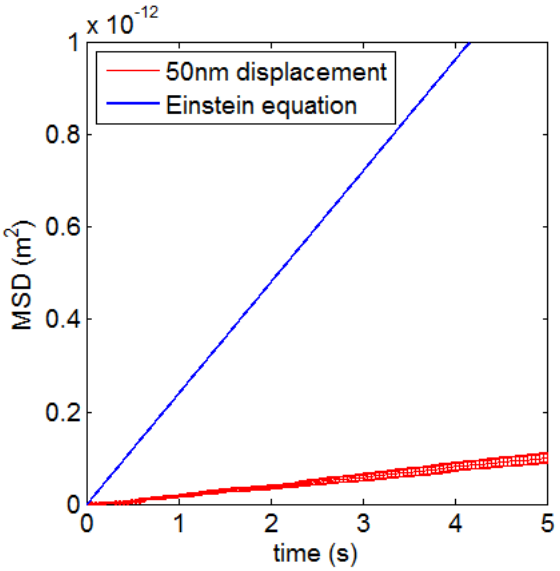

Figure 31 - 50nm gold experimental msd compared with Einstein's prediction in glycerol-water mixture 9:1 at $5x10^{-6}$mg/ml. Six measurements performed by single nanoparticle tracking on different nanoparticles from the same sample.

In Einstein's relation (45), that linearly relates the mean square displacement to the time in an isotropic fluids, the slope of the trend is the diffusion of the particle, which consequently has to be constant. The 50nm gold particle essentially diffuses, in both cases shown in Figure 30-31, slower than what Einstein's equation predicts for the diffusion of a 50nm particle in distilled water and a glycerol-water mixture of 9:1. The experimental data in Figure 30-31 were collected at about 30 frames/second, at 30°C and a particle concentration of $5x10^{-6}$mg/ml.

The diffusion coefficient was calculated following the approach of Ernst and Kohler [137], using the Einstein's equation (45) for each time step and averaged over the whole period of observation. This method was chosen so to consider possible variation of the diffusion coefficient at each time step over the period of observation and to consider possible anomalies of the motion, such as exponential trends.

In Figure 32a, values of the diffusion coefficient are shown for gold nanoparticles from 150nm to 10nm diameter dispersed in water, at a concentration of 5×10^{-6} mg/ml, which in the experiments of this thesis represents the least crowded case with about 10^8 particles/ml, when the particle diameter is 10nm.

The diffusion coefficient was found to be about 100 times lower than predicted using the Stokes-Einstein relation for the 10nm diameter gold particles and less than 10 times lower for the 150nm diameter particles.

The over-prediction of the diffusion coefficient was less when the viscosity was higher. At the higher viscosity of 0.15Pa·s (9:1 glycerol-water mixture), the 10nm diameter gold particle diffused about 40 times slower than predicted by the Stokes-Einstein relation whereas for the 150nm diameter particle there was only a factor or two of difference.

The experiments were repeated using polystyrene nanoparticles from 150nm to 20nm to investigate both the possible influence of the surfactant and the material density. The density of gold is nominally 19.3g/cm^3 compared to 1.05 g/cm^3 for polystyrene, i.e. a difference of more than an order of magnitude. The results are

shown in Figure 33 for the same conditions of concentration and viscosity as in

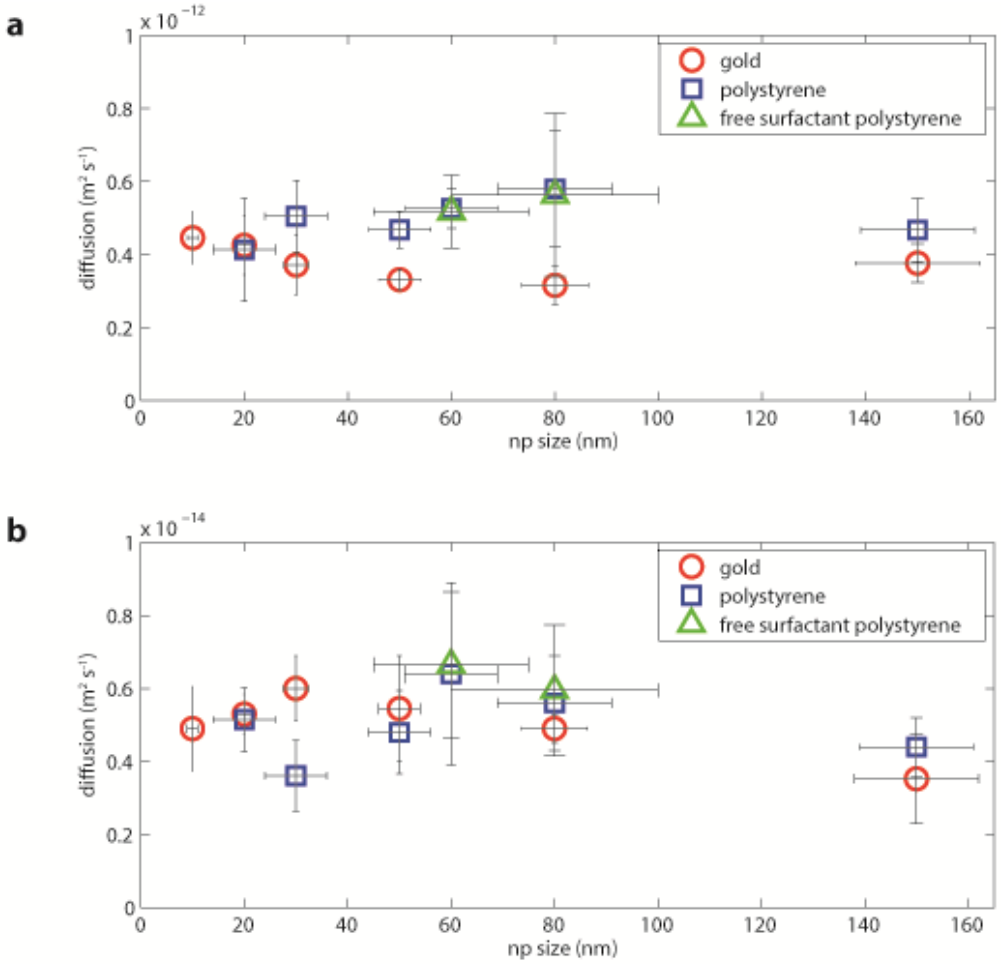

Figure 33 - Diffusion of gold (nominal density of 19.3g/cm^3) and polystyrene (nominal density of 1.05g/cm^3) nanoparticles as a function of particle diameter in (**a**) water with a viscosity of 0.0008Pa·s and (**b**) a 9:1 glycerol-water mixture with a viscosity of 0.15Pa·s. Data for surfactant-free and silica nanoparticles are included for comparison. The horizontal error bars are based on uncertainty data provided by the manufacturer about the size of the particles and the vertical error bars are based on the standard deviation of 6 measurements of the mean square displacement for each material and size.

Figure 32, and compared with the diffusion data of the gold nanoparticles. It is immediately noticeable that there are no significant differences between the two

types of material, implying that diffusion is independent of particle density, as predicted by the Stokes-Einstein relation.

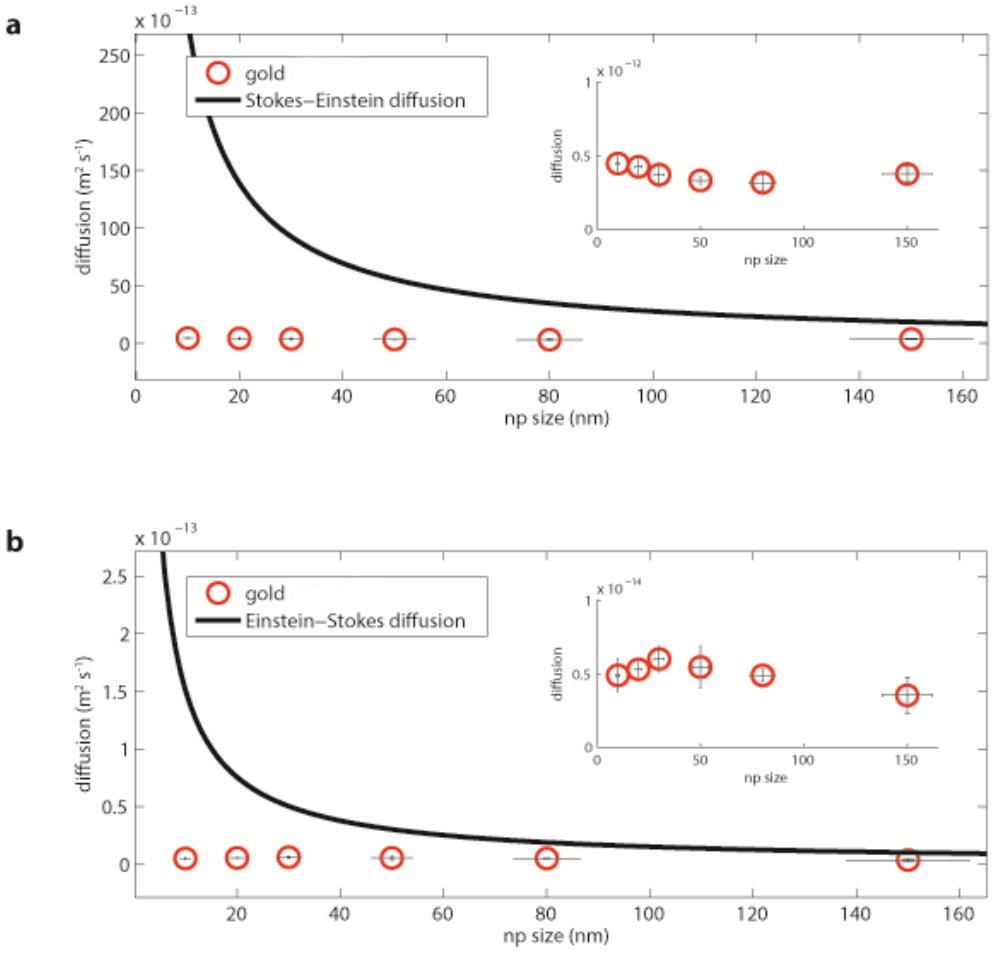

Figure 32 - Diffusion of gold nanoparticles calculated from measured mean square displacements and predicted using the Stokes-Einstein relation as a function of particle diameter in (**a**) water of viscosity 0.0008Pa·s and (**b**) a 9:1 glycerol-water mixture of viscosity 0.15Pa·s; both at particle concentrations of 5×10^{-6}mg/ml. Each point represent the average diffusion coefficient calculated over six measurements on different nanoparticles from the same sample with relative error bar (±σ). Horizontal error bar are based on the standard deviation (±σ) stated from the manufacturer.

The most surprising result is that the diffusion coefficient was found to be independent of the particle size for the range of viscosities under investigation,

which contradicts the Stokes-Einstein relation. Indeed the Stokes-Einstein relation postulates that the diffusion of a spherical particle increases as the particle size decreases, for the same temperature and viscosity. Figure 32 and Figure 33 suggest that the constant diffusion is independent of the particle size, under these experimental circumstances, with values close to $5x10^{-13}m^2/s$ both for the gold and polystyrene nanoparticles when dispersed in distilled water and close to $4x10^{-15}$ m^2/s when dispersed in a 9:1 glycerol-water mixture.

In Figure 33, vertical and horizontal error bars are included for each data point to demonstrate that the errors cannot account for the trends observed. The horizontal error bars are based on uncertainty data provided by the manufacturer for the size of the particles. The vertical error bars are based on the standard deviation of 6 measurements of the mean square displacement for each material and size.

Stabilizing agent is generally added to all commercially-available dispersions to reduce the aggregation of particles. The surfactant was suspected of being responsible for lowering the surface tension around the particle by changing the chemistry of the matrix, which in turn would change the fluid-particle and the particle-particle interaction inducing a change in the predicted diffusion. However, the data in Figure 33 show that there are no appreciable differences for 60nm and 80nm diameter polystyrene particles with and without surfactant. Some surfactant is used in the production of surfactant-free particles so that there may be trace amounts present but these are expected to have a negligible effect.

5.4 – Low concentrations of nanoparticles do not affect the value of the fluid viscosity

The value of the fluid viscosity was evaluated for each solution using the empirical formula proposed by Cheng [138], which allows the calculation of the viscosity of glycerol-water mixtures for mass concentrations in the range 0-100% and temperatures varying from 0 to 100°C. To confirm that low concentrations of nanoparticles dispersed in simple fluids do not significantly affect the viscosity of the fluid, experiments were performed on one solution (9:1 mixture of glycerol and water) using a rheometer (AR1000N, TA Instruments). The mean and the standard deviation of the viscosities in Table 1 are based on 15 measurements on each solution.

	Viscosity (Pa s)
glycerol-water 9:1 [138]	0,14732
glycerol-water 9:1 (measured)	0.14688±0.0012
adding 150nm gold ($5x10^{-3}$mg/ml)	0.15128±0.0036
adding 150nm gold ($5x10^{-6}$mg/ml)	0.14576±0.0016
adding 80nm gold ($5x10^{-3}$mg/ml)	0.14839±0.0008
adding 80nm gold ($5x10^{-6}$mg/ml)	0.14602±0.0020
adding 20nm gold ($5x10^{-3}$mg/ml)	0.14751±0.0004
adding 20nm gold ($5x10^{-6}$mg/ml)	0.14693±0.0012

Table 1 – Experimental viscosities adding concentrations of $5x10^{-3}$ and $5x10^{-6}$mg/ml gold nanoparticles with diameters of 20nm, 80nm and 150nm to a 9:1 glyerol-water mixture.

Adding concentrations of $5x10^{-3}$ and $5x10^{-6}$mg/ml of gold nanoparticles with diameters of 20nm, 80nm and 150nm to the solution had no significant effect on

the viscosity, at a 99.9% confidence level. At these low concentrations, the addition of nanoparticles does not change significantly the viscosity of the base fluid and cannot account for the breakdown of the Stokes-Einstein diffusion, which falls orders of magnitude below the prediction.

5.5 – Appearance of a critical concentration

The effect of the particle concentration was investigated to understand whether it could have caused the breakdown of the Stokes-Einstein diffusion. Experiments on gold nanoparticles were performed for a range of concentrations from $5x10^{-3}$mg/ml to $5x10^{-6}$mg/ml, maintaining a constant temperature while varying the viscosity from 0.0008Pa·s (distilled water) to 0.15Pa·s (9:1 glycerol-water mixture). The results for the measured diffusion of gold nanoparticles were plotted in Figure 34 as a function of concentration, up to the maximum value at which it was possible to track individual particles, i.e. 5×10^{-3}mg/ml.

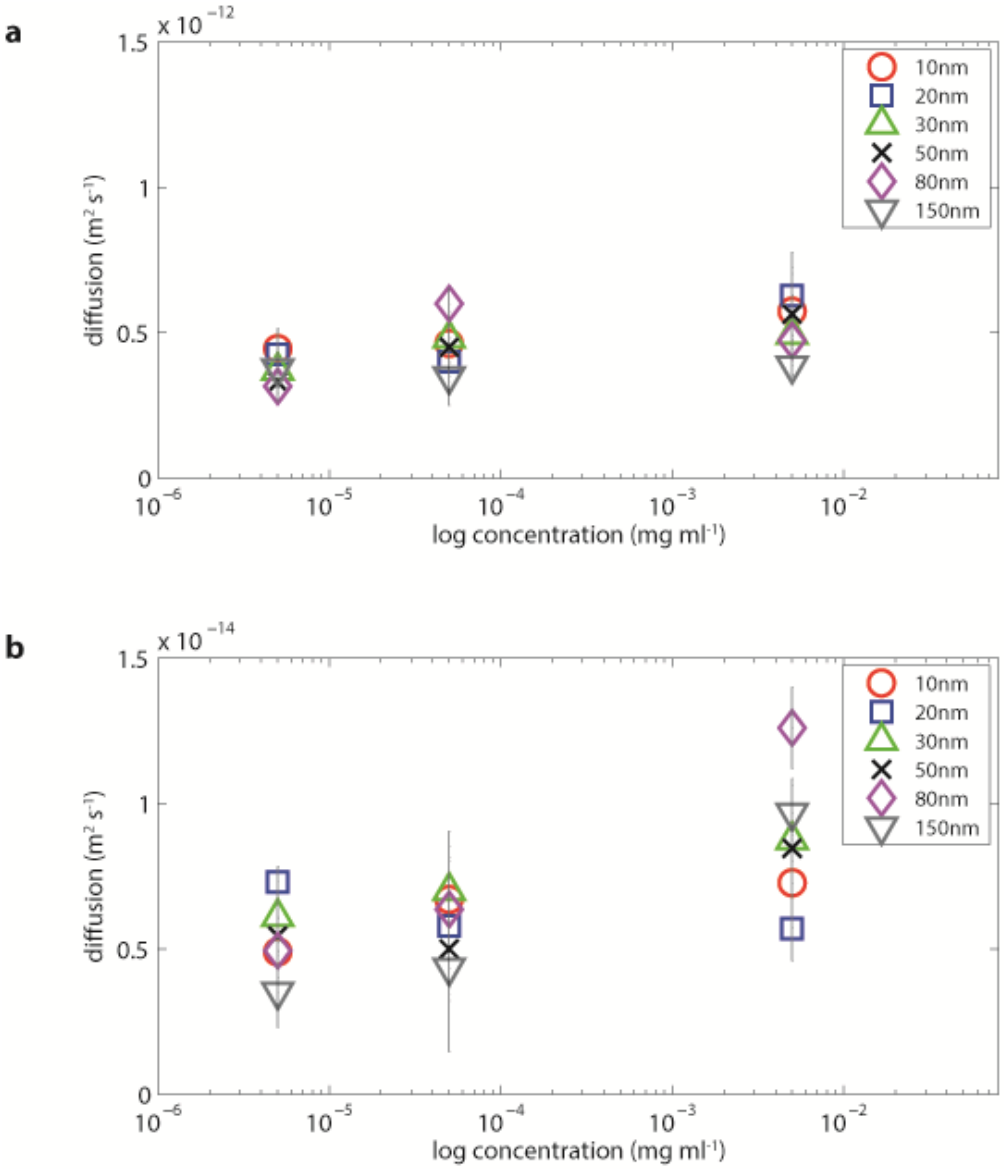

Figure 34 - Diffusion of gold nanoparticles, ranging in size from 10nm to 150nm, and from $5x10^{-6}$mg/ml to $5x10^{-3}$mg/ml in concentration, calculated from measured mean square displacements as a function of concentration in (**a**) water with a viscosity of 0.0008Pa·s and (**b**) a 9:1 glycerol-water mixture with a viscosity of 0.15Pa·s

At this concentration, the 150nm diameter particles in water have a diffusion coefficient of about 3×10^{-13} m^2/s, which is an order of magnitude less than predicted

using the Stokes-Einstein relationship and the experimental value found by Koenig et al. [139].

Koenig et al. purchased the same type of 150nm diameter gold nanoparticles as those used in this study and measured the diffusion coefficient at the supplied concentration as a calibration for their work on the diffusion of functionalized nanoparticles. For the particles dispersed in water at 5×10^{-2} mg/ml, which is ten times more crowded than the highest concentration in this study, they obtained a value of $D\approx30\times10^{-13}m^2\ s^{-1}$ which was in good agreement with the Stokes-Einstein relation.

Figure 34 shows, again, the diffusion of the nanoparticles to be independent by the particle diameter, for the whole range of tested concentrations and at both values of viscosity. Considering for instance, the diffusion of the 150nm gold nanoparticle, it was found to be $3.76x10^{-13}m^2/s$ at $5x10^{-6}$mg/ml, $3.5x10^{-13}m^2/s$ at $5x10^{-5}$mg/ml and $3.87x10^{-13}m^2/s$ at $5x10^{-3}$mg/ml, when dispersed in water. Looking at Figure 34b and considering always the same 150nm gold particle, the diffusion was found to be $3.53x10^{-15}m^2/s$ at $5x10^{-6}$mg/ml, $4.35x10^{-15}m^2/s$ at $5x10^{-5}$mg/ml and $9.68x10^{-15}m^2/s$ at $5x10^{-3}$mg/ml. The diffusion appears to be, at these concentrations, for nanoparticles ranging from 150nm to 10nm, independent to the size and almost constant if the concentration of the particles is very low. The diffusion increases slightly with concentration but remains substantially less than the Stokes-Einstein prediction.

Since Koenig et al also used optical microscopy, these data would suggest that there is a critical concentration below which the dynamics of a particle are no longer governed by the Stokes-Einstein equation, lying between $5x10^{-2}$mg/ml and $5x10^{-3}$mg/ml.

Above the critical concentration one could observe the formation of the caustics, due to the interaction between the light beam and the nanoparticles, but the single particle tracking was not possible because of the overwhelmed field of view and the noise caused by the interference of the diffraction patterns. From a qualitative analysis one can say that the nanoparticles moved faster above 5×10^{-3}mg/ml, but this observation it is not supported by experimental data because of the limit of this technique. For this reason experiments above 5×10^{-3}mg/ml were performed with the Nanosight system.

5.6 – The emergence of a critical size

Polystyrene particles of 300nm and 500nm diameter were purchased to extend the range of investigation and understand the importance of the particle size in the breakdown of diffusion described by the Stokes-Einstein relation. The choice of polystyrene nanoparticles was obliged by the unavailability of gold nanoparticles over 150nm diameter from the same manufacturer who provided the previously tested nanoparticles.

The concept of a critical size, below which the Stokes-Einstein relation is not able to represent the particle diffusion, was proposed by Li [140] based on molecular

dynamics simulations. To test this hypothesis we performed further experiments with 300nm and 500nm diameter polystyrene particles. The results for the whole range of polystyrene nanoparticles particles are shown in Figure 35. The experimental data indicate the existence of a critical size at which there is a transition between behaviour that can be characterised by the Stokes-Einstein and fractional Stokes-Einstein relationships.

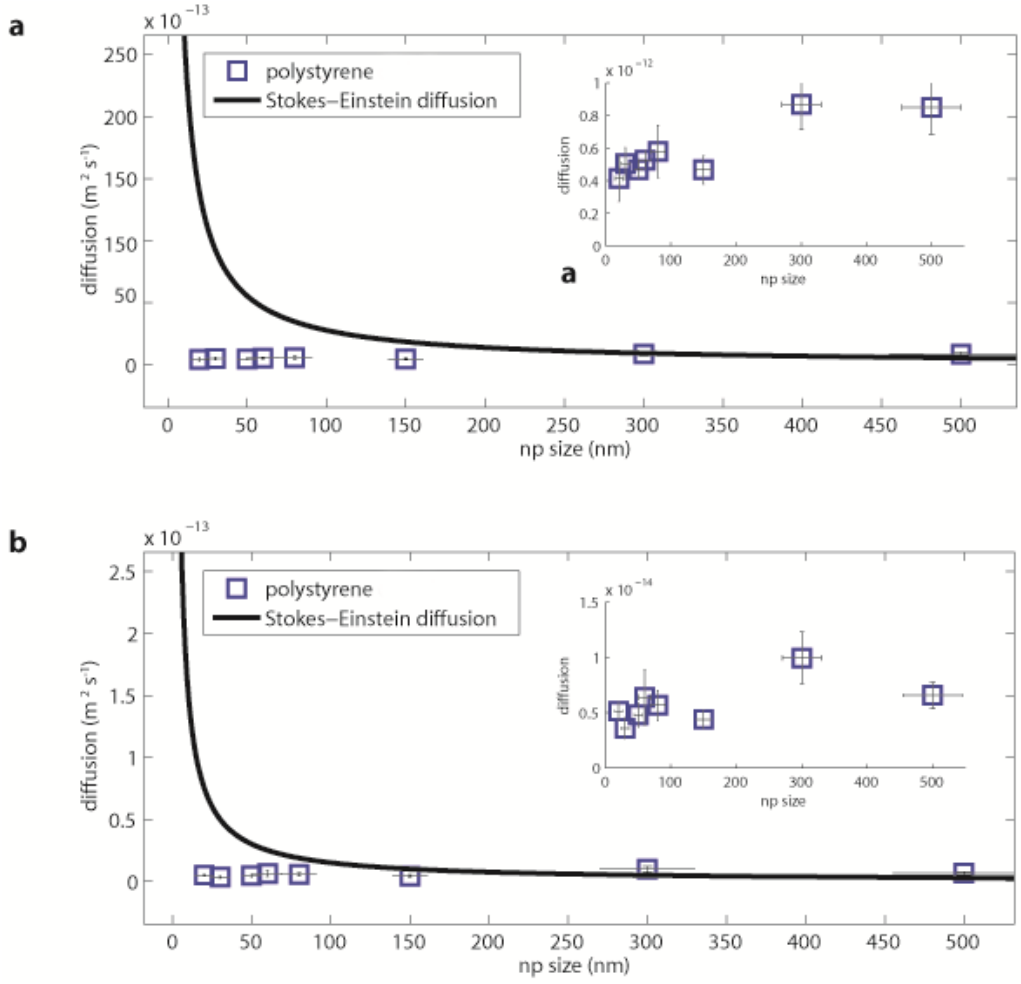

Figure 35 – Diffusion of polystyrene particles up to 500nm calculated from measured mean square displacements and predicted using the Stokes-Einstein relation as a function of particle diameter in (a) water of viscosity 0.0008Pa·s and(b) a 9:1 glycerol-water mixture of viscosity 0.15Pa·s both at concentrations of 5×10^{-6}mg/ml.

As already mentioned, we were unable to obtain spherical gold nanoparticles at these diameters, but based on the data in Figure 33 we would not expect the results to change significantly with material or density. In Figure 35a it can be noticed that the diffusion of polystyrene nanoparticles dispersed in water is constant and independent to the size below a particle diameter of 150nm, for which the diffusion is $4.7x10^{-13}m^2/s$ (for the 150nm gold particle diffusion is similarly $4.3x10^{-13}m^2/s$), which is seven times slower than Stokes-Einstein prediction. Considering, in Figure 35a, the 300nm polystyrene particle, it nicely matches with Stokes-Einstein diffusion; at this size, from Figure 35a inset, it can be noticed an increase of the diffusion coefficient compared to those of nanoparticles below 150nm, leading to a good agreement with the Stokes-Einstein prediction. For the 500nm polystyrene particle, Stokes-Einstein relation is again able to predict the nanoparticle diffusion at low concentration. As for the gold nanoparticles, polystyrene from 20nm to 150nm present value of the diffusion coefficients below Stokes-Einstein prediction. In Figure 35b, the diffusion of the 300nm and 500nm polystyrene particles dispersed in a glycerol-water mixture 9:1 is well represented by the Stokes-Einstein relation. In this case, the diffusion of the 150nm particle is just a couple of times lower than Stokes-Einstein model, while the same nanoparticle dispersed in water is seven times slower than Stokes-Einstein diffusion. At both viscosities, the critical size, representing the transition between classical and fractional Stokes-Einstein equation, lies between 150nm and 300nm For water it seems to be closer to 300nm while for the 9:1 glycerol-water mixture it is closer to 150nm. The critical size appears to be an inverse function of viscosity, that is, it decreases with increasing viscosity from about 300nm at 0.0008 Pa·s to about 150-200nm at 0.15Pa·s.

5.7 – NTA failure below a critical size and concentration

Nanoparticle Tracking Analysis (NTA) allows a quick analysis of the particle size distribution, because of its user-friendly setup and automated data analysis, which gives as a final outcome a report containing information on the particles diameters. The typical image, taken from a Nanosight report, in which the particle size distribution is represented, is shown in Figure 36.

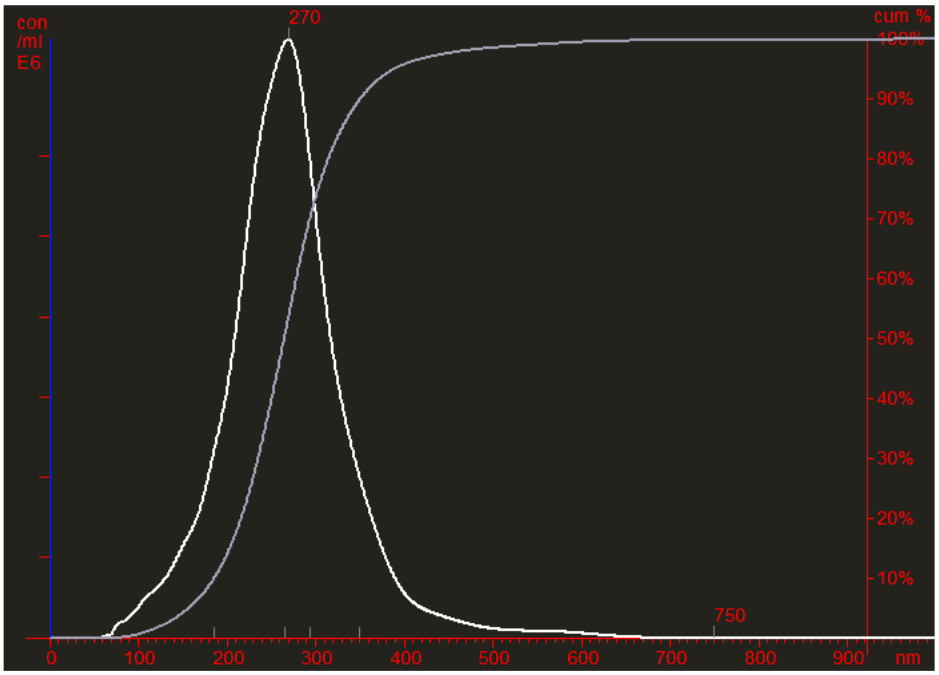

Figure 36 – Nanosight Particle size distribution obtained with 300nm polystyrene particles in water. Distribution data are based on simultaneous single particle tracking; nanoparticles dispersed in water are tracked individually by Nanosight at the same time.

Figure 36 shows the particles size distribution from the Nanosight system for a 300nm polystyrene particle dispersed in distilled water, at a concentration of $5x10^{-6}$mg/ml. The system measured a mean in the distribution of 270nm, with a standard

deviation of ±73nm. The manufacturer datasheet states, for the same polystyrene nanoparticles, an average size of 300±30nm. The overlap of the two intervals in terms of size confirms that in this case, i.e. low concentration but above the critical size, the Nanosight system correctly measures the size distribution of the nanoparticles. When the system is able to measure correctly the diameter of the particles, it means the diffusion is well represented by the Stokes-Einstein diffusion, because Nanosight evaluates the size distribution of particles using the classical Stokes-Einstein relation and measured displacement data, so that the diffusion is determined from equation (45) and the diameter from equation (25) and (26).

On the same plot, the grey curve represents the cumulative frequency distribution. The Nanosight report gives information about three typical intercepts of the distribution, i.e. 10%, 50%, 90%. In Figure 36, the intercepts of these three values correspond, respectively to 185nm, 265nm, 350nm, that means that the 10% of all the particles are below 185nm, there will be 50% below 265nm and the 90% of all the measured particles is below 350nm.

To support the results obtained with the caustic method, solutions of gold particles with nominal diameters of 20nm, 80nm and 150nm were tested in a Nanosight system (Nanosight LM10, Malvern Instruments Ltd) which had been calibrated by the manufacturer six months prior to the experiments.

When 150nm gold nanoparticles, dispersed in distilled water at the supplied concentration, were introduced in the Nanosight chamber, the system correctly measured the size of the particles, giving a mean of 157±10nm, as shown in Figure 37. According to the manufacturer's datasheet, the tested gold nanoparticles should

have a size of 150±12nm. This result confirms the findings of by Koenig et al [139], who tested the same particles in water at the supplied concentration using darkfield microscopy. The experiment was repeated six times over which the system gave an average diameter of 153±18nm.

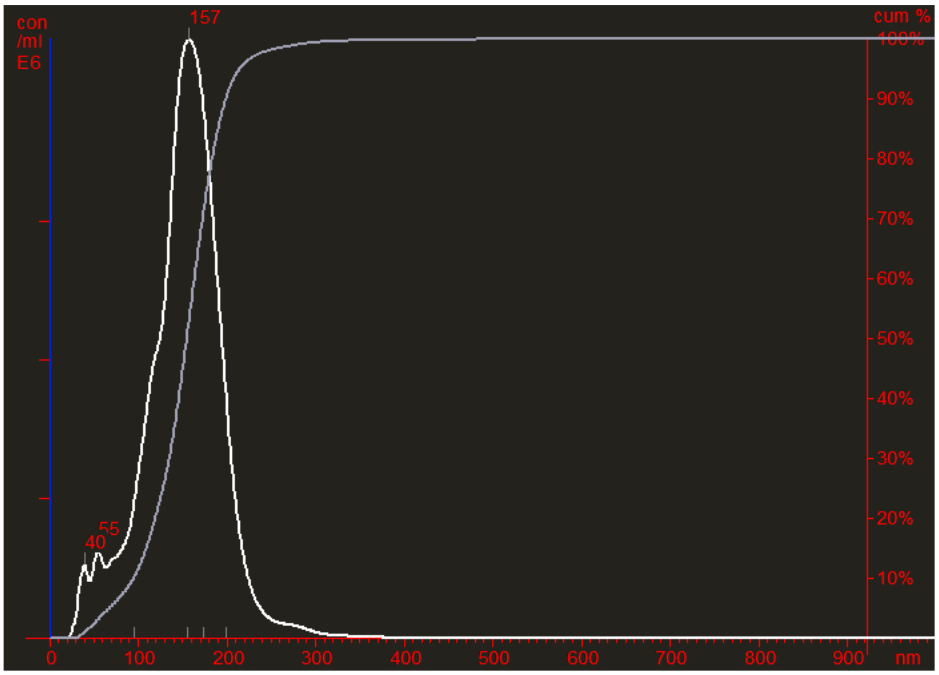

Figure 37 – Nanosight Particle size distribution obtained with 150nm gold particles in water at the supplied concentration. Distribution data are based on simultaneous single particle tracking; nanoparticles dispersed in water are tracked individually by Nanosight at the same time.

Conversely, the Nanosight system was not able to give an appropriate estimate when the same 150nm, or the 80nm or the 20nm gold particles were dispersed in water at lower concentrations, i.e. below the supplied concentration of $5x10^{-2}$mg/ml. In this cases, as shown in Figure 38 the peak of the size distribution, for instance, for the 20nm gold particles, was found to be about 200nm.

Below the critical size and concentration, over six experiment for each size, a peak in the size distribution of about 200nm was obtained for every tested size for particle concentrations of $5x10^{-6}$ and $5x\ 10^{-3}$mg ml^{-1} as shown in Table 2.

Concentration [mg ml^{-1}]	Nominal diameter		
	20nm	80nm	150nm
$5x10^{-6}$	202±30nm	190±28nm	215±22nm
$5x10^{-3}$	220±34nm	202±15nm	236±20nm
$5x10^{-2}$			153±18nm

Table 2: Nanoparticle size measured using Nanosight system. Nanosight measures the displacement of each particle in the field, giving a distribution in terms of size based on calculation through the Stokes-Einstein relation. The measurements were performed at different concentrations. The data in the table are based on six consecutive measurements with Nanosight on different samples.

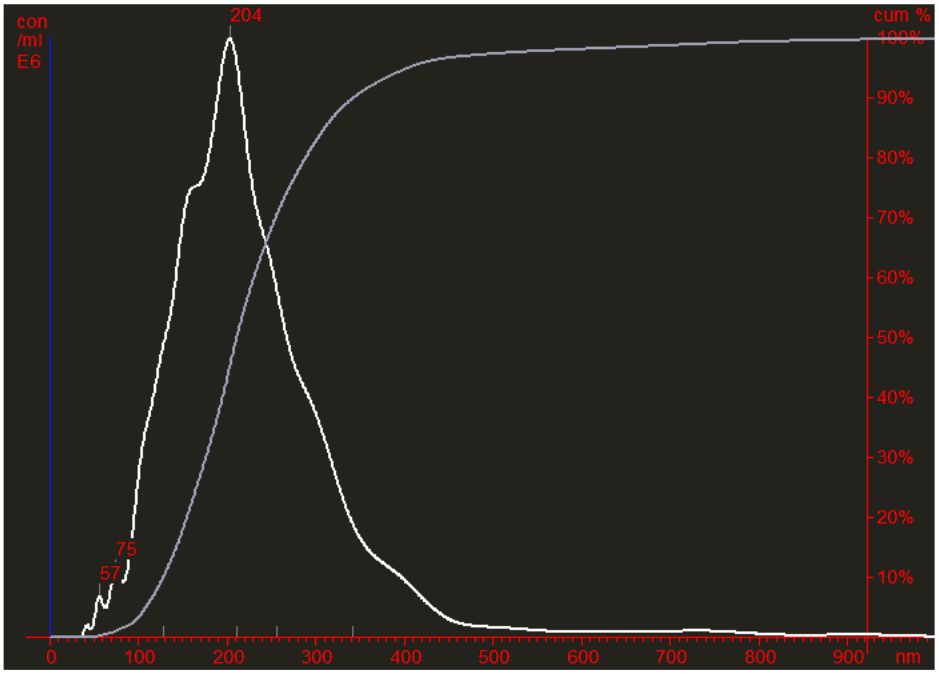

Figure 38 – Nanosight Particle size distribution obtained with 20nm gold particles in water at low concentration ($5x10^{-6}$mg/ml). Distribution data are based on simultaneous single particle tracking; nanoparticles dispersed in water are tracked individually by Nanosight at the same time.

These results support the concept of a critical size and concentration, below which the displacement, and hence diffusion, of the particle is constant and independent of the size, leading the Nanosight system to misinterpret the real dimensions of the nanoparticles.

Indeed, when the system measures the size distribution above the critical size and concentration, it is able to evaluate the real dimension of the particle through the Stokes-Einstein equation. When the experiments were performed below the critical size and below the critical concentration, Stokes-Einstein diffusion is not able to represent the particle motion. As a consequence of the breakdown, the system gave wrong measurements, almost the same for any of the nanoparticles tested below the critical size and concentration, implying that the diffusion, in this regime, is constant and independent to the size.

Concentration could be an essential parameter for Nanosight and DLS users, which are systems based on the validity of the Stokes-Einstein equation. If the particles or molecules under investigation are dispersed in fluid at low concentration, they could exhibit anomalous behaviour from the classical Stokes-Einstein model and lead to wrong result in sizing the particle or in the calculation of the diffusion coefficient. Aggregation and the formation of the hydrodynamic radius are possible explanations of unexpected results in dynamic light scattering systems, but a direct observation of the particle motion seems to be essential for a better understanding of the particle dynamic.

5.8 – The fractional Stokes-Einstein equation

The fractional Stokes-Einstein equation was proposed by Hiss and Cussler [59] to explain the diffusion of small solutes in liquids with viscosity ranging between 0.0005Pa·s to 5Pa·s at 25°C. They found the diffusion to be proportional to a fractional power of the viscosity, based on their experimental data for the diffusion of naphthalene and n-hexane in hydrocarbon liquids. The general fractional Stokes-Einstein relation is expressed as

$$D = C/\eta^p \qquad (46)$$

where p=1 for the classical Stokes-Einstein relation, and C is a numerical constant [59]. 'Fractional' refers to the diffusion coefficient D being inversely proportional to a fractional power of viscosity, i.e. p is less than unity [62].

In order to establish the dependency of diffusion on viscosity implied by the fractional Stokes-Einstein relation (46), experiments were performed at four values of viscosity, from 0.0008Pa·s to 0.15Pa·s, on gold nanoparticles, with sizes from 150nm to 10nm. Data were collected at 30°C for the whole range of concentration, from $5x10^{-3}$mg/ml to $5x10^{-6}$mg/ml. In this range, diffusion was found to be constant for the considered concentration and independent of the size, as shown in the previous paragraphs of this chapter and extended, as represented in Figure 39, to the intermediate viscosities, adding glycerol to distilled water so to obtain solutions with 20% and 50% of glycerol in the mixture.

The relationship in equation (46) was fitted to the experimental data, as shown in Figure 39. To better represent the dependence to the viscosity, a log-log scale was

chosen to make the plot clearer. The two empirical parameters of the fractional Stokes-Einstein equation, *C* and *p*, were found to be independent of the size and density of the particles with values of p = 0.84 and $C=10^{-15}$ for all concentrations tested with regression coefficients of $R^2=0.98$ at 5×10^{-6}mg/ml and 5×10^{-5}mg/ml, and $R^2=0.96$ at 5×10^{-3}mg/ml. The significant change in diffusion with viscosity implies that it is unlikely that systematic errors are present in the data.

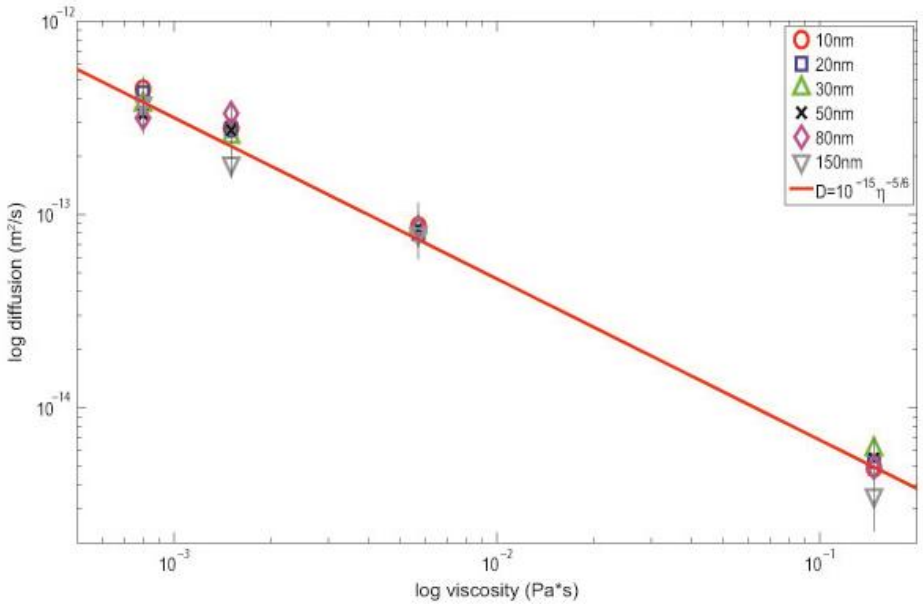

Figure 39 – Diffusion of gold nanoparticles ranging in diameter from 10 to 150nm diameter calculated from measured mean square displacements as a function of viscosity together with the fractional Stokes-Einstein equation fitted to the data. The inset shows the Gaussian distribution of measured displacements of a 20nm and 150nm polystyrene nanoparticles in distilled water and confirms the random nature of the measured motion.

The increase in terms of viscosity lead to the decrease of the particle motion. A particle dispersed in water has a diffusion in the order of $\sim10^{-13}m^2/s$, while when dispersed in the 9:1 glycerol-water mixture of $\sim10^{-15}m^2/s$. Stokes-Einstein

behaviour would be expected to breakdown if there is constraint from the container walls or from neighbouring particles and when there is convection or thermal non-equilibrium. However, care was taken to ensure that these conditions did not occur by collecting data away from the influence of the container walls, by using very low concentrations of isolated single particles, and by controlling and monitoring a spatially and temporally constant temperature.

CHAPTER 6

Discussion

6.1 – Stokes-Einstein breakdown at low concentrations

One of the most used techniques to measure nanoparticle diffusion is dynamic light scattering, which has been used extensively for sizing nanoparticles. Sabunca et al [141] used dynamic light scattering to measure the diameter of gold nanoparticles with nominal diameters 10, 25, 50 and 100nm at a concentration of 5 μg/ml (0.5%) in water, i.e. three order of magnitude higher than the most concentrated solution in this thesis. They obtained average measured diameters of 24, 41, 65 and 97nm with substantially larger scatter in the results at the smaller diameters. They measured the same nanoparticles in a Dulbecco's Modified Eagle's Medium (DMEM), which is a liquid able to support the growth of micro-organisms or cells with very high concentration of amino acids and vitamins and obtained respectively peaks in the size spectra at 108, 95, 88 and 110nm. They attributed these large deviations from the expected results to aggregation and the tendency, in this kind of medium, to form large complexes. Yang et al [142] found that in the absence of stabilizer, DLS measurements of 40nm diameter Al_2O_3 particles gave diameters of 320-330 nm at concentrations of 0.24 to 0.024% by volume but 39nm with stabilizer at 0.24%, while they were not able to obtain data at 0.024% for the same nanoparticles. They attributed the measured diameters and the large deviation from the nominal size to agglomeration of particles. In their work, agglomeration is ascribed to be caused mainly by the viscosity of the fluid; according to the authors,

higher viscosity can result is less agglomeration due to lower probabilities of collision between particles. Egerton and Tooley [143] reached a similar conclusion for TiO_2 particles between 7 and 200nm diameter at a concentration of 0.1% by weight. The volume percentages used in this thesis are significantly lower than those in the cited studies, ranging from $2.6x10^{-3}$ % to $2.6x10^{-7}$ % as the weight percentages, with a maximum of 0.0005% both for the gold and the polystyrene nanoparticles. The caustic method used for single nanoparticle tracking allows single particles to be visualized and distinguished from agglomerations, which have caustics of different size and shape. Lee et al [144] found that DLS was unable to identify 50nm silica particles in a mixture of 50nm and 100nm diameter particles while others, for instance He et al [145], Vareene et al [146] and Gollwitzer et al [147] using DLS and Chon et al [148] using fluorescence lifetime correlation spectroscopy (FLCS), have not observed any anomalous behaviour of 100nm or smaller nanoparticles at concentrations that were at least two order of magnitude greater than those used in these experiments. Verpillat et al [149] calibrated their dark-field digital holographic microscope for 3D-tracking purposes using 100nm gold nanoparticles at a concentration of about 10^6 particles/ml, i.e. similar values to this experimental investigation, and obtained values for the diffusion coefficient that agreed with predictions using the Stokes-Einstein relation. However, although they captured data over a period of at least 10s at about 30 frames/second, they calculated the diffusion coefficient using a linear fit just over the first six frames. According to the study of Michalet [134], the use of few points for the calculation of the diffusion coefficient lead to an overestimation of its value. The experimental

data in this investigation gave similar results when only six frames were used to calculate the diffusion coefficient.

To provide more evidence of the behaviour observed at low concentrations with the caustic method in an inverted optical microscope, additional experiments were performed with a Nanosight system both at low concentrations and at higher concentrations, for which the Stokes-Einstein relation was verified for a 150nm gold nanoparticle with an optical technique by Koenig et al [139]. The Nanosight is essentially a dynamic light scattering microscope for the visualization of particles, but it uses the characteristics of Brownian motion to measure the particle dimension, whereas a classical dynamic light scattering system calculates the diffusion coefficient, hence the size of the particle, based on the intensity of the speckle representing the nanoparticle. The Nanosight was able to measure the particle size above the critical concentration, confirming that, both with an optical microscope [139] and with a dynamic light scattering system, Stokes-Einstein diffusion is able to predict nanoparticle diffusion. Below the critical concentration, the Nanosight was unable to provide the correct size, giving always the same diameter whatever was the size of the nanoparticle under investigation. This result provides a confirmation of the data collected with the caustics method at low concentrations, since particles of different diameters were all considered as a ~200nm particle by the Nanosight at low concentrations.

At higher concentration than the critical value, Stokes-Einstein equation well represents the diffusion of nanoparticles. The reason could be attributed to a higher level of thermal energy, corresponding to k_bT in equation 25: the presence of a

higher number of particles, the increase of the number of particle-particle collisions, the decrease of the inter-particle distance, could lead to an increase of the total thermal energy of the system. Conversely, below the critical concentration, where only particle-fluid interactions can be considered, a decrease of the total energy of the system could cause the breakdown of the Stokes-Einstein relation.

6.2 – Stokes-Einstein breakdown at low concentrations: a spatial interpretation

The cited studies about dynamic light scattering, at higher concentrations than those of this experimental investigation and the work of Koenig et al [139] with darkfield microscopy, suggest that Stokes-Einstein diffusion is able to represent the diffusion of the nanoparticles when the concentration of particles is high enough. In some case, the failure of the dynamic scattering system in sizing the nanoparticles has been ascribed to the particle agglomeration. Comparing the results of other works at high concentrations with those in this investigation, it seems likely that below a critical value of concentration the population of particles is sufficiently sparse that individual nanoparticles are isolated from one another and do not influence each other's diffusion, so that their motion is almost entirely controlled by collisions with fluid molecules and the particle-particle interaction can be neglected. For instance, if we consider a concentration of 5×10^{-3}mg/ml, for every 10nm diameter particle there are 58 billion water molecules and this rises to 58 thousand billion molecules

per nanoparticle when the concentration decreases to 5×10^{-6}mg/ml. To put this into perspective, imagine for a static situation, at the lowest tested concentration (5×10^{-6}mg/ml), on average the water molecules would surround each particle for a radius of ~6μm (Figure 40), while at the highest concentration of 5×10^{-3}mg/ml the corresponding radius would be 600nm and this compares to 270nm (Figure 41) in the supplied concentration used by Koenig et al [139]. Hence, even in the most concentrated solution, the nanoparticles are mostly surrounded by water molecules, lowering the probability that particle-particle interactions could happen.

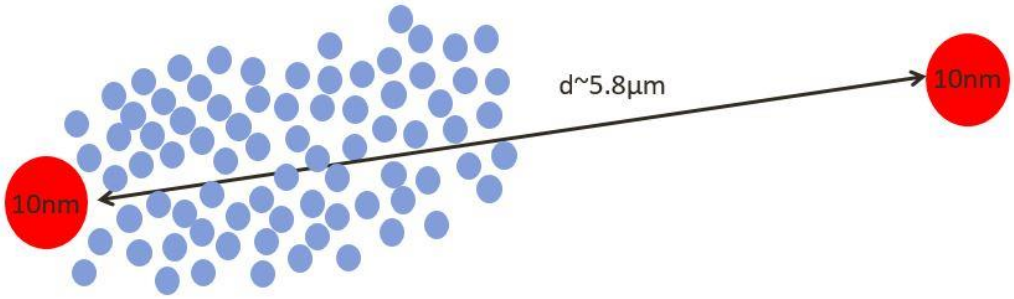

Figure 40 – Interparticle distance when the nanoparticle concentration is $5x10^{-6}$mg/ml

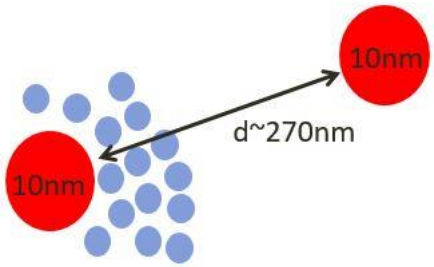

Figure 41 – Interparticle distance when the nanoparticle concentration is $5x10^{-2}$mg/ml (supplied concentration)

6.3 – Small nanoparticles follow the fluid regime

Neglecting collisions between particles at very low concentrations, the nanoparticles motion seems to follow the regime of the fluid, implying a dependence on the behaviour of the fluid molecules and consequently dominated by the viscosity. Water has been found experimentally to follow a fractional Stokes-Einstein equation [72], but also other fluids follow this relation, as described in Chapter 2.5. Looking in particular at the water case, Xu et al [72] found experimentally that below a crossover temperature of about 27°C, water molecule diffusion is better represented by a fractional Stokes-Einstein relation, while they follow the classical Stokes-Einstein equation above it. They attributed the transition from one to another regime to the water local structure, which becomes similar to that of low-density amorphous solid water, which, differently from the common ice, is not characterized by an ordered molecular arrangement. It was not possible to test the Stokes-Einstein breakdown of the nanoparticles diffusion as a function of temperature with the setup used for these experiments. For the experimental data, collected at 30°C, it may possible to find a physical explanation in the behaviour of the water as it approaches the crossover temperature found by Xu et al, when the particles are below the critical concentration. A similar interpretation perhaps could be given for the glycerol-water mixtures, but cannot be confirmed since neither experimental nor computational works were found to support this explanation. In order to observe the transition from the classical Stokes-Einstein diffusion to the fractional Stokes-Einstein relation below the critical concentration, a further requirement is that the particle diameter must be below a critical size. It was found

to be an inverse function of viscosity and in the range 200 to 300nm for the conditions in these experiments. Below the critical size, the nanoparticle behaviour is not predictable using Stokes-Einstein diffusion, but the fractional Stokes-Einstein approach is more effective.

6.4 – Critical size: the role of van der Waals forces

Li [140] in his computational work suggested the existence of a critical size below which the Stokes-Einstein equation breaks down. He described the liquid with a Lennard-Jones potential [150], to understand the interactions nanoparticles-surrounding molecules:

$$U(r) = 4\varepsilon\left[\left(\frac{\sigma}{r}\right)^{12} - \left(\frac{\sigma}{r}\right)^{6}\right] \quad (47)$$

Where r is the distance between two molecules or the particle-molecule distance, σ is the collision diameter and ε the binding energy, which takes into account attraction forces like the van der Waals interactions.

Li's main findings are shown in Figure 42. The diffusion is plotted as a function of the inverse of the hydrodynamic radius. It can be noticed that, when the value of ε grows, the Stokes-Einstein trend breaks down. For ε=584K, the trend tends to be a plateau, which means constant diffusion and size independence. The author attributed the breakdown to the van der Waals forces, which play an important role in the simulation when the size approaches the molecular scale. Van der Waals forces are core-core attractive interactions and so they could be decisive when the

distance between the core of the particle and, for instance, the core of a water molecule is reduced, like at the nanoscale.

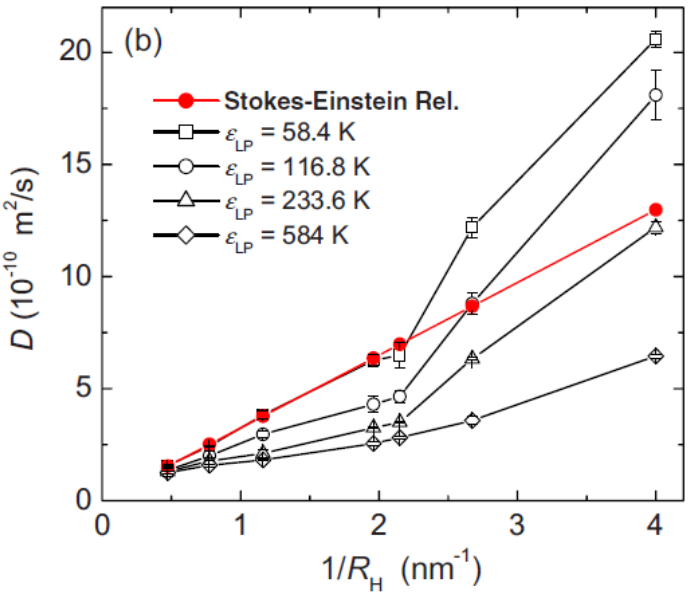

Figure 42 – Diffusion coefficient as a function of the inverse of the hydrodynamic radius for different liquid-particle binding energies [140}

Li was unable to determine the critical dimension due to computational limitations, though he stated it should be of the order of few nanometres. This investigation provides an experimental demonstration of the existence of the critical size. In addition, the critical size was found to be an inverse function of viscosity and in the range 200 to 300nm for the conditions in the experiments. Moreover, it was found that nanoparticle motion, below the critical size, is represented by the fractional Stokes-Einstein equation.

In general particle-particle, molecule-particle and molecule-molecule interactions can be summarized by the DLVO potential (Derjaguin, Landau, Verwey and Overbeek). This potential is a combination of two potentials, the Debye-Hückel U_{DH} and the van der Waals U_{SR} contributions [151]:

$$U_{DLVO} = U_{DH} + U_{SR} \tag{48}$$

One can neglect the Debye-Hückel potential if the nanoparticles are at their isoelectric point, where the charge is Q = 0 [73]. If this approximation is acceptable, one could disregard the Debye-Hückel contribution and assume the DLVO potential as given only by the van der Waals forces, and write [73]:

$$U_{DLVO} = U_{SR}(\rho, H_A) = -\left[\frac{H_A}{12}\frac{1}{(1+\rho)^2} + \frac{1}{(\rho+\rho)^2} + 2\ln\left[\frac{2\rho+\rho^2}{(\rho+\rho)^2}\right]\right] \tag{49}$$

where ρ is the interparticle distance normalized by the particle diameter:

$$\rho = \frac{r-2R}{2R} \tag{50}$$

At very low concentrations, the interparticle distance can be consider effectively infinite, since the nanoparticles are isolated and not interacting with their neighbours. In this case the short range (or van der Waals) potential depends only on the Hamaker contant H_A. This constant has a value ranging from 10^{-20} to 10^{-19}J [152], and it is used essentially to determine the van der Waals forces between two bodies. For the conditions in the experiments of this thesis, i.e. low concentrations of nanoparticle, and looking to equation (49) the Hamaker constant is not reduced by the interparticle distance ρ, so that the van der Waals forces between the

nanoparticles and the fluid molecules are so strong as to create a big shell of layers of fluid molecules, The nanoparticle real dimension becomes unimportant and the motion is regulated by the fluid shell.

6.5 – Hydrodynamic interactions between nanoparticles and fluid molecules

The importance of the van der Waals forces at the nanoscale, the role of the particle-fluid molecule interactions can be read from another point of view. Assuming a hard sphere model, where both the nanoparticle and the fluid molecule are considered as impenetrable spheres [153], the increase in the attraction forces could generate an increase in terms of friction. Felderhof [154] proposed a modified Stokes-Einstein relation in order to take into account the hydrodynamic interactions between two spheres in a fluid:

$$D = \frac{k_b T}{6\pi\eta R(1-\zeta)} \tag{51}$$

where the parameter ζ describes the hydrodynamic boundary conditions between the two spheres and takes values between 0 and 1/3. The two extremes ζ=0 and ζ=1/3 correspond, respectively to complete stick and slip boundary conditions. In the first case, the two spheres stick together, leading to the formation of a hydrodynamic radius. In the second case, the spheres slip ideally without any friction. Even if equation (51) cannot explain the experimental data of this investigation because it is size dependent, it can give some hint about the

mechanical phenomena behind the fractional Stokes-Einstein relation. The possibility that van der Waals forces are crucial at the nanoscale could lead to the formation of layers of fluid molecules, bigger than expected, so that the fluid molecules completely adhere to the nanoparticles forming fluid molecule layers around the nanoparticle. The length of this fluid layer depends on the strength of the attraction forces. The "sticking tendency" could increase the friction between the nanoparticle and the fluid molecules and, consequently, slow down the particle motion. Once the nanoparticle is covered by fluid molecules, which tend to adhere to its surface, the nanoparticle follows the fluid regime rather than the Stokes-Einstein model.

The hydrodynamic radius (or Stokes radius) often replaces the real particle radius in the Stokes-Einstein equation. Small variations or unexpected values of the particle diffusion coefficient are often justified by its formation. In this investigation it was chosen to use the physical size of the nanoparticles, trying to understand the mechanisms behind the Stokes-Einstein breakdown and point out the characteristics of the nanoparticle motion. Indeed, the formation of the hydrodynamic layer cannot explain the size independence of the nanoparticle diffusion. The hydrodynamic radius accounts for the geometric core dimension of the particle and the Debye layer of attached charged ions that makes the effective diameter of the particle larger. Henry's function [155] is used to relate the zeta potential to the electrophoretic mobility

$$U_E = \frac{2\varepsilon_r z * f(kr)}{3\eta} \tag{52}$$

where U_E is the electrophoretic mobility, ε_r is the dielectric constant, *f(kr)* is Henry's function and η the fluid viscosity. This function represents the ratio of the particle radius *r* and the reciprocal of the Debye layer *k*, and can be

$$f(kr) = 1 \tag{53}$$

$$f(kr) = 1.5 \tag{54}$$

where the first equation is the Hückel approximation for non-polar media, the second the Smoluchowski approximation for polar media [155]. In both cases there is a dependence of the Debye layer *1/k* to the particle radius. Henry's function implies a constant ratio of core particle diameter to Debye layer thickness. For a given ionic strength, the increase of the particle radius *r* corresponds to a decrease of *k*, which means an increase of the Debye layer *1/k*. The data collected in this investigation imply a constant hydrodynamic diameter, which does not change with the variation of the particle size and is several times bigger than the physical diameter. For this reason the use of the physical diameter of the nanoparticles was preferred, since the formation of the hydrodynamic radius and Debye layer cannot explain the constant diffusion despite the particle size.

6.6 – Fractional Stokes-Einstein behaviour below the critical size and concentration

The fractional Stokes-Einstein equation was found to be a good fit for the experimental data of this thesis, for three concentrations and four viscosities.

Zwanig and Harrison [74] criticized the use of the fractional Stokes-Einstein equation for molecular fluids on the grounds that molecules cannot be considered hard spheres. However, this criticism is not applicable to the spherical nanoparticles used in this work, whose shape was confirmed by TEM images from the manufacturer's datasheet and by observations shown in Figure 9. Anyway, Zwanig and Harrison stated that, after the formation of the layers of fluid molecules, standard hydrodynamics, where diffusion is proportional to the first power of viscosity, may not be strictly applicable and a "local viscosity" could account for deviations due to the energy dissipation by friction, which is caused by the presence of the particle. This "local viscosity" should be responsible of the diffusion to be proportional to a fractional power of the viscosity. Harris [68] stated that the fractional Stokes-Einstein equation is commonly accepted to apply to molecular liquids and compared its results with those from other authors. The behaviour of particles characterized by the fractional Stokes-Einstein relationship has been observed previously in biological media, where Chirico et al [73] found bovine serum albumin to follow a fractional Stokes-Einstein relation, and other complex systems, such as polymer melts [156, 159], but not in simple systems, such as water and glycerol-water mixture. The observation in a simple system was unexpected because it has been postulated that the constraint imposed by a crowded or structured medium was responsible for the changes in the diffusion of suspended particles and the consequent breakdown of the Stokes-Einstein diffusion. However the results of this thesis imply that at the other extreme, i.e. low concentrations, single particles follow the behaviour of the fluid in which they are suspended. There is a critical concentration below which nanoparticles smaller than a critical

size would be expected to follow the fractional, rather than classical Stokes-Einstein relationship. The experiments were performed only at close to ambient conditions; however the self-diffusion of water has been shown previously, both experimentally [72] and computationally [70], to follow the fractional Stokes-Einstein relation at, or close to, this temperature.

Differently from fractional Brownian motion, which was described in the literature review section, the fractional Stokes-Einstein relationship maintains, at least in this investigation, some of the typical features of simple diffusion, described by the classical Stokes-Einstein relation: a linear dependence of the mean square displacement with the time and Gaussian statistics. In the other cited works the mean square displacement trend and the Gaussian distribution of the displacement data were not mentioned, so it is not possible to make a comparison. The empirical exponent p and the empirical coefficient C in the fractional equation, which were found to be respectively 0.84 and 10^{-15} by fitting to the experimental data, need to be studied more deeply, since their dependence on other parameters could reveal the physical reasons underlying the behaviour characterised by the fractional Stokes-Einstein equation.

CHAPTER 7

Conclusions

In this thesis the motion of nanoparticles in simple fluids has been investigated. The research has addressed the question of the validity of the Stokes-Einstein diffusion at the nanoscale, for which theoretical studies have predicted deviations, due to microscopic parameters, such as molecular interactions, but no experimental evidence had been presented to validate these predictions for simple fluids. The idea that there could have been violations for small particles whose size approaches the molecular scale, because of a central role for van der Waals forces, was the motivation leading to this research. Indeed, classical models have shown the Stokes-Einstein equation to be often not appropriate to represent diffusion of molecules whose diameter is of few nanometres or angstroms. The relation has been verified for microparticles, both over short [56] and long time periods [57], while for nanoparticles was still an open question. Deviations were experimentally found for nanoparticles moving in biological media [23] and complex systems [157, 158], such as polymer melts, but not in simple systems, such as simple isotropic fluids.

In order to test if the equation could represent the diffusion of nanoparticles, a new optical technique for single particle tracking was employed [126]. This technique allows the visualization, in an inverted optical microscope adjusted to have Kohler illumination, of the nanoparticles thanks to the formation of caustics, which are characterized by an intense central spot surrounded by diffraction rings several orders of magnitude larger than the particles. In this way, it was straightforward to

locate a single nanoparticle and follow its motion. Through a camera fitted to the microscope, it was possible to record videos and the in-plane coordinates of a single nanoparticle were collected frame by frame. Consequently the particle displacements and diffusion coefficient were calculated.

Single particle tracking is an essential tool to characterize the dynamic of the nanoparticles, from simple fluids to more complex environment, such as a biological entity. In the latter case, single particle tracking could reveal important characteristics both of the particle dynamic, both of the response of, for instance, a cell membrane or of organelles in the cytoplasm. If the mean square displacement of the particle could be expected to be linear in the liquid matrix, particle approaching the cell membrane or other organisms could exhibit behaviour far from the classical Stokes-Einstein diffusion, such as super or subdiffusion, or both of them at the same time depending on the type of interaction.

Experiments were performed on gold and polystyrene nanoparticles moving in water and glycerol-water mixtures, with the aim of improving the understanding of the dynamics of both metallic and non-metallic nanomaterials at various viscosities and concentrations. The choice of the temperature equal to 30°C was taken, both for stability of the experimental setup and experiments, and to be close to relevant temperature to biological interest. Indeed no relevant changes can be expected increasing the temperature up to, for instance, the body temperature.

For all the nanoparticles under investigation, the mean square displacement was found to be a linear function of the time in all the fluids in which they were dispersed. This behaviour was expected for nanoparticles diffusing in isotropic

fluids. At the same time the displacement data were found to be Gaussian distributed, confirming the random nature of the motion.

Even though the nanoparticles moving in simple fluids verified these two requirements, it was clear from the beginning the Stokes-Einstein relationship was not able to predict the nanoparticle diffusion at low concentrations. Indeed the slope of the linear trend was found to be several times lower than what predict by Einstein's equation, which linearly relates the mean square displacement of the particle to time through the diffusion coefficient, i.e. the slope of the linear trend. Moreover, the Gaussian distribution of nanoparticles of different sizes where all characterized by the same variance, which implies they have the same diffusion coefficient despite of their different particle diameters.

The nanoparticle concentrations in water and in the glycerol-water mixtures varied from $5x10^{-6}$ to $5x10^{-3}$mg/ml. Gold and polystyrene nanoparticles from 10 to 150nm diameter, in this range of concentration, were shown to deviate from the prediction. Stokes-Einstein equation, indeed, overpredicted the diffusion coefficients: the measured diffusion was found to be up to 100 times slower for the smallest particles in water and up to 40 times slower when moving in the most viscous fluid employed in this work. The deviation decreased with increasing the nanoparticle size and the viscosity of the fluid: the 150nm particles were found to be below the prediction just of a factor or two. So in conclusion it can be stated that at very low concentrations the diffusion of small nanoparticles deviates from the Stokes-Einstein relation.

Even though the values of the diffusion coefficients were below the predictions for nanoparticles whose diameter was below 150nm, experiments on both metallic and non-metallic nanomaterials confirmed that there were no significant differences between the two types of material. In other words, diffusion was independent of material density, as predicted by the Stokes-Einstein relation.

The diffusion coefficients of nanoparticles were independent of their size at the temperature, in the range of concentrations and viscosities of these experiments. The Stokes-Einstein equation postulates that diffusion increases as the particle size decreases. The experimental diffusion was found to be constant for nanoparticles below 150nm and showed no significant differences among the range of concentrations under investigation.

Comparing the results with experimental data found in the literature and performing experiments with a Nanosight system, at a higher concentration than the top end of the investigated range, a critical concentration emerged below which the Stokes-Einstein diffusion deviates from the classical behaviour. Above this concentration Stokes-Einstein diffusion is able to predict the nanoparticles diffusion in isotropic fluids. For the experimental conditions of this research, the critical concentration lies between $5x10^{-2}$ and $5x10^{-3}$ mg/ml.

Prior work had suggested the existence of a critical size below which the Stokes-Einstein diffusion is no longer able to represent the particle motion [140]. The size range was extended to test this hypothesis, performing experiments, at low concentrations, over 150 and up to 500nm diameter. The results showed agreement with Stokes-Einstein diffusion for the tested 300 and 500nm diameter particles,

proving the existence of a critical size. The critical size appears to be an inverse function of viscosity, decreasing with increasing the viscosity. It was found to be close to 300nm diameter when the nanoparticles were dispersed in water at low concentrations, and close to 150nm when dispersed in a glycerol-water mixtures whose viscosity was three orders of magnitude higher than water.

Since the results showed a strong influence of viscosity on the nanoparticle motion, the experimental data were fitted with the general fractional Stokes-Einstein equation, where "fractional" refers to a fractional power of the viscosity. For the range of viscosities and concentrations investigated, this relation represented well the measured diffusion coefficients of nanoparticles characterized by different sizes.

A first reason for the deviation from Stokes-Einstein diffusion can be found in the low concentrations that characterized this research. At low concentrations the inter-particle distance is such that the collisions between nanoparticles can be neglected, and, since each nanoparticle is completely surrounded by fluid molecules, just the particle-molecule interactions considered. This provides a first explanation for the strong dependence of the nanoparticle motion at low on the fluid viscosity and consequently its behaviour. Water molecules, indeed, were experimentally found to follow a fractional Stokes-Einstein relation close to the same temperature of this work by Xu et al [72], who attributed this behaviour to a change in the structure of the water molecules at temperatures close to 17°C. Computational works have extended the application of the fractional Stokes-Einstein relation for water up to 350°C [70].

Theoretical studies attributed deviations at the nanoscale from classical models to the van der Waals forces. The experimental data of this research could support the explanation involving the central role of the van der Waals interactions, which become important at this scale. DLVO theory supports this hypothesis, by providing a theoretical justification for the strong effect of the van der Waals forces at low concentrations, where they could lead to the formation of several layers of fluid molecules, which make the nanoparticle's real size unimportant and regulate the motion. It has been discussed that classical concepts, such as the hydrodynamic radius and Debye length, are not able to explain the nanoparticle dynamic at low concentrations. These attraction forces can be interpreted also as an increase in the friction between the nanoparticles and the fluid molecules, with a consequent slowdown in the diffusion.

The findings of this research have potential implications for predicting nanoparticle transport for which current models are often unreliable [159]. A deep understanding of the nanoparticles behaviour is important for managing the benefits and disadvantages in the use of nanomaterials. Among the factors that are crucial to evaluate the risks associated with engineered nanoparticles, one must consider their mobility [160]. Miendl et al have shown that nanoparticles of the material and size used in this investigation are responsible for cell membrane damage and apoptosis [161]. Diffusion and concentration are essential to assess the nanoparticle toxicity [162]. Particles in general and nanoparticles specifically, diffuse, settle, and agglomerate in cell culture media as a function of systemic and particle properties: media density and viscosity and particle size, shape, charge and density, for

example. Particles at low concentration have less probability to agglomerate and settle and cause obstruction of the biological environment. Moreover and more important, it was studied [162] that slow dynamic avoid cell damage or death, do not interfer with protein or mRna expression and in general have a time scale so that do not interfer with the biological responses. Nanoparticles diffusion and concentration are also important parameters in understanding of enhanced heat transfer in nanofluids, which is important in designing systems such as for cooling for electronics, solar collectors and nuclear reactors [163]. Diffusion behaviour is likely also to be important in understanding the transport of nanoparticles used for drug delivery [164] for instance, via the nasal passage to the central nervous system, for which the factors governing the transport are not clear [165].

Future work

The finding of this research could find a wide application where nanoparticles dispersed a fluid matrix are employed.

A first step to continue this research will be to pursue the parametric study that have characterized this thesis. Chemical or physical quantities have to be considered. Temperature, for instance, could play a decisive role in the breakdown. Stokes-Einstein relation may be able to represent nanoparticle diffusion at higher temperatures than 30°C. A critical temperature could emerge varying the temperature of the experiments. The ph of the solution could play an important role

too. The addition of salt and the consequent presence of ionic current are expected to cause an increase in the dynamic of the nanoparticles.

The study can be extended in three dimension, even if no appreciable changes are to be expected because of the isotropic host. Two and three dimensional tracking can be important in non-isotropic host, complex biological environment, where the characteristics of the mean change based on the direction. Important information could be evaluated by single particle tracking, locating the particle and following its path, understanding its dynamic for a better comprehension of the particle-biological entity interaction. Experimental data are necessary to check the validity of widely used models and could be not surprising to observe behaviours far from the expected ones. Even in these cases, a parametric approach could reveal important and novel characteristics for a better understanding of the nanoparticles related phenomena in a biological matrix.

Modifications to the microscope setup could allow optical trapping. No studies were performed with such an experimental apparatus on nanoparticles dispersed in biological means. An optical trap could help to limit the region of interest of the study, reducing the number of nanoparticles and biological bodies involved in the interactions. A simplification of the unresolved problem of the particle biointeraction is necessary to improve the knowledge and test theoretical models. Low concentrations of nanoparticles, with their slower dynamics than the expected, could lead, for instance, to lower levels of toxicity in the cytoplasm.

APPENDIX

First year experiments

The parametric study of this research, contained in the chapter of the thesis, began in the second year. Gold and polystyrene nanoparticles of different size were purchased to test different physical quantities.

The first year was focused on testing nanoparticles of different material and size to check the potential and the limits of the caustic technique, and in order to become more confident both with the experimental setup and the theoretical models that had to be tested.

The nanoparticles under investigation, during the first year of phd, were provided by the System Toxicology Unit of the Joint Research Centre of the European Commision (table 3), as follows:

Nanomaterial	Size	manufacturer	shape	Dispersed in water Y/N	Stabilized with oleic acid Y/N
Iron Oxides Fe2O3	~8nm	PlasmaChem	spherical	Y	Y
Gold	~11nm	Mintek	spherical	Y	N
Silver	<20nm	JRC	spherical	Y	Y
Cerium	<25nm	Aldrich	spherical	Y	N

Table 3 – List of nanoparticles, their size, manufacturer, shape, fluid in which they were dispersed. Experiments on these nanoparticles were performed to calculate MSD and diffusion coefficients.

The decision to move to commercial nanoparticles was due to practical consideration:

- I was not able to independently produce nanoparticles, and as a consequence was difficult to obtain particles with the desired characteristics.
- Commercial nanoparticles are widely employed in all kinds of applications
- Commercial nanoparticles are available in a large range of characteristics

These are the main reasons that pushed me to investigate the dynamic of commercial gold and polystyrene nanospheres.

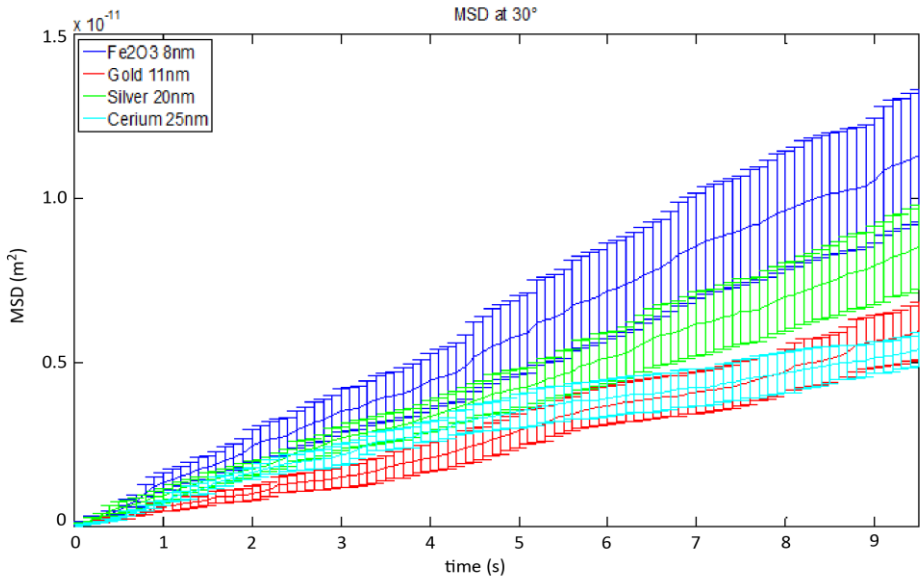

Figure 43 – MSD of three different nanoparticles at 30°C dispersed in water. All nanomaterials exhibited linear behaviour. Stokes-Einstein equation was not able to predict the value of the diffusion coefficient.

Anyway, experimental data were obtained with the nanoparticles in the table, confirming that, below a critical value of concentration, nanoparticles obey to a fractional Stokes-Einstein relation

In figure 43, the linear trend of the mean square displacement of iron oxide, gold, silver and cerium nanoparticles can be observed, as for the gold and polystyrene particles in the results chapter. The related diffusion coefficients are shown in table 4:

Nanomaterial	**Diffusion coefficient (m^2/s)**
Iron Oxide 8nm	$(8.2\pm1.6)\ x10^{-13}$
Gold 11nm	$(5.1\pm1.2)x10^{-13}$
Silver 20nm	$(7.2\pm1.4)\ x10^{-13}$
Cerium 25nm	$(5.5\pm0.9)x10^{-13}$

Table 4 – Experimental diffusion coefficients of the nanoparticles provided from the JRC

The temperature at which the experiment were performed was 30°C and the concentration was roughly $5x10^{-6}$mg/ml. The preparation of the sample was the same described in the thesis. The results were considered as a first hint of the Stokes-Einstein breakdown for nanoparticles below a critical concentration and critical size.

References

1. R. Brown, “A brief account of microscopical observations made in the months of June, July and August 1827, on the particles contained in the pollen of plants; and on the general existence of active molecules in organic and inorganic bodies,” Philos. Mag. Ser. 2, vol. 4, no. 21, pp. 161–173, 1828.
2. G. Gamow, “One, Two, Three…Infinity”, The Viking Press, 1955
3. A. Einstein, “On the movement of small particles suspended in stationary liquids required by the molecular-kinetic theory of heat,” Annalen der Physik, vol. 322. pp. 549–560, 1905.
4. J. Philibert, “One and a Half Century of Diffusion: Fick, Einstein, Before and Beyond”, Diffusion Fundamentals, vol. 2, pp. 1-10, 2005
5. E. L. Cussler, “Diffusion: Mass Transfer in Fluid Systems”, Cambridge University Press, 1997.
6. A. Fick, “Uber Diffusion”, Poggendorff’s Annalen, vol, 94, pp.59-86, 1855.
7. A. Fick, “On Liquid Diffusion”, Philosophical Magazine, Vol.10, pp. 30-39, 1855.
8. W.C. Roberts-Austen, “Bakerian Lecture: on the Diffusion in Metals”, Philosophical Transaction of the Royal Society of London, vol. 187, pp. 383-415, 1896.
9. L.G. Gouy, “Note Sur Le Mouvement Brownien, Journal de Physique (Paris), vol. 7, pp. 561-564, 1888.
10. A. Einstein, “On the theory of Brownian movement”. Annales de Physique (Leipzig), vol.19, pp. 371-381, 1908.
11. M. von Smoluchowski, “Zur kinetischen Theorie der Brownschen Molekularbewegung und der Suspensionen”, Annalen der Physik, vol. 4, pp. 756-780, 1906.
12. P. Langevin, “On the theory of Brownian motion”, Comte Rendus de l’Académie des sciences, vol. 146, pp. 530-533, 1908.
13. J. Perrin, “Les Atomes”, Librairie Félix Alcan, Paris, 1913.

14. D.H. Deutsch, “Did Robert Brown observe Brownian Motion: probably not”, Bulletin of the American Physical Society, vol. 36, pp 1374, 1991.
15. G.C Cadée, “Brownian Emotion”, Nature, vol. 354, pp. 180, 1991.
16. B.J. Ford, “Brownian Movement in Clarkia Pollen: a reprise of the first observations”, The Microscope, vol. 40, pp. 235-241, 1992.
17. K. Pearson, “The problem of the random walk”, Nature, vol. 72, pp. 294, 1905
18. L. Bachelier, “Théorie de la Spéculation”, Thèse Annales Scientifique de l’Ecole Normal Supérieure, 3° série, Tome 17, Gauthier-Villars, Paris, 1900.
19. G. Vogl, “Diffusion and Brownian Motion. Analogies in the migration of atoms, animals, men and ideas”, Diffusion Fundamentals, vol. 2, pp. 1-15, 2005
20. D.T. Gillespie, “Simple Brownian Diffusion”, Oxford University Press, 2013.
21. C.C. Miller, “The Stokes-Einstein law for diffusion in solution”, Proceeding of the royal society A, vol. 106, pp. 724-749, 1924.
22. R. Metzler, J. Klafter, “The random walk’s guide to anomalous diffusion: a fractional dynamics approach”, Physical Reports, vol. 339, pp. 1-77, 2000.
23. J.A. Dix, A.S. Verkman, “Crowding effects on diffusion in solutions and cells”, Annual Review of Biophysics, vol. 37, pp. 247-263, 2008.
24. K. Luby-Phelps. 2000. “Cytoarchitecture and physical properties of cytoplasm: volume, viscosity, diffusion, intracellular surface area”, International Review of Cytology, vol. 192, pp. 189–221, 2000.
25. J.P. Bouchaud, A. Georges, “Anomalous diffusion in disordered media-statistical mechanisms, models and physical applications”, Phys. Rep.-Rev. Sec. Phys. Lett, vol. 195, pp. 127–293, 1990.
26. H.X. Zhou, G. Rivas, A.P. Minton, “Macromolecular crowding and confinement: biochemical, biophysical, and potential physiological consequences”, Annual Review of Biophysics, vol. 37, pp. 375–397, 2008.

27. L.F. Richardson, “Atmospheric diffusion shown on a distance-neighbour graph”, Proceeding of the Royal Society, vol. 110, pp. 709-727, 1926
28. E.W. Montroll, H. Scher, “Random walks on lattices, IV: Continuous-time walks and influence of absorbing boundaries”, Journal of Statistical Physics, vol. 9, pp. 101-135, 1973.
29. R. Metzler and J. Klafter, “The random walk’s guide to anomalous diffusion: a fractional dynamics approach”, Physical Rep., vol. 339, pp. 1–77, 2000.
30. F. Amblard, A.C. Maggs, B. Yurke, A.N. Pargellis, S. Leibler, “Subdiffusion and Anomalous Local Viscoelasticity in Actin Networks”, Physical Review Letters, vol. 77, pp. 4470-4473, 1996.
31. E. Barkai, J. Klafter, Comment on “Subdiffusion and Anomalous Local Viscoelasticity in Actin Networks”, Physical Review Leters, vol. 81, pp. 1134, 1998.
32. E.R. Weeks, H.L. Swinney, “Anomalous Diffusion Resulting from Strongly Asimmetric Random Walk”, Physical Review E, vol. 57, pp. 4915-4920, 1998.
33. O.V. Bychuk, B. O'Shaugnessy, “Anomalous Diffusion at Liquid Surfaces”, Physical Review Letters, vol. 74, pp. 1795-1798, 1994.
34. S. Stapf, R. Kimmich, R.-O. Seitter, “Proton and Deuteron Field-Cycling NMR Relaxometry of Liquids in Porous Glasses: Evidence for Lévy-Walk Statistics”, Physical Review Letters, vol. 75, pp. 2855-2858, 1995
35. J. Bodurka, R.O. Seitter, R. Kimmich, A. Gutsze, “Field-cycling nuclear magnetic resonance relaxometry of molecular dynamics at biological interfaces in eye lenses: The Lévy walk mechanism”, The Journal of Chemical Physics, vol. 107, pp. 5621-5624, 1997.
36. G. Zumofen, J. Klafter, “Spectral random walk of a single molecule”, Chemical Physics Letters, vol. 219, pp. 303-309, 1994.
37. E. Barkai, R. Silbey, “Distribution of single-molecule line widths”, Chemical Physics Letters, vol. 310, pp. 287-295, 1999.

38. J. Klafter, B.S. White, M. Levandowsky, “Microzooplankton Feeding Behavior and the Lévy Walks in “Biological Motion”, Lecture Notes in Biomathematics, ed. W. Alt and G. Hoffmann, vol. 89, Springer, Berlin, 1990.
39. M. Levandowsky, B.S. White, F.L. Schuster, “Random movements of soil amebas”, Acta Protozoologica, vol. 136, pp. 237-248, 1997.
40. R. Nossal, “Stochastic aspects of biological locomotion”, Journal of Statistical Physics, vol. 30, pp. 391-400, 1983.
41. J.B. Metzler, “Linder Biologie”, J.B.Metzler´sche Verlagsbuchhandlung, 1984.
42. C.K. Matthews, K.E. van Holde, “Biochemistry”, 2nd Edition, Benjamin/Cummings, 1996.
43. G.M. Viswanathan, V. Afanasyev, S.V. Buldyrev, E.J. Murphy, P.A. Prince, H.E. Stanley, “Lévy flight search patterns of wandering albatrosses”, Nature, vol. 381, 413-415, 1996.
44. B. O'Shaugnessy, I. Procaccia, “Analytical Solutions for Diffusion on Fractal Objects”, Physical Review Letters, vol. 54, pp. 455-458, 1985.
45. R. Kubo, M. Toda, N. Hashitsume, “Statistical Physics II”, Solid State Sciences, Vol. 31, Springer, 1985.
46. J. Klafter, M.F. Shlesinger, G. Zumofen, “Beyond Brownian Motion”, Physics Today, vol. 49, pp. 33-39, 1996.
47. B.B. Mandelbrot, J.W. van Ness, “Fractional Brownian motions, fractional noises and applications”, SIAM Review, vol. 10, pp. 422-437, 1968.
48. J. Szymanski and M. Weiss, “Elucidating the origin of anomalous diffusion in crowded fluids”, Physical Review Letters, vol. 103, pp. 1–4, 2009.
49. V. Balakrishnan, “Anomalous diffusion in one dimension”, Physica A, vol. 132, pp. 569-580, 1985.
50. W. Wyss, “The fractional diffusion equation”, Journal of Mathematical Physics, vol. 27, pp. 2782-2785, 1986.
51. W.R. Schneider, W. Wyss, “Fractional diffusion and wave equations”, Journal of Mathematical Physics, vol. 30, pp. 134-144, 1989.

52. F. Peseckis, “Statistical dynamics of stable processes”, Physical Review A, vol. 36, pp. 892-902, 1987.
53. H.C. Fogedby, “Lévy Flights in Random Environments”, Physical Review Letters, vol. 73, pp. 2517-2520, 1994.
54. H.C. Fogedby, “Langevin equations for continuous time Lévy flights”, Physical Review E, vol. 50, pp.1657-1660, 1994.
55. G.E. Uhlenbeck, L.S. Ornstein, “On the Theory of the Brownian Motion”, Physical Review, vol. 36 , pp. 823-841, 1930.
56. T. Li, S. Kheifets, D. Medellin, M.G. Raizen, “Measurement of the Instantaneous Velocity of a Brownian Particle”, Science, vol. 328, pp. 1673-1675, 2010.
57. R. Huang, I. Chavez, K.M. Taute, B. Lukic, S. Jeney, M.G. Raizen, E.L. Florin, “Direct observation of the full transition from ballistic to diffusive Brownian motion in a liquid”, Nature Physics, vol. 7, pp. 576–580, 2011.
58. J. Crane, A.S. Verkman. “Long-range nonanomalous diffusion of quantum dotlabeled aquaporin-1 water channels in the cell plasma membrane”, Biophys. Journal, vol. 94, pp. 702–713, 2008
59. T.G.T. Hiss, E.L. Cussler, “Diffusion in high viscosity liquids”, AIChE Journal, vol. 19, pp. 698–703, 1973.
60. W. Hayduk, S. Cheng, “Review of Relation between Diffusivity and. Solvent Viscosity in Dilute Liquid Solutions”, Chemical Engineering Science, vol. 26, pp. 635-646, 1971.
61. W. Hayduk,W.D. Buckley, “Effect of molecular size and shape on diffusivity in dilute liquid solutions”, Chemical Engineering Science, vol. 27, pp. 1997-2003, 1972.
62. D. Fennell Evans, T. Tominaga, C. Chan, “Diffusion of symmetrical and spherical solutes in protic, aprotic, and hydrocarbon solvents,” Journal of Solution Chemistry, vol. 8, pp. 461–478, 1979.
63. C. Wakai, M. Nakahara, “Pressure Dependencies of Rotational, Translational, and Viscous Friction Coefficients in Water-D(2), cetonitrile-

D(3), Acetonitrile, Choloroform and Benzene", Journal of Chemical Physics, vol. 100, pp. 8347-8358, 1994.

64. T. Funazukuri, C. Yi, S. Kagei, "Predictive correlation of binary diffusion and self-diffusion coefficients under supercritical and liquid conditions", The Journal of Supercritical Fluids, vol. 46, pp. 280–284, 2008.
65. H. Sillescu, "Heterogeneity at the glass transition: A review, Journal of Non-Crystalline Solids", vol. 243, pp. 81-108, 1999.
66. M. D. Ediger, "Spatially Heterogeneous Dynamics in Supercooled Liquids, Annual Review of Physical Chemistry, vol. 51, pp. 99-128, 2000.
67. P. Kumar, S. V. Buldyrev, S. R. Becker, P. H. Poole, F. W. Starr, H. E. Stanley, "Relation between the Widom line and the breakdown of the Stokes–Einstein relation in supercooled water", Proceeding of the National Academy of Scieinces of the United States of America, vol. 104, pp. 9575-9579, 2007.
68. K. R. Harris, "The fractional Stokes-Einstein equation: Application to Lennard-Jones, molecular, and ionic liquids", Journal of Chemical Physics, vol. 131, 054503, 2009.
69. K. Meier, A. Laesecke, S. Kabelac, "Transport coefficients of the Lennard-Jones model fluid. II Self-diffusion", Journal of Chemical Physics, vol. 121, pp. 9526–9535, 2004.
70. K. R. Harris, "Communications: The fractional Stokes-Einstein equation: Application to water", Journal of Chemical Physics, vol. 132, 231103, 2010.
71. K. Yoshida, T. Yamaguchi, S. Kittaka, M. C. Bellissent-Funel, P. Fouquet, "Thermodynamic, structural, and dynamic properties of supercooled water confined in mesoporous MCM-41 studied with calorimetric, neutron diffraction, and neutron spin echo measurements", Journal of Chemical Physics ,vol. 129, 054702, 2008.
72. L. Xu, F. Mallamace, Z. Yan, F. W. Starr, S. V. Buldyrev, H. Eugene Stanley, "Appearance of a fractional Stokes–Einstein relation in water and a structural interpretation of its onset", Nature Physics, vol. 5, pp. 565–569, 2009.

73. G. Chirico, M. Placidi, S. Cannistraro, “Fractional Stokes-Einstein relationship in biological colloids: role of mixed stick-slip boundary conditions,” Journal of Physical Chemistry B, pp. 1746–1751, 1999.
74. R. Zwanzig, A. K. Harrison, “Modifications of the Stokes–Einstein formula”, Journal of Chemical Physics, vol. 83, pp. 5861-5862, 1985.
75. S.Weiss, “Fluorescence spectroscopy of single biomolecules”, Science, vol. 283, pp. 1676-1683, 1999.
76. V. Levi, E. Gratton, “Three-dimensional particle tracking in a laser scanning fluorescence microscope”, Single Particle Tracking and Single Molecule Energy Transfer, Wiley-VCH, 2010.
77. V. Levi, E. Gratton, “Exploring dynamics in living cells by tracking single particles”, Cell Biochemistry and Biophysics, vol.48, pp.1-15, 2007.
78. A. Yildiz, “Single-molecule fluorescent particle tracking”, Handbook of Single-Molecule Biophysics, Springer, pp.1-18, 2009.
79. C. Manzo, M.F. Garcia-Parajo, “A review of progresss in single particle tracking: from methods to biophysical insights”, Reports on Progress in Physics, vol.78, 124601, 2015.
80. D. Axelrod, D.E. Koppel, J. Schlessinger, E. Elson, W.W. Webb, “Mobility measurement by analysis of fluorescence photobleaching recovery kinetics”, Biophysics Journal, vol. 16 , pp. 1055-1069, 1976.
81. D. Magde, E. Elson, W.W. Webb, “Thermodynamics fluctuations in a reactin system: measurement by fluorescence correlation spectroscopy”, Physical Review Letters, vol. 29, pp. 705-708, 1972.
82. H. Qian, M.P. Sheetz, E.L. Elson, “Single particle tracking. Analysis of diffusion and flow in two-dimensional systems”, Biophysics Journal, vol. 60, pp. 910-921, 1991.
83. J. Gelles, B.J. Schnapp, M.P. Sheetz, “Tracking kinesin - driven movements with nanometre-scale precision”, Nature, vol. 331, pp. 450-453, 1988.
84. G.M. Lee, A. Ishihara, K. Jacobson, “Direct observation of brownian motion of lipids in a membrane”, Proceeding of the National Academy of Sciences of the United States of America, vol. 88 , pp. 6274-6278, 1991.

85. H. Geerts, M. de Brabander, R. Nuydens, “Nanovid microscopy”, Nature, vol. 351, pp. 765-766, 1991.
86. H Quian, MP Sheetz, EL Elson, “Single particle tracking Analysis of diffusion and flow in two-dimensional systems”, Biophysics Journal, vol. 60, pp. 910-921, 1991.
87. C.J.R. Sheppard, D.M. Shotton, “Confocal laser Scanning microscopy”, Royal Microscopical Society Microscopy Handbooks, 1997.
88. I. Rasnik, T. French, K. Jacobson, K. Berland, “Electronic cameras for low-light microscopy”, Methods in Cell Biology, vol. 81, pp. 219-249, 2007.
89. R. Graf, J. Rietdorf, T. Zimmermann, “Live cell spinning disk microscopy”, Advances in Biochemical Engineering/Biotechnology, vol. 95, pp. 57-75, 2005.
90. T. Wazawa, M. Ueda, “Total internal reflection fluorescence microscopy in single molecule nanobioscience”, Advances in Biochemical Engineering/Biotechnology, vol. 95, pp. 77-106, 2005.
91. D. Axelrod, “Total internal reflection fluorescence microscopy in cell biology”, Traffic, vol. 2, pp. 764-774, 2001.
92. S.W. Hell, “Far-field optical nanoscopy”, Science, vol. 316, pp. 1153-1158, 2007.
93. E. Betzig, G.H. Patterson, R. Sougrat, O.W. Lindwasser, S. Olenych, J.S. Bonifacino, M.W. Davidson, J. Lippincott-Schwartz, H.F. Hess, “Imaging intracellular fluorescent proteins at nanometer resolution”, Science, vol. 313, pp. 1642-1645, 2006.
94. S.T. Hess, T.P. Girirajan, M.D. Mason, “Ultra-high resolution imaging by fluorescence photoactivation localization microscopy”, Biophysics Journal, vol. 91, pp. 4258-4272, 2006.
95. B. Huang, W. Wang, M. Bates, X. Zhuang, “Three-dimensional super-resolution imaging by stochastic optical reconstruction microscopy”, Science, vol. 319, pp. 810-813, 2008.
96. R.R. Kellner, C.J. Baier, K.I. Willig, S.W. Hell, F.J. Barrantes, “Nanoscale organization of nicotinic acetylcholine receptors revealed by stimulated

emission depletion microscopy", Neuroscience, vol. 144, pp. 135-143, 2007.

97. J.J. Sieber, K.I. Willig, C. Kutzner, C. Gerding-Reimers, B.Harke, G. Donnert, B. Rammner, C. Eggeling, S.W. Hell, H. Grubmuller, T. Lang, "Anatomy and dynamics of a supramolecular membrane protein cluster", Science, vol. 317, pp. 1072-1076, 2007
98. G. Wang, N. Fang, "Detecting and tracking nonfluorescent nanoparticle probes in live cell", Methods in Enzymology, vol.54, pp. 83-108, 2012.
99. K. Miura, "Tracking Movement in Cell Biology, Microscopy Techniques", Springer-Verlag Berlin, pp. 267-295, 2005.
100. M.J. Saxton, K. Jacobson, "Single-particle tracking: Applications to membrane dynamics", Annual Review of Biophysics and Biomolecular Structure, vol. 26, pp. 373-399, 1997.
101. Y. Luo, W. Sun, Y. Gu, G.F. Wang, N. Fang, "Wavelength-dependent differential interference contrast microscopy: Multiplexing detection using nonfluorescent nanoparticles", Analytical Chemistry, vol. 82, pp. 6675-6679, 2010.
102. C.J. Murphy, A.M. Gole, J.W. Stone, P.N. Sisco, A.M. Alkilany, E.C. Goldsmith, S.C. Baxter, "Gold nanoparticles in biology: Beyond toxicity to cellular imaging", Accounts of Chemical Research, vol. 41, pp. 1721-1730, 2008.
103. Hu, R., Yong, K. T., Roy, I., Ding, H., He, S., and Prasad, P. N. (2009). Metallic nanostructures as localized plasmon resonance enhanced scattering probes for multiplex dark-field targeted imaging of cancer cells. J. Phys. Chem. C 113, 2676–2684
104. G. Mie, "Contributions to the optics of turbid media, particularly of colloidal metal solutions", Annalen der Physik, vol. 25, pp. 377-445, 1908.
105. M. Pluta, "Advanced Light Microscopy vol. 1 Principles and Basic Properties", Elsevier, 1988.
106. M.A. Dijk, A.L. Tchebotareva, M. Orrit, M. Lippitz, S. Berciaud, D. Lasne, L. Cognet, B. Lounis, "Absorption and scattering microscopy of single metal

nanoparticles", Physical Chemistry Chemical Physics, vol. 8, pp. 3486-3495, 2006.

107. L. Cognet, V. Octeau, D. Lasne, S. Berciaud, B. Lounis, "Photothermal detection and tracking of individual non-fluorescent nano-objects in live cells", Digest of the Leos Summer Topical Meetings, Ieee, pp. 65–66, 2008
108. M. Born, E. Wolf, "Principles of Optics: Electromagnetic Theory of Propagation, Interference and Diffraction of Light", Cambridge University Press, 7th edition, 1999.
109. G.F. Wang, A.S. Stender, W. Sun, N. Fang, "Optical imaging of non-fluorescent nanoparticle probes in live cells", Analyst, vol. 135, pp.215-221, 2010.
110. V. Jacobsen, P. Stoller, C. Brunner, V. Vogel, V. Sandoghdar, "Interferometric optical detection and tracking of very small gold nanoparticles at a water-glass interface", Optical Express, vol. 14, pp.405-414, 2006.
111. P. Kukura, H. Ewers, C. Muller, A. Renn, A. Helenius, V. Sandoghdar, "High-speed nanoscopic tracking of the position and orientation of a single virus", Nature Methods, vol. 6, pp.923-985, 2009.
112. P. Zakharov, F. Scheffold, "Advances in dynamic light scattering techniques", Light Scattering Reviews, vol. 4, pp.433-467, 2009.
113. S.K. Brar, M. Verma, "Measurement of nanoparticles by light-scattering techniques", Trends in Analytical Chemistry, vol. 30, pp. 4-17, 2011.
114. B.J. Berne, R. Pecora, "Dynamic Light Scattering", Courier Dover Publications, 2000.
115. S.R. Aragón, R. Pecora, "Theory of dynamic light scattering from polydisperse systems", The Journal of Chemical Physics, vol. 64, pp.2395-2404, 1976.
116. W.R. Hamilton,"Theory of systems of rays", Transactions of the Royal Irish Academy, vol. 15, pp. 69–174, 1828.
117. J.A. Lock, J.H. Andrews, "Optical caustics in natural phenomena", American Journal of Physics, vol. 60, pp. 397–407, 1992.

118. L.A. Weinstein, “Open Resonators and Open Waveguides”, The Golem Press, 1969.
119. P. Ball, "Light tamers", New Scientist, vol. 217, pp. 40–43, 2013.
120. P. Manogg, “Anwendung der schattenoptik zur untersuchung des zerreissvorgangs von platen”, PhD Thesis Albert-Ludwigs-Universitat Freiberg, 1964.
121. J.D. Carazo-Alvarez, E.A. Patterson, “A general method for automated analysis of caustics”, Optical Lasers Engineering, vol. 32, pp. 95–110, 1999.
122. I.R. Wallhead, S. Gungor, L. Edwards, “Optimisation of the optical method of caustics for the determination of stress intensity factors”, Optics Lasers Engineering, vol. 20, pp.109-133, 1994.
123. M. Sereno, “On gravitomagnetic time-delay by extended lenses”, Monthly Notices of the Royal Astronomical Society, vol.357, pp. 1205–1210, 2005
124. G.N. Gyulchev, S.S. Yazadjiev, “Kerr-Sen dilaton-axion black hole lensing in the strong deflection limit”, Physical Review D, vol. 75, 023006, 2007
125. K. Kanaya, E. Oho, K. Adachi, Y. Yamamoto, H. Doi, “Caustic patterns combined with second and third order astigmatism in high resolution scanning electron microscopes”, Micron Microscopy Acta, vol. 21, pp. 57-68, 1990.
126. E.A. Patterson, M.P. Whelan, “Tracking nanoparticles in an optical microscope using caustics”, Nanotechnology, vol. 19, 105502, 2008.
127. G. Wang, “Diffractive approach to image dynamic optically-bound assembly in real time”, Optical Express, vol. 14, pp. 4584–4588, 2006.
128. G. Mu W, Wang, L. Luan, G.C. Spalding, J.B. Ketterson, “Dynamic control of defects in a two-dimensional optically assisted assembly”, New Journal Physics, vol. 8, 70, 2006.
129. R.W. Kelsall, M. Geoghegan, I.W. Hamley, “Nanoscale Science and Technology”, Wiley, 2005.
130. I. Fedosov, I. Nefedov, B. Khlebtsov, V. Tuchin, “Particle image velocimetry for visualizing laser-induced motion of nanoparticles”, SPIE Newsroom, doi:10.1117/2.1200707.0803, 2007.

131. A. Kohler, “Gedanken zu einem neuen Beleuchtungsverfahren fur mikrophotographische Zwecke (a new systemof illumination for photomicrosgraphic purposes)”, Z Wiss Mikrosk, vol. 10, pp. 433-440, 1983.
132. H. Shao, Y. Huang “Effect of surfactants on the shape and size of cobalt nanoparticles synthesized by thermal decomposition”, Journal of Applied Physics, vol. 99, 08N702, 2006.
133. NTK Thanh, LAW Green, “Functionalisation of nanoparticles for biomedical applications”, Nano Today, vol. 5, 213-230, 2010
134. X. Michalet, “Mean square displacement analysis of single-particle trajectories with localization error: Brownian motion in an isotropic medium”, Physical Review E, vol. 82, 041914, 2010.
135. G. Milne, “Optical Sorting and Manipulation of Microscopic Particles”, PhD Thesis St. Andrews University, 2007.
136. B. Carr, M. Wright, “Nanoparticle tracking Analysis”, Nanosight Ltd, 2013.
137. D. Ernst, J. Kohler, “Measuring a diffusion coefficient by single-particle tracking: statistical analysis of experimental mean squared displacement curves”, Physical Chemistry Chemical Physics, vol. 15, pp. 845-849, 2013.
138. N.S.Cheng, “Formula for the viscosity of a glycerol-water mixture”, Industrial & Engineering Chemistry Research, vol. 47, pp. 3285-3288, 2008.
139. G. Koenig, R. Ong, A. Cortes, J. Moreno-Razo, J. de Pablo, N. Abbot, “Single nanoparticle tracking reveals influence of chemical functionality of nanoparticles on local ordering of liquid crystal and nanoparticle diffusion coefficients”, Nano Letters, vol. 9, pp. 2794-2801, 2009.
140. Z. Li, “Critical particle size where the Stokes-Einstein relation breaks down”, Physical Review E, vol. 80, 061204, 2009.
141. A.C. Sabuncu, J. Grubbs, S. Qian, J.M. Abdel-Fattah, M.W. Stacey, A. Beskok, “Probing nanoparticle interactions in cell culture media”, Colloids and Surfaces B: Biointerfaces, vol. 95, pp. 96-102, 2012.
142. Y. Yang, A. Oztekin, S. Nete, S. Mohapatra, “Particle agglomeration and properties of nanofluids”, Journal of Nanoparticle Research, vol. 14, pp. 852-861, 2012.

143. T.A. Egerton, I.R. Tooley, “Physical characterization of titanium dioxide nanoparticles”, International Journal of Cosmetic Science, vol. 36, pp. 195-206, 2014.
144. D.H. Lee, G.S. Cho, H.M. Lee, “Comparisons of particle size measurement method for colloidal silica”, Journal of Ceramic Processing Research, vol. 14, pp. 274-278, 2013.
145. K. He, M. Spannuth, J.C. Conrad, R. Krishnamoorti, “Diffusive dynamics of nanoparticles in aqueous dispersions”, Soft Matter, vol. 8, 11933, 2012.
146. F. Varenne, J. Bolton, C. Merlet, M. Beck-Broichsitter, F.X. Legrand, C. Vauthier, “Standardization and validation of a protocol of size measurements by dynamic light scattering for monodispersed stable nanomaterial characterization”, Colloids and Surfaces A, vol. 486, pp. 124-138, 2015.
147. C. Gollwitzer, D. Bartczak, H. Goenaga-Infante, V. Kestens, M. Krumrey, C. Minelli , M. Pálmai, Y. Ramaye, G. Roebben, A. Sikova, Z. Varga, “A comparison of techniques for size measurement of nanoparticles in cell culture medium”, Analytical Methods, vol. 8, 5272, 2016.
148. B. Chon, K. Briggman, J. Hwang, “Single molecule confocal fluorescence lifetime correlation spectroscopy for accurate nanoparticle size determination”, Physical Chemistry Chemical Physics, vol. 16, 13418, 2014.
149. F. Verpillat, F. Jond, P. Desbiolles, M. Gross, “Dark-field digital holographic microscopy for 3D-tracking of gold nanoparticles”, Optical Express, vol. 19, 26044, 2011.
150. J.E. Lennard-Jones, "On the Determination of Molecular Fields", Proceeding of the Royal Society of London A, vol. 106, pp. 463–477, 1924.
151. J.K.G. Dhont, “An introduction to dynamics of colloids”, Elsevier, 1996.
152. J.N. Isrealachvili, “Intermolecular and Surface Forces”, Elsevier, 2011.
153. J. P. Hansen and I. R. McDonald, “Theory of Simple Liquids”, Academic Press, 1986.
154. B.U. Feldherof, “Hydrodynamic interactions between two spheres”, Physica A: Statistical Mechanics and its Applications, vol. 89, pp. 373-384, 1977.

155. D.C. Henry, “Cataphoresis of suspended particles. I. The equation of Cataphoresis”, Proceeding of the Royal Society of London A, vol. 133, pp. 106-129, 1931.

156. M. von Smoluchowski, “Contribution to the Theory of Electro-osmosis and Related Phenomena”, Bullettin International de l’Academie des Sciences de Cracovie, vol.3, pp. 184-199, 1903.

157. A. Tuteja, M.E. Mackay, “Breakdown of the continuum Stokes-Einstein relation for nanoparticle diffusion”, Nano Letters, vol. 7, pp. 1276-1281, 2007.

158. J. Liu, D. Cao, L. Zhan, “Molecular dynamics study on nanoparticle diffusion in polymer melts: A test of the Stokes-Einstein law”, Journal of Chemical Physics C, vol. 112, pp. 6653-6661, 2008.

159. E. Goldberg, M. Scheringer, T. Buchelli, K. Hungerbuhler, “Prediction of nanoparticle transport behaviour from physicochemical properties: machine learning provides insights to guide the next generation transport models”, Environmental Science: Nano, vol. 2, pp. 352-360, 2015.

160. T.O. Poulen, K.J. Wilkinson, “Diffusion of Nanoparticles in a Biofilms”, Environmental Science and Technology, vol.45, pp. 3367-3373, 2011.

161. C. Miendl, T. Kueznik, M. Bosch, E. Roblegg, E. Frohlich, “Intracellular Calcium Levels as Screening Tool for Nanoparticle Toxicity”, Journal of Applied Toxicology, vol. 35, pp. 1150-1159, 2015.

162. J.G. Teeguarden, P.M. Hindelliter, G. Orr, B.D. Thrall, J.G. Pounds, “Particokinetics In Vitro: Dosimetry Considerations for In Vitro Nanoparticle Toxicity Assessments”, Toxicological Sciences, vol. 95, pp. 300-312, 2007.

163. K. Solangi, S. Kazi, M. Luhur, A. Badarudin, A. Amiri, R. Sadri, M. Zubir, S. Gharahknami, K. Teng, “A comprehensive review of thermo-physical properties and convective heat transfer to nanofluids”, Energy vol. 89, pp. 1065-1086, 2015.

164. T. Sun, Y. Zhang, B. Pang, D. Hyun, Y. Xia, “Engineered nanoparticles for drug delivery in cancer therapy”, Angewandte Chemie International Edition, vol. 53, pp.12320-12364, 2014.

165. A. Mistry, S. Stolnik, L. Illum, “Nose-to-brain delivery: investigation of the transport of nanoparticles with different surface characteristics and sizes in excised porcine olfactory epithelium”, Molecular Pharmaceutics, vol. 12, pp. 2755-2766, 2015.